big bang, a novel regulator of tissue growth in *Drosophila melanogaster*

DISSERTATION

zur Erlangung des akademischen Grades

Doctor of Philosophy (Ph. D.)

vorgelegt

der Fakultät Mathematik und Naturwissenschaften der
Technischen Universität Dresden

von

Georgios Tsoumpekos

geboren am 07. April 1985 in Volos, Griechenland

Dresden, 2015

Gutachter: **Prof. Dr. Elisabeth Knust**
Prof. Dr. Christian Dahmann

Eingereicht am: 21.12.2015
Tag der Verteidigung: 01.04.2016

"Dies slowly he who does not travel, does not read,
Dies slowly he who abandons a project before starting it,
Who does not ask over a subject that he does not know".

Pablo Neruda

Dedicated to my parents Manolis and Maria and my sister Olga

Table of Contents

Index of Figures

Index of tables

Abbreviations

4.1 protein/Erzin/Radixin/Moesin (FERM)

a-catenin (a-cat)

Adherens junctions (AJ)

Amino acids (a.a.)

Atypical protein kinase C (aPKC)

Big bang (bbg)

Canoe (cno)

Crumbs (crb)

Dachsous (Ds)

DE-cadherin (DE-cad)

Disc large (Dlg)

Drosophila homolog of mammalian Patj (DPATJ)

Echinoid (Ed)

Electron microscopy (EM)

Epidermal growth factor (EGF)

Fat(ft)

Fluorescence-activated cell sorter (FACS)

Guanylate kinase domain (GUK)

Heat shock (hs)

Lin-2/Lin-7 (L27)

Mass spectrometry (MS)

Membrane associated guanylate kinase homologue (MAGUK)

Neurotactin (Nrt)

Partitioning defective 6 (Par6)

Phosho histone 3 (PH3)

Polychaetoid (pyd)

PSD-95, Dlg, ZO-1 (PDZ)

Septate junctions(SJ)

Spaghetti Squash (Sqh)

Stardust (Sdt)

Stranded at second (SAS)

Sup apical region (SAR)

Src-homology 3 domain (SH3)

Terminal deoxynucleotidyl transferase dUTP nick end labeling (TUNEL)

Toucan (tok)

Wild-type (wt)

Wingless (wg)

Yorkie (Yki)

Zyxin (zyx)

B-spectrin (β-spec)

Summary

Multicellular organisms need to control their size throughout development and adult life in the face of challenges such as rapid growth. Unraveling the mechanisms that regulate tissue growth in epithelial tissues, in order to generate organs of correct size and proportion, remains a crucial goal of developmental biology. A suitable epithelial tissue for studying tissue growth in *Drosophila* is the proliferative monolayer epithelial sheet of imaginal wing discs, which gives rise to the adult wing. The Hippo signaling pathway regulates tissue growth in wing development. There are several observations that link tissue growth/Hippo signaling with cell polarity and the actin cytoskeletal organization.

The aim of this thesis was the study of the interplay between cell polarity, cytoskeletal organization and tissue growth. To gain further insight into how apical polarity proteins regulate tissue growth, an enhancer/suppressor screen that was previously conducted in our lab by Linda Nemetschke, was used. The screen was based on the modification of a dominant smaller wing phenotype induced upon overexpression of $Crb^{extraTM}$-*GFP*. One of the enhancers identified in this screen is a gene called *big bang* (*bbg*). The absence of *bbg* results in smaller wings with a slower cell cycle and increased apoptosis in wing discs. *bbg* encodes a protein expressed in the apical cortex in wing disc cells and is required for the proper localization of apical proteins, like Crb, in wing disc epithelia. Bbg is also in the same complex with Spaghetti Squash (Sqh) in the apical cortex of the wing disc epithelia. *sqh* encodes an actin-binding protein that has actin cross-linking and contractile properties. Bbg stabilizes Sqh in the apical compartment of the cell. In conclusion, Bbg regulates wing tissue growth, acting as a scaffolding molecule, through the proper localization of apical components of the cells like Crb and the cytoskeletal component Sqh.

Introduction

Cell polarity

Cell polarity is the non-symmetric distribution of several cellular components, including plasma membrane molecules, cytoskeletal components and/or organelles. In epithelia, the main functions of this asymmetry are the formation of cellular barriers, the secretion of different molecules, the mechanical support of the cells, the sensation of external environmental cues and cell-cell communication. At the cellular level the plasma membrane is separated in apical and basolateral surfaces by the adhesive junctions. The adhesive junctions keep the cells tightly together. Each plasma membrane domain of the cell, either is apical or basolateral has a defined protein composition, giving to the cells specific characteristics like cellular stability and controlled excretion and resorption of different molecules. A basic question that remains still unanswered in biology is how cell polarity is established and maintained. However, several molecules have been already identified to play essential roles in cell polarity.

Three major protein complexes play essential roles in the establishment and maintenance of cell polarity. The first is the apical Par complex consisting of Par3 (in *Drosophila*: Bazooka)-Par6-aPKC [Chen and Zhang, 2013]. The second is the apical Crumbs complex consisting of Crumbs-Pals1 (in *Drosophila*: Stardust)-Patj-Lin-7 [Tepass et al., 1990; Wodarz et al., 2000; Bachmann et al., 2001; Hong et al., 2001; Lemmers et al., 2002; Bachmann et al., 2008]. Finally the third is the basolateral Scribble complex consisting of Lethal giant larvae (Lgl)-Scribble (Scrib)-Disc large (Dlg) proteins [Bilder and Perrimon, 2000; Bilder et al., 2003]. The above three cell polarity protein complexes are evolutionary highly conserved from invertebrates to vertebrates (Fig. 1). The sub-cellular localization of the polarity complexes is also highlighted in the schematic representation of the cells (Fig. 1).

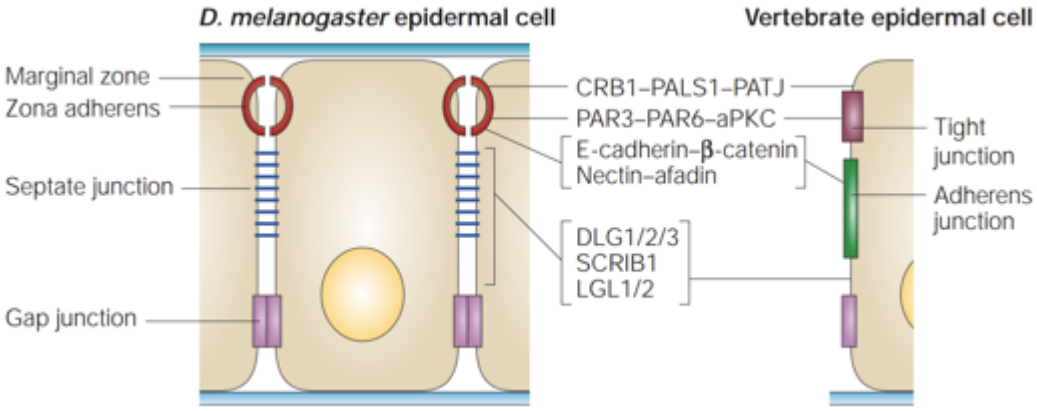

Figure 1: Comparison of the epithelial structure and the polarity protein localization in invertebrates (*D. melanogaster*) and vertebrates. The scheme represents a late embryonic cell from *D.*melanogaster and a mammalian epithelial cell. The structures of the cells, e.g. marginal zone and adherens junctions, are shown on the left and right. The polarity proteins, e.g. CRB1, PATJ are categorized in the middle, in their specific sub-cellular loclization along the lateral membrane of the cell. Only the mammalian names of the proteins are listed. aPKC, atypical protein kinase C; CRB1, Crumbs homologue-1; DLG1/2/3, Discs large homologue-1/2/3; LGL1/2, Lethal giant larvae homologue-1/2; PALS1, protein associated with LIN7; PATJ, PALS1-associated tight-junction protein; SCRIB1, Scribble homologue 1 (Adapted from Macara, 2004).

The role of *crumbs (crb)* in epithelial cell polarity

The transmembrane protein Crumbs (Crb) was the first 'polarity determinant' to be identified in *Drosophila* [Tepass et al., 1990]. In *Drosophila*, Crb is expressed in all ectodermally derived epithelial tissues, like epidermis, foregut, hindgut, Malpighian tubules, trachea and salivary glands. In embryonic epithelia Crb is localized in the sup-apical region of the cell (also called marginal zone) (Fig. 1 A), a membrane domain that can be found apical to the zonula adherens (Fig. 1 B). Regarding the function of the gene, *crb* mutant is embryonic lethal [Jürgens et al., 1984; Tepass et al., 1990]. More specifically, *crb* mutant *Drosophila* embryos show disorganization of the polarity structure and maintenance of epithelial cells, and disruption in the formation of the zonula adherens [Tepass and Knust, 1993]. Similar phenotypes are observed in *stardust* (*sdt)* mutant embryos [Bahmann et al., 2001] (Fig. 2 C). *crb* overexpression in embryos leads to an expansion of the size of the apical membrane at the expense of the basolateral membrane [Wodarz et al. 1995]. The previous data suggests that indeed Crb is a master apical determinant of epithelial cell polarity (Fig. 2 A-C).

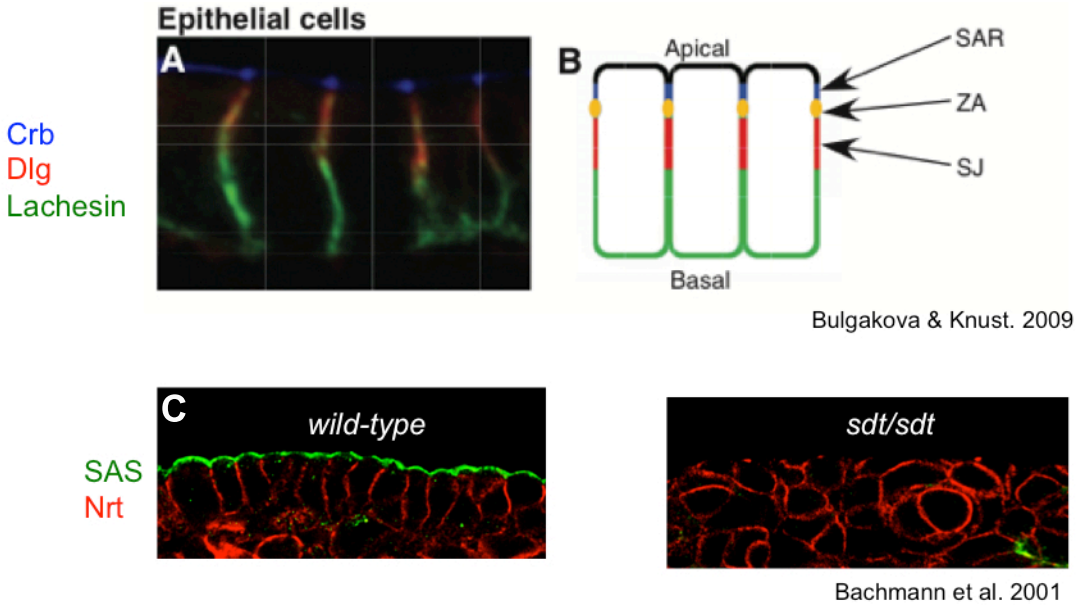

Figure 2: Crb localization and its function in maintaining epithelial cell polarity. (A-B) Localization of Crumbs in *Drosophila* embryonic epithelial cells (A) and schematic structure of the Drosophila embryonic epithelial cells (B). Vertical confocal section through embryonic epithelial cells and immunostained with: Crb, localised to the subapical region (SAR); Dlg, localized to septate junctions (SJ); and Lachesin, highlighting basolateral plasma membrane. **(C)** Lateral sections of stage 12 wild-type (left) and *sdt* mutant (right) embryos stained with Stranded at Second (SAS) and Neurotactin (Nrt), apical and basolateral marker, respectively. (Adapted from: (A-B) Bulgakova and Knust, 2009; (C) Bachmann et al., 2001]

As already mentioned, Crb is a type I transmembrane protein, with a huge extracellular domain consisting of 29 epidermal growth factor (EGF)-like repeats (like Notch) [Chillakuri et al., 2012] and four laminin-A globular-domain-like repeats (Fig. 3). The highly conserved intracellular domain of Crb consists of 37 amino acids and has two conserved binding motifs, the FERM- (4.1 protein/Erzin/Radixin/Moesin) and the PDZ- (PSD-95, Dlg, ZO-1) [Bulgakova and Knust, 2009] -binding motifs. After the identification of Crb in *Drosophila*, several homologous of Crb were identified in humans, mice and zebrafish and in *C. elegans* [den Hollander et al., 1999, Bossinger et al., 2001, Mehalow et al., 2003, Omori et al., 2006, Tepass 2012]. Vertebrates contain multiple paralogs of Crb (*CRB1*, *CRB2* and *CRB3*), although flies have a single *crb* gene, suitable for genetic analyses to identify potential downstream interactors.

Crb is a master regulator of apical cell polarity, and several interactors, direct or indirect of the intracellular or the extracellular domain were identified, respectively [Thompson et al., 2013]. It is already mentioned that the core complex of Crumbs, which regulates cell polarity consists of: Crb, Sdt, PATJ

(protein associated with tight junctions or Pals1-associated tight junction protein) and Lin-7 (Fig. 3). *Drosophila sdt* encodes a PDZ domain protein of the membrane-associated guanylate kinase (MAGUK) family. *sdt* encodes several protein isoforms. Sdt, as a member of the MAGUK family proteins, contains a PDZ domain, two Lin-2/Lin-7 (L27) domains, a Src-homology 3 (SH3) domain and a guanylate kinase (GUK) domain [Bachmann et al., 2001; Berger et al., 2007; Bulgakova et al., 2008; Hong et al., 2001]. The PDZ binding motif of Crb directly binds to the single PDZ domain of Sdt [Bachmann et al., 2001, Hong et al., 2001] (Fig. 3). PATJ is a PDZ domain protein, like Sdt, containing four PDZ domains and a single L27 domain [Pielage et al., 2003]. Lin-7 is a small protein that has a L27 domain and a C-terminal PDZ domain [Bachmann et al., 2004]. Sdt recruits the other scaffolding molecules PATJ and Lin-7 in the Crumbs core complex [Roh et al., 2002; Bachmann et al., 2004] (Fig. 3).

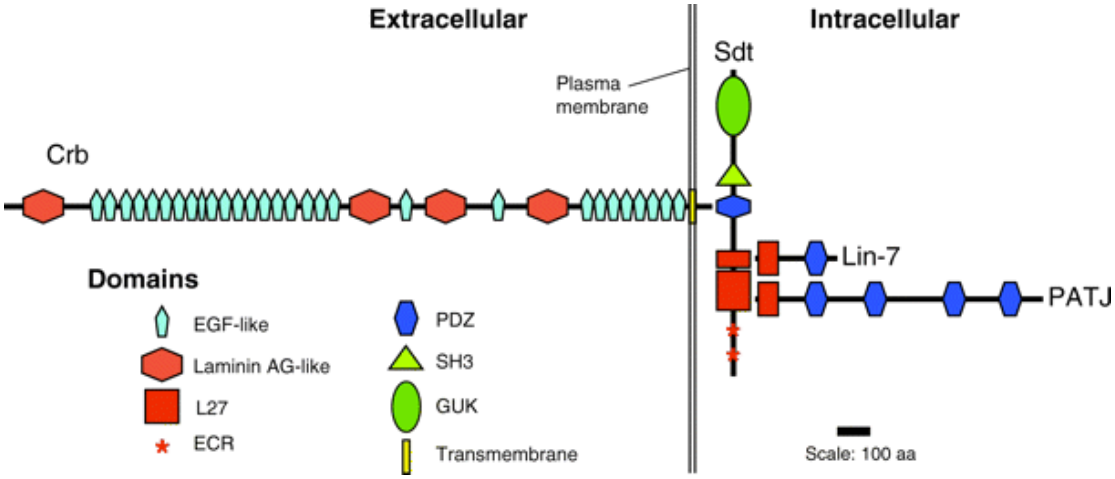

Figure 3: Schematic representation of the Crumbs core complex. The Crumbs core complex conxists of Crb, Sdt, PATJ and Lin-7. The protein domains are designed in scale (100 amino acids). (Adapted from Bulgakova and Knust 2009).

Crb and Sdt have essential roles in establishment and maintenance of epithelial cell polarity [Tepass and Knust, 1990; Tepass and Knust, 1993; Bachmann et al., 2001; Hong et al., 2001]. However PATJ and Lin-7 seem to play complementary roles in epithelial cell polarity in the *Drosophila* embryo [Zhou and Hong, 2012; Krahn et al., 2010; Bachmann et al., 2008]. In *Drosophila* the expression of the membrane-bound cytoplasmic domain of Crb can partially rescue the *crb*-mutant embryonic phenotype. Therefore, the intracellular domain of Crb is the important domain of the protein for the

establishment and maintenance of epithelial cell polarity in *Drosophila* embryos [Wodarz et al., 1995; Klebes and Knust, 2000; Klose et al., 2013].

Apart from Sdt several partners of Crb were identified. The intracellular domain of Crb also interacts with partitioning defective 6 (Par6), atypical protein kinase C (aPKC), Moesin, Yurt and Expanded [Tepass 2012]. All of the previous partners of Crb except from Expanded regulate the establishment and maintenance of apical cell polarity [Tepass 2012]. Recently it was reported that the extracellular domain of Crb directly interacts with the extracellular domain of Notch in zebrafish, an essential interaction that leads to a down regulation of the Notch activity in the zebrafish neuroepithelium [Ohata et al., 2011].

At the same time there were identified mutations in one of the human Crb proteins, CRB1 that uncovered a novel function for Crb. Specifically, loss of CRB1 leads to severe forms of the inherited, degenerative eye diseases retinitis pigmentosa (RP12) and Leber congenital amaurosis [den Hollander et al., 1999, den Hollander et al., 2008]. Similar data were obtained for mouse CRB2, as loss of CRB2 leads to gradual disorganization of the mouse retina [Alves et al., 2012]. *Drosophila* and human Crb are localized to the stalk membrane and the inner segment of *Drosophila* and human photoreceptor cells, respectively [Bulgakova and Knust, 2009]. The function of Crb in those cells is the maintenance of the integrity of the apical light-sensing organelle, the rhabdomere in *Drosophila* and the outer segment in vertebrates [Pellikka et al., 2002, Izaddoost et al., 2002]. This function is connected with the function of Crb to prevent light-dependent retinal degeneration in invertebrates and vertebrates [Johnson et al., 2002, Mehalow et al., 2003, van de Pavert et al., 2004, Chartier et al., 2012].

Crumbs and tissue growth

Recently, a novel function of Crb was identified, the regulation of tissue growth through the interaction with the signaling pathway Hippo [Robinson et al., 2010, Grzeschik et al., 2010, Ling et al., 2010, Chen et al., 2010] and the Notch signaling pathway [Herranz et al., 2006, Richardson and Pichaud 2010, Ohata et al., 2011]. More specifically, Crumbs has an impact on the activity of

the transcription factor Yorkie (Yki), the human homologues are Yes-associated protein (YAP) and transcription co-activator with PDZ-binding motif (TAZ) in the Hippo pathway. This probably occurrs through a direct interaction of Crb with an upstream regulator of the Hippo pathway, the FERM domain-containing protein Expanded [Robinson et al., 2010, Ling et al., 2010]. In conclusion, *crb* was identified as a central component of epithelial polarity specification and remodeling during development, but recent data suggests that *crb* is also a main regulator of epithelial tissue growth and organ size control.

Linking apical proteins with tissue growth: *bbg*, as a novel enhancer, in a screen specific for *crb*

Various observations indicate that polarity and growth are linked. For instance, during the development of the *Drosophila* and vertebrate nervous system, non-polarized progenitor cells are closer to cell cycle exit than polarized progenitors [Arai et al., 2011]. It is notable that the majority of human cancers (approximately 90%) are correlated with loss of polarity and functional aberrations of apico-basal polarized epithelial cells [Lee and Vasioukhin, 2008]. A genetic screen conducted in *Drosophila* uncovered novel tumor suppressor genes, some of which encode components of the apico-basal polarity complexes [Gateff, 1978; Bilder et al., 2000]. Loss- or gain-of-function mutations in these genes are associated with uncontrolled proliferation during cancer progression and stem cell renewal [Wodarz and Nathke, 2007; Lee and Vasioukhin, 2008]. However, the mechanisms that establishes and maintains cell polarity and the correlations that they show with proliferation and tissue growth are not fairly elucidated yet.

There is some evidence indicating that cell polarity and especially lateral polarity proteins, like Lgl and Scribbled play crucial roles in the control of tissue growth [Lee et al. 2006, Grusche et al. 2011]. However less clear is the role of the apical proteins and the crosstalk with tissue growth. For instance, it has been shown that the apical determinant *crb* regulates wing size through the Hippo signaling pathway [Robinson et al., 2010, Ling et al., 2010, Chen et al., 2010]. In mammals, homophilic interactions of E-cadherin (E-cad), a component of the adherens junctions, in cultured cells decrease

cell proliferation and promote nuclear export of YAP (the homologue of Yorkie in vertebrates) [Kim et al 2011]. Conditional deletion of another adherens junction marker, α-Cat, which serves as a link between the actin cytoskeleton and adherens junctions [Baum et al., 2011], causes nuclear accumulation of YAP in *α-catenin* (*α-cat*) mutant keratinocytes *in vitro* and *in vivo* [Schlegelmilch et al., 2011, Silvis et al., 2001]. Bearing these few examples, the connections between polarity proteins of epithelial cells and tissue growth have not been studied in detail. This has been addressed to some extent in the following work.

To gain further insight into how exactly apical proteins regulate tissue growth, Linda Nemetschke previously conducted an enhancer/suppressor screen in our lab. The screen was based on the modification of a dominant smaller wing phenotype induced upon overexpression of $Crb^{extraTM}$*-GFP* (the intracellular domain of Crb is replaced by GFP). Here, we show that one of the enhancers of that screen is a gene called *big bang* (*bbg*). *bbg* encodes a protein with a novel apical localization in cells and regulates tissue growth during wing development in *Drosophila*. We also identified that Bbg localizes in the same complex with Spaghetti Squash (Sqh) in the apical cortex of the wing disc epithelium. *sqh* encodes an actin-binding protein that has actin cross-linking and contractile properties and is regulated by the phosphorylation of its light and heavy chains [Manzanares et al., 2009]. Bbg stabilizes Sqh in the apical compartment of the cell. In conclusion, Bbg regulates wing tissue growth, acting as a scaffolding molecule, through the proper localization of apical components of the cells like Crb and the cytoskeletal component Sqh.

Bbg is a PDZ domain protein that is dynamically expressed throughout *Drosophila* development

bbg encodes a PDZ-domain protein with multiple isoforms that is expressed dynamically throughout development in *Drosophila* including the wing margin of larval imaginal discs [Kim et al., 2006]. The PDZ domain is a modular protein-protein interaction domain composed of 80-100 amino acids and derives its name from the first letter of the three proteins in which this domain was first identified, namely postsynaptic density-95 (PSD-95),

Disc large 1 (DLG1) and zonula occludens-1 (ZO-1) [Kornau, 1995]. PDZ domains are among the most abundant protein interaction domains. A recent examination of the genomic SMART database shows that there are a plethora of PDZ domain proteins in metazoan species (e.g. 90 in *C. elegans*, 88 in *D. melanogaster*, 160 in *H. sapiens*). The majority of the PDZ domain proteins usually function as scaffolding molecules and are involved in the assembly, maintenance and function of localized macromolecular complexes or networks. The establishment and maintenance of cell polarity is an important process for which genetic analyses have uncovered crucial roles of PDZ domain proteins (e.g. as is mentioned above Sdt, Baz, Dlg, Scribble). Signal transduction is another major process involving PDZ domain proteins such as InaD that is required for phototransduction in photoreceptor cells in *Drosophila*. Finally, PDZ domain protein-encoding genes can acquire functional diversity through alternative splicing, like Bbg.

Bbg was characterized in 2006 [Kim et al., 2006] and was found to be predominantly expressed in the developing gut during embryogenesis, as well as in the external sensory organs found in the epidermis. In late third instar larva, Bbg is expressed except from the presumptive wing margin in the wing disc, in the eye, leg and haltere discs as well as in the brain. The expression patterns for Bbg are dynamic and specific during development, suggesting that Bbg plays important roles in multiple developmental processes.

As previously reported, flies, which are homozygous mutant for *bbg* are viable and fertile [Kim et al. 2006]. However, the exact function of the gene is not clear. Recent work identified that RNAi-mediated knockdown of *bbg* disrupts border cell migration during *Drosophila* oogenesis through the JAK-STAT signaling pathway [Aranjuez et al., 2012]. Bbg was also shown to mediate the gut immune response [Bonnay et al., 2013]. It was shown that in the adult *Drosophila* midgut, Bbg is present at the level of the apical side of the enterocytes of the midgut. In *bbg* mutants, these junctions loosen, enabling the intestinal flora to trigger a constitutive activation of the midgut immune response. The function of Bbg in tissue growth is currently not well characterized. In this project, I analyzed the role of Bbg in wing size control and the potential interaction of Bbg with Crb and other proteins, like Sqh, linking cell polarity and cytoskeletal organization to tissue growth.

Results

To gain further insight into the molecular mechanisms by which the apical proteins in association with *crb* regulate tissue growth, an enhancer/suppressor screen was conducted in our lab (Linda Nemetschke, unpublished), to identify regulators of a wing phenotype occurring from the overexpression of *Crb^{extraTM}-GFP*. This screen was based on a dominantly smaller wing defect (Fig. 10 A-C). Two of the enhancers picked up in this genetic screen were *RabX6* and *big bang (bbg)*, which were analyzed further in this project.

The critical developmental stage of the overexpression of *Crb^{extraTM}-GFP* smaller wing phenotype is at least the L3 stage

The first question addressed was, which was the developmental stage that produced the growth defect after overexpression of *Crb^{extraTM}-GFP*. To achieve that, the overexpression of *Crb^{extraTM}-GFP* was conditionally turned on using the GAL80 system. In this conventional GAL4/UAS system, a P element carrying the GAL4 coding region drives the expression of GAL4 protein in a specific tissue, on the basis of proximity of the P element to a tissue-specific enhancer [McGuire et al., 2003]. GAL4 protein then binds to its cognate UAS binding site and activates transcription of the downstream effector gene. In the target system, a temperature-sensitive GAL80 protein (GAL80ts) expressed ubiquitously from the tubulin 1α promoter, represses the transcriptional activity of GAL4 at 19°C and thus prevents the expression of the UAS-*Crb^{extraTM}-GFP* transgene, but becomes inactive at 30°C, allowing GAL4 to drive the expression of the UAS-*Crb^{extraTM}-GFP* transgene in the imaginal wing tissue.

As shown in Fig. 4 the overexpression of *Crb^{extraTM}-GFP* was switched on in different developmental stages: embryogenesis, L1, L2, L3, L3-early pupal, early pupal and late pupal. Then, the size of the adult wings was measured. Overexpression of *Crb^{extraTM}-GFP* from embryogenesis until L3 stage produced the smaller wing phenotype (green arrows in Fig. 4). However, upon overexpression of *Crb^{extraTM}-GFP* later in the pupal stages the

wings were the same size (red arrows in Fig. 54) as the control. Finally, the overexpression of *Crb*^{extraTM}*-GFP* only in the L3 stage again gave the smaller wing phenotype (small green arrow in Fig. 4). The L3 stage is sufficient for the overexpression of *Crb*^{extraTM}*-GFP* to show an effect in the adult wing size.

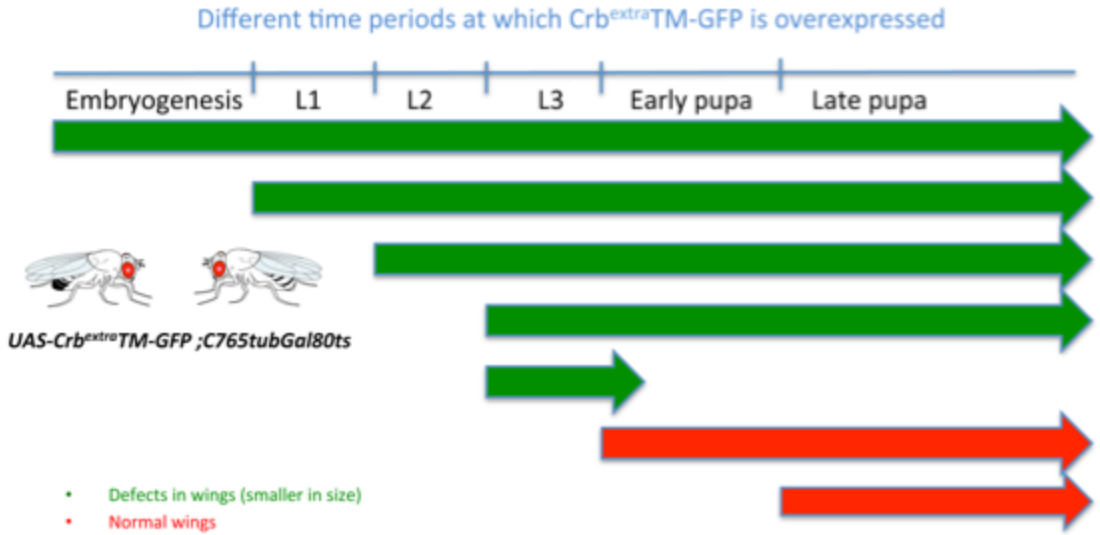

Figure 4: The critical developmental stage of the overexpression of *Crb*^{extraTM}*-GFP* smaller wing phenotype is at least the L3 stage. Conditional overexpression of *Crb*^{extraTM}*-GFP*, using the *C765tubGal80ts*, in different developmental stages. Specifically, the overexpression of *Crb*^{extraTM}*-GFP* was switched on from the developmental stages: embryogenesis, L1, L2, L3, L3-early pupal, early pupa and late pupa (the duration of the overexpression of CrbextraTM-GFP is analogous to the length of the arrows. Green arrows correspond to smaller wings in size. Red arrows correspond to normal wings in size.

Cell cycle arrest does not occur upon overexpression of *Crb*^{extraTM}*-GFP* in wing discs

Given that overexpression of *Crb*^{extraTM}*-GFP* gives smaller wings (Fig. 10 A-C), the possibility of a cell cycle arrest in the L3 wing disc stage was analyzed (e.g. in G1 or G2 phase). *Crb*^{extraTM}*-GFP* was overexpressed specifically in the posterior compartment of the wing disc and then the numbers of EdU positive cells were counted. Edu treated cells completed one cell cycle and proceeded to the next S-phase (Fig. 5 C-D'). The overexpression of *GFP* was used as a negative control in order to exclude the possibility that the *GFP* by itself produces any phenotype (Fig. 5 A-B'). The Edu positive cells were 48 in the specific frame from the pouch area (read square in Fig. 5 B'). Seven individual discs were used from each genotype and they showed similar numbers of EdU cells (Fig. 5 E). Thus there was no cell cycle arrest upon overexpression of *Crb*^{extraTM}*-GFP* in wing discs.

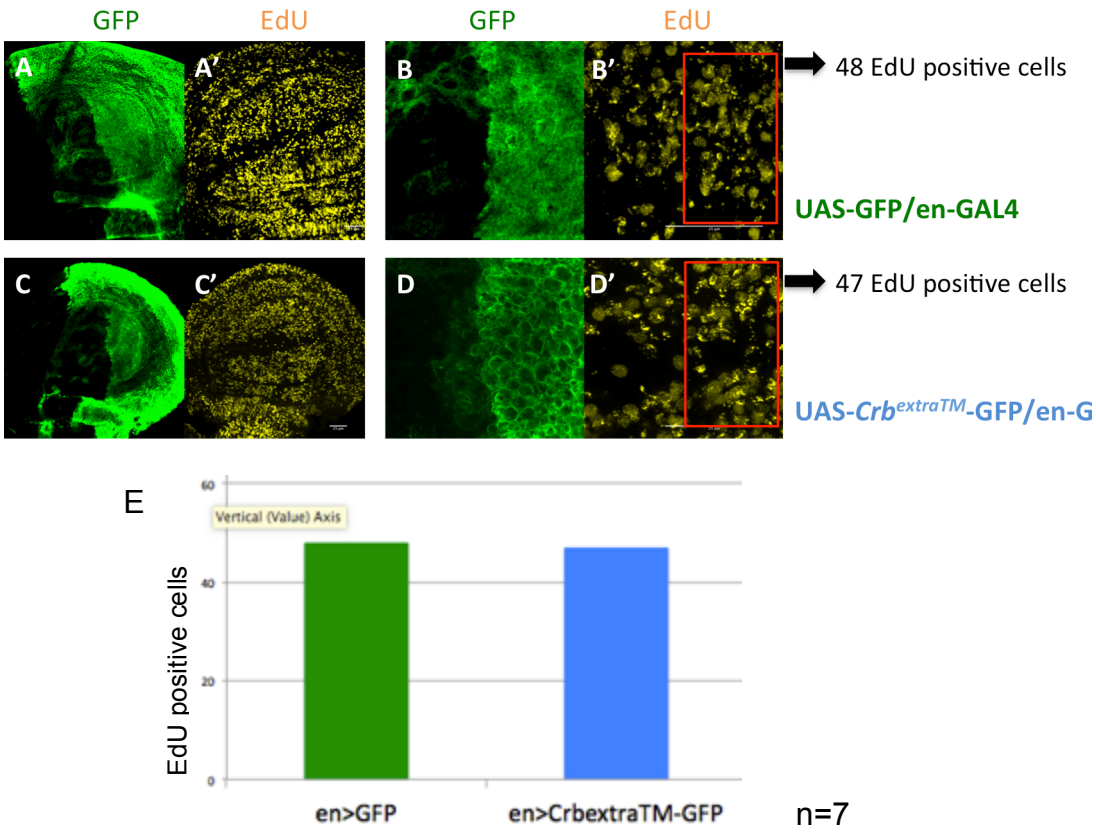

Figure 5: Cell cycle arrest does not occurr upon overexpression of *Crb^{extraTM}-GFP* in wing discs. Overexpression of *GFP* **(A-B')** or *Crb^{extraTM}-GFP* **(C-D')** in the posterior compartment of the wing disc and measurement of the EdU positive cells. B-B' are magnifications from A-A' and D-D' from C-C', respectively. Staining with GFP (A,B,C,D) and EdU Scale bars, 25 μm. **(E)** Statistical analysis of the number of the EdU positive from *en>GFP* and *en>Crb^{extraTM}-GFP* wing discs. TTEST did not show any statistical significant differences. Error bars show standard deviation. There were measured seven independent wings/ condition that showed similar observation.

The overexpression of *Crb^{extraTM}-GFP* or *Crb^{full}* in clones results in slower proliferation or/and less cell number in the wing disc epithelium

In order to analyze further the growth defects in wing discs upon overexpression of *Crb^{extraTM}-GFP*, clones of overexpression of *Crb^{extraTM}-GFP*, *Crb^{full} and* GFP, as control, were generated, in wing discs. In the clones overexpressing *Crb^{extraTM}-GFP* or *Crb^{full}*, the size of the clones was measured in the pouch area and was compared with the size of the clones overexpressing *GFP* (Fig. 6). Two independent time points were used to induce clone formation (72h and 96h induction of clones after egg laying, left and right panel respectively). The overexpression of *Crb^{extraTM}-GFP* clones compared with *GFP* clones, showed that the overexpression of *Crb^{extraTM}-GFP* produces clones (quantification of the surface area of all clones in the wing

pouch) -40% less (heatshock - hs - after 72h) and 30% less (hs after 96h) (compare Fig. 6 B, B', E, E' to A, A', D, D', left and right panels, G-H). Overexpressing *Crb*^{full} produces -70% lesser clones (hs after 96h) (compare Fig. 6 C,C', F, F' to A, A', D, D', left and right panels, H). The overexpression of *Crb*^{full} in clones probably leads to apoptosis. Apoptosis is characterized by a series of typical morphological features, such as shrinkage of the cell [Saraste and Pulkki, 2000]. This is suggested by the smaller size and the roundish morphology of the cells inside the *Crb*^{full} clones (Fig. 6 F, the arrow indicates clones that are composed from one cell, probably undergoing apoptosis). Notably, the only one clone upon overexpression of *Crb*^{full} after 72h is in the peripodial membrane and not in the monolayered epithelium tissue (maybe due to apoptosis) of the wing disc (Fig. 6 C', the arrow indicates that the cells are bigger in size, therefore indicates the peripodial membrane). That was the reason that the size of the *Crb*^{full} clones was not measured after 72h of hs. In general the defects that were noticed are more severe when the clones are induced in earlier time points (compare hs after 72h to 96h). In conclusion, overexpression of *Crb*^{extraTM}*-GFP* or *Crb*^{full} in clones in wing discs decreased the number of the dividing cells inside the clone. This can be attributed due to slower proliferation and/or apoptosis. These two events are not mutually exclusive.

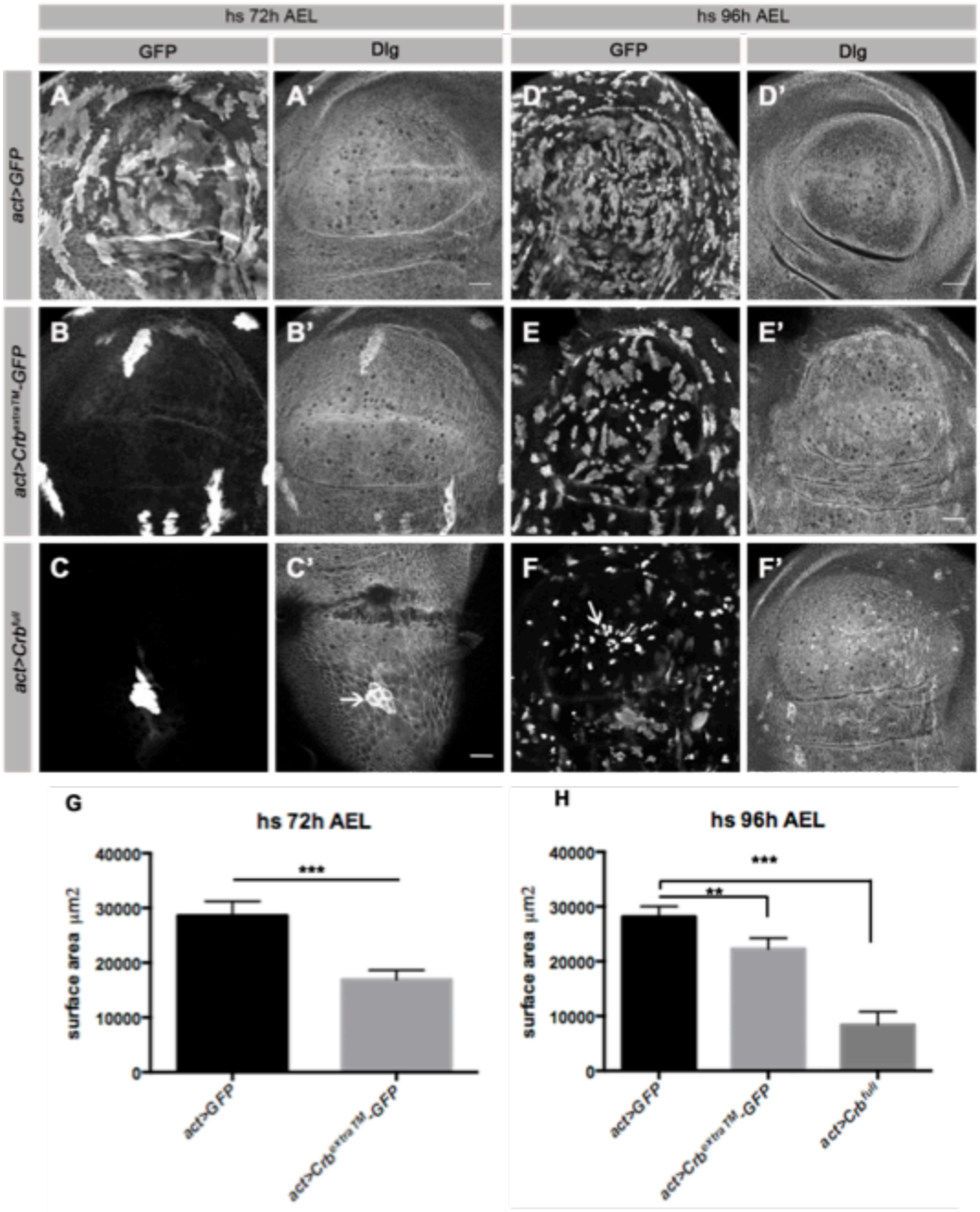

Figure 6: Overexpression of *Crb^{extraTM}-GFP* or *Crb^{full}* in clones in wing discs decreases the number of divisions or eliminates the cells. Generation of overexpression clones in wing discs of **(A, A', D, D')** *GFP*, **(B, B', E, E')** *Crb^{extraTM}-GFP* and **(C, C', F, F')** *Crb^{full}* in two independent time points (hs after 72h AEL left panel and 96h AEL right panel) and stained with GFP and Dlg, respectively. Scale bars, 25 µm **(G, H)** Statistical analysis of measuring the size of the clones in the pouch area of overexpression of GFP, *Crb^{extraTM}-GFP* and *Crb^{full}* after 72h of hs **(G)** and 96h **(H)** using 9 independent discs/condition. For the analysis (G-H) it was used TTEST and ANOVA test. Two asterisks indicate $p \leq 0.01$, three asterisks indicate $p \leq 0.001$. Error bars show standard deviation.

Hippo upstream components suppress the wing phenotype upon overexpression of *Crb^{extraTM}-GFP*

Crb has been shown previously to regulate wing size through the Hippo signaling pathway [Robinson et al., 2010, Ling et al., 2010, Chen et al., 2010]. More specifically, *crb* mutant wings are overgrown or bigger in size. Since the overexpression of *Crb^{extraTM}-GFP* gives the opposite phenotype where the wings are smaller in size compared to the control, the relationship between the overexpression of *Crb^{extraTM}-GFP* and the Hippo components was studied. Deficiency lines for nine components of the Hippo pathway, namely *fat*, *expanded*, *merlin*, *kibra*, *mats*, *salvador*, *warts*, *hippo*, and *yorkie* were used for this study. (Fig. 7). These deficiency lines were crossed with flies over-expressing *Crb^{extraTM}-GFP*, in order to identify any genetic interaction between *Crb^{extraTM}-GFP* and any component of the Hippo pathway.

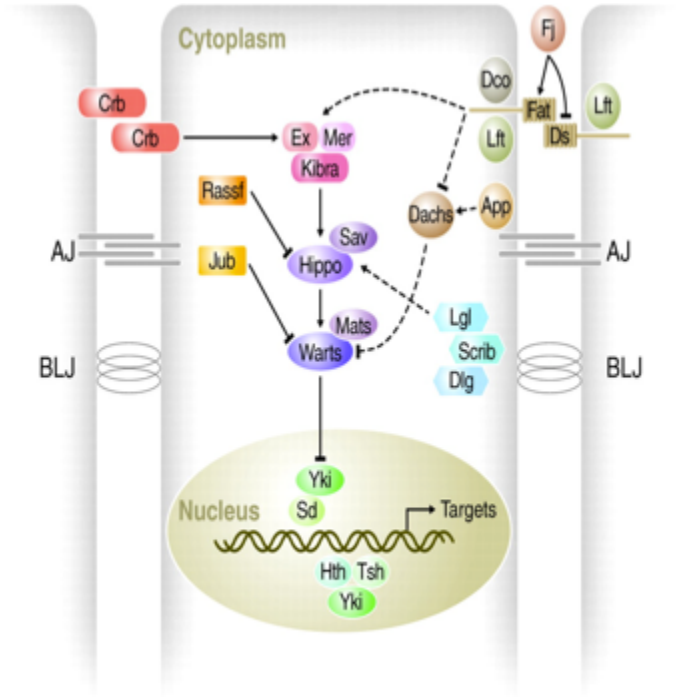

Figure 7: Hippo signaling pathway in *Drosophila*. Cells (outlined in grey, nuclei in green) are shown with adherens junctions (AJ) and basolateral junctions (BLJ). Hippo pathway components in various colors, with pointed and blunt arrowheads indicating activating and inhibitory interactions, respectively. Continuous lines indicate direct interactions, whereas dashed lines indicate unknown mechanisms. Abbreviations: Jub, Ajuba; App, Approximated; Crb, Crumbs; Dco, Discs overgrown; Dlg, Discs large; Ds, Dachsous; Ex, Expanded; Fj, Four-jointed; Hth, Homothorax; Jub, *Drosophila* Ajuba; Lats, Large tumor suppressor; Lft, Lowfat; Lgl, Lethal giant larvae; Mer, Merlin; Mats, Rassf, Ras-associated factor; Sav, Salvador; Scrib, Scribble; Sd, Scalloped; Tsh, Teashirt; Yap, Yes associated protein; Yki, Yorkie (Adapted from Halder and Johnson 2011).

The deficiency lines that include either *kibra* or *expanded* were able to suppress the smaller wing phenotype obtained upon the overexpression of *Crb^{extraTM}-GFP* (Fig. 8 A-H). The wings were bigger in size (Fig. 8 A-E, H). These are the upstream components of Salvador and Hippo kinases of the Hippo pathway. The previous result was verified using a mutant line for *expanded* (Fig. 8 F-H). To verify the above results obtained with deficiency lines that include either *kibra* or *expanded*, the experiments were repeated using the deficiency lines alone. The size of the wing obtained when one copy of the gene *kibra* was missing, was the same compared to that obtained of the same deficiency but in the background of overexpression of *Crb^{extraTM}-GFP* (Fig. 8 I-K). However, the wing size when one copy of *expanded* is missing is bigger than when the mutated gene is in the background of *Crb^{extraTM}-GFP* overexpression (Fig. 8 L-Q). This suggests an interaction between the Hippo pathway components *kibra* and *expanded* with *Crb^{extraTM}-GFP.*

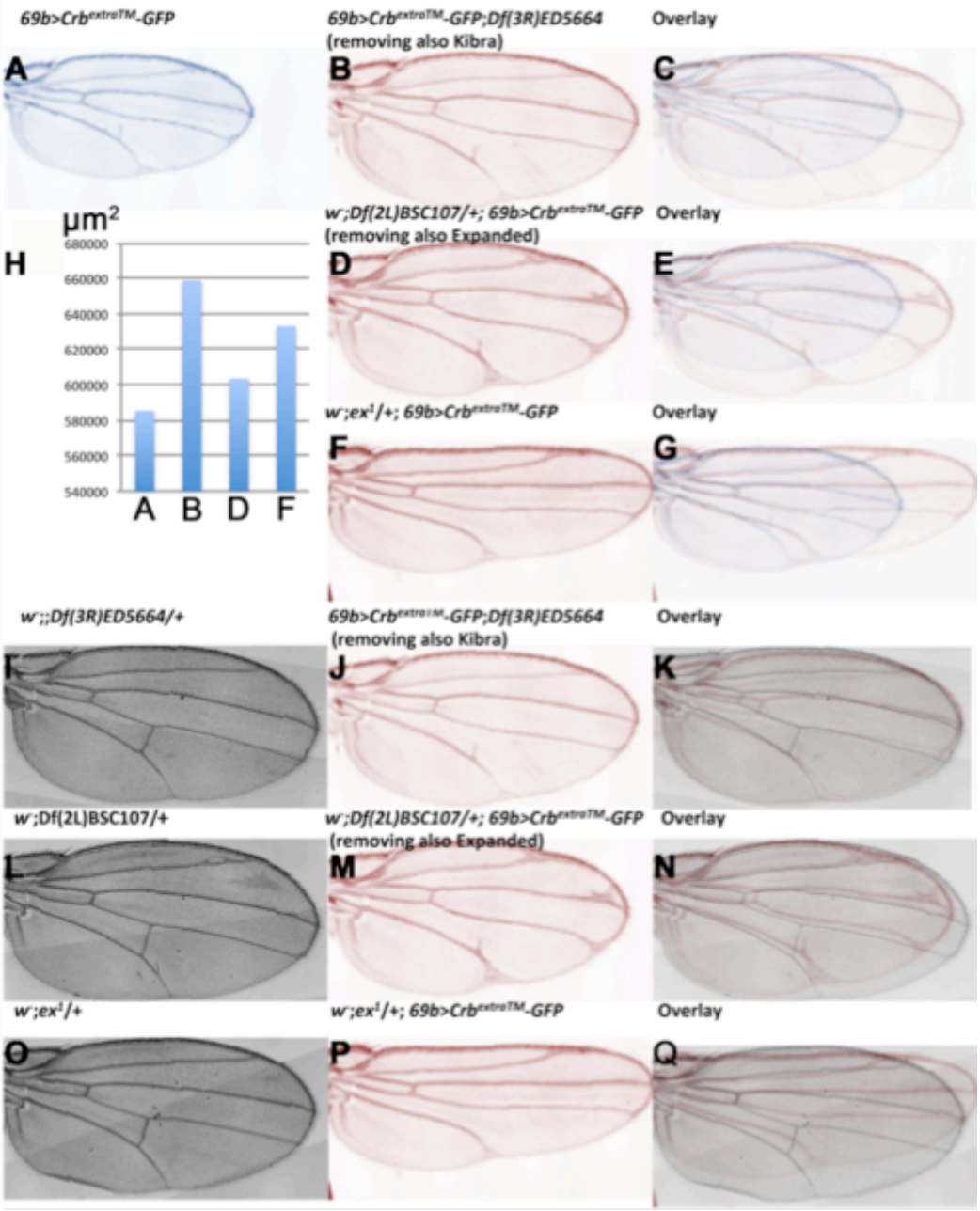

Figure 8: Hippo components suppress the wing phenotype upon overexpression of *Crb^{extraTM}-GFP*. (A-G) Genetic interactions between overexpression of *Crb^{extraTM}-GFP* with *expanded* and *kibra*. **(H)** Statistical analysis of measuring the surface area of 15 adult wings per genotype (A,B,D and F). **(I-Q)** Control wing measurements from (A-G).

Overexpression of *Crb^{extraTM}-GFP* in wing discs does not affect the levels of the Hippo downstream transcription factor Yorkie

Given that Crb interacts with Expanded [Robinson et al., 2010, Ling et al., 2010, Chen et al., 2010] and Yorkie regulates *expanded* transcriptionally, the relationship between the overexpression of *Crb^{extraTM}-GFP* and the localization of the downstream component of the Hippo pathway, Yorkie, was analyzed in wing discs (Fig. 9). *Crb^{extraTM}-GFP* was overexpressed specifically in the posterior compartment, using the Engrailed-Gal4 driver and stained with Rabbit-anti-Yorkie (Fig. 9 C-D'). Comparing the posterior compartment where *Crb^{extraTM}-GFP* is overexpressed with the anterior one, where the overexpression is not induced, the localization of Yorkie remained unaltered (Fig. 9 D'). As control, *GFP* alone was overexpressed in the posterior compartment of the wing disc (Fig. 9 A-B'). The localization of Yorkie in the posterior compartment remained unaffected, too (Fig. 9 B'). However, the quality of the antibody is not good enough to distinguish if Yorkie is nuclear or cytoplasmic, even at higher magnification.

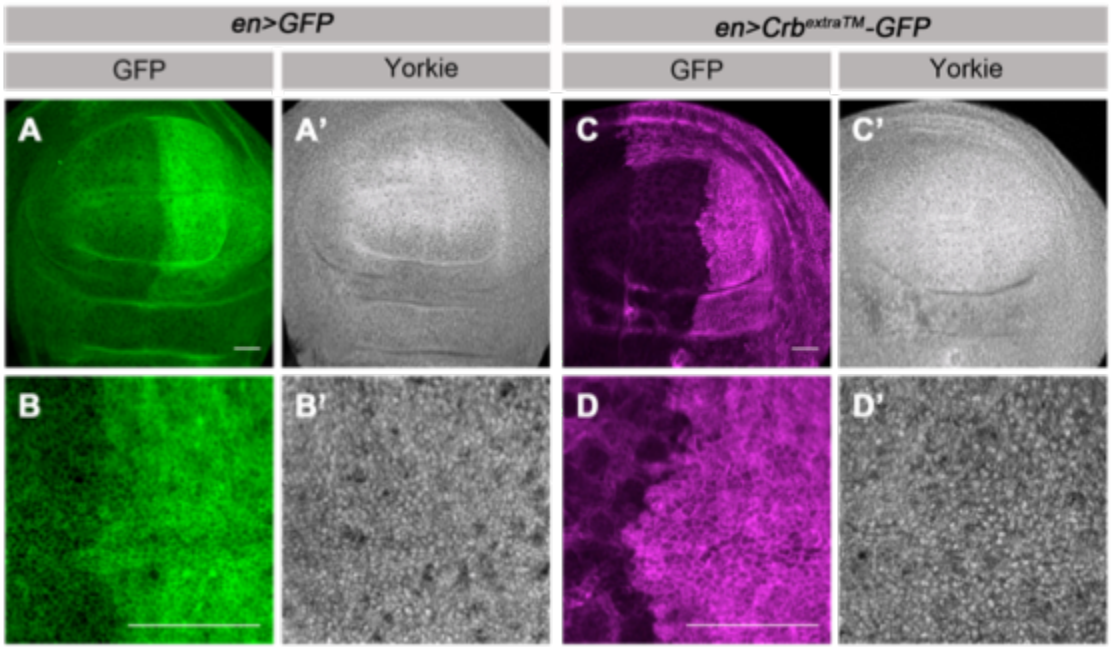

Figure 9: Overexpression of *Crb^{extraTM}-GFP* in wing discs does not affect the levels of the Hippo downstream transcription factor Yorkie. (A-D') Overexpression of *GFP* or *Crb^{extraTM}-GFP* in the posterior compartment of the wing disc and immunostaining with Yorkie (GFP is endogenous). Scale bars, 25 µm.

RabX6 genetically interacts with *crb*

After the characterization of the overexpression of *Crb*^{extraTM}*-GFP* phenotype, the genetic relationship between the overexpression of *Crb*^{extraTM}*-GFP* and the candidate genes *RabX6* and *bbg* was analyzed. The knock down of *RabX6* simultaneously with the overexpression of *Crb*^{extraTM}*-GFP* enhanced the small wing phenotype obtained upon overexpression of *Crb*^{extraTM}*-GFP* alone (Fig. 10 D-F). However knocking down RabX6 alone showed a smaller wing phenotype (Fig. 10 G and A). Knock down of RabX6 either in wild-type background or upon overexpression of *Crb*^{extraTM}*-GFP*, gave a blistering phenotype in wings (Fig. 10 G and H). Blistering phenotypes are caused by defects in the attachment of the two epithelia of the wings. This defect is translated into defects in integrins in the basal membrane of the cells. In mammalian cells, Rab4 regulates integrin recycling from early endosomes and is required for cell adhesion and spreading [Chen et al., 2012].

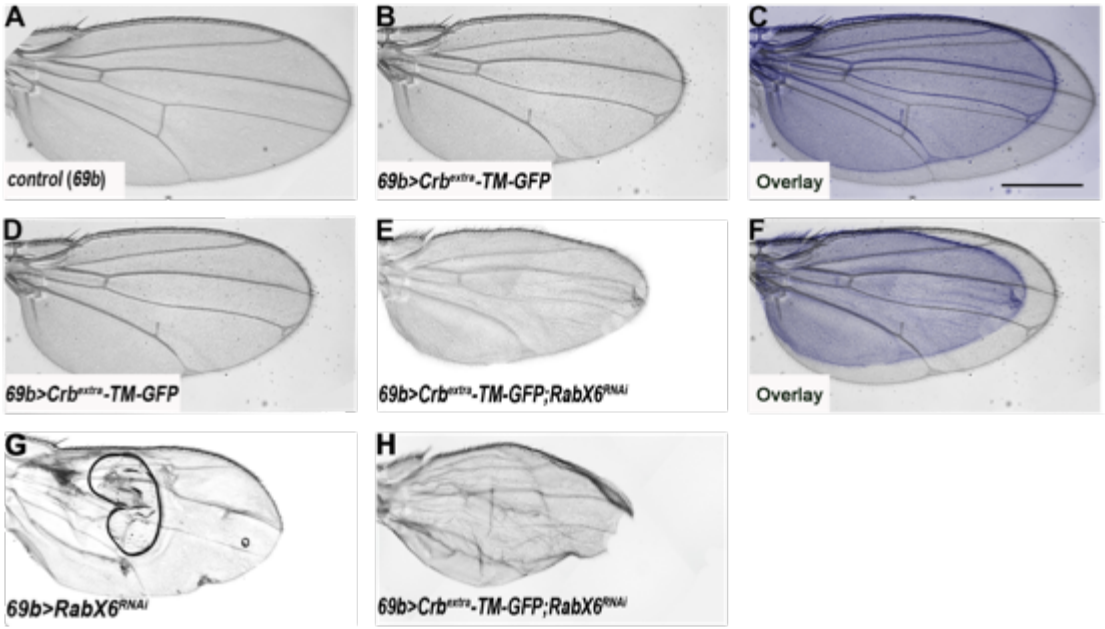

Figure 10: *RabX6* genetically interacts with *crb*. (A) Control (*69b-Gal4*) wing, **(B)** Expression of UAS-*Crb*^{extraTM}*-GFP* with *69b-Gal4* wing and **(C)** overlay, respectively. **(D)** Expression of UAS-*Crb*^{extraTM}*-GFP* with *69b-Gal4* wing, **(E)** Expression of UAS-*Crb*^{extraTM}*-GFP* & *UAS-RabX6*^{RNAi} with *69b-Gal4* wing and **(F)** overlay, respectively. **(G)** Expression of *UAS-RabX6*^{RNAi} with *69b-Gal4* wing and **(H)** Expression of UAS-*Crb*^{extraTM}*-GFP* & *UAS-RabX6*^{RNAi} with *69b-Gal4* wing, respectively. 15 independent wings per condition. B and D are identical. Data information: Scale bars, 500 µm (A-H).

RabX6 is highly expressed in L3 wing and eye discs

In order to understand further the role of RabX6, the RabX6:YFP transgenic line was used, as there was no antibody available for this protein. RabX6:YFP is a transgenic line that is produced from homologous recombination of the YFP-tagged *RabX6* allele [Dunst et al., 2015]. The L3 wing discs were used as a model. The wing disc contains about 30 cells at the beginning of the first instar larva and reaches to a number of about 50,000 cells at metamorphosis around four days later [Milan et al., 1996]. The adult wing is produced by the eversion of the wing disc. The *Drosophila* wing discs have become a very convenient model to study tissue growth, as it is composed from a monolayer epithelium tissue with apicobasal polarity and a high capacity of proliferation. RabX6:YFP was found to be highly expressed in the monolayer epithelium of the disc (Fig. 11 B' and C'). The expression was from the apical side of the cell (Fig. 11 B') to the lateral side (Fig. 11 C'). RabX6:YFP showed a cytoplasmic staining and maybe linked to the plasma membrane

RabX6:YFP was found to be expressed in the epithelium of the eye discs as well (Fig. 11 C' and D'). The eye is derived from the eye-antennal disc. The area anterior to the morphogenetic furrow is rich in synchronously dividing cells. The area posterior to the furrow shows preclusters of cells, each with a recognizable core of five cells, corresponding to cells 2, 3, 4, 5 and 8 of the photoreceptor. The small GTP-ase was also highly expressed both in the posterior and the anterior compartment of the eye discs (Fig 11 C' and D'). In both tissues the expression of Crb is shown in the apical membrane of the cells.

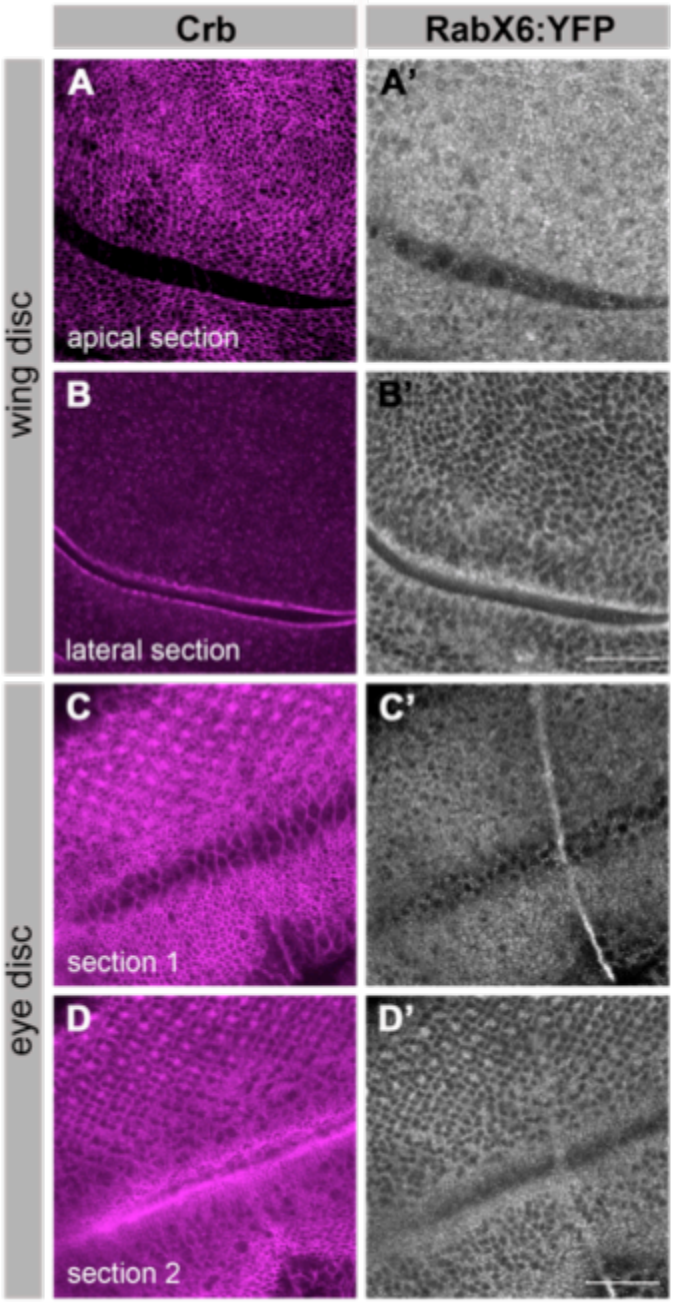

Figure 11: RabX6 is highly expressed in L3 wing and eye discs. (A, A') Apical section of a third-instar *RabX6:YFP* wing disc pouch stained with Crb and GFP, respectively. **(B, B')** Lateral section of the same third-instar *RabX6:YFP* wing disc pouch stained with Crb, GFP and Dlg, respectively. **(C, C')** Section 1 of a third-instar *RabX6:YFP* eye disc stained with Crb and GFP, respectively. **(D, D')** Section 2 of the same third-instar *RabX6:YFP* eye disc stained with Crb and GFP, respectively. Data information: Scale bars, 25 µm (A-D').

The reduction of Crb and RabX6:YFP does not affect the localization of RabX:YFP and Crb, respectively

In order to understand further the relationship between Crb and RabX6, Crb was knocked down and the localization of RabX6 in wing discs was

analyzed in this background. The localization of RabX6 does not seem to be affected in the wing disc epithelium (Fig. 12 C').

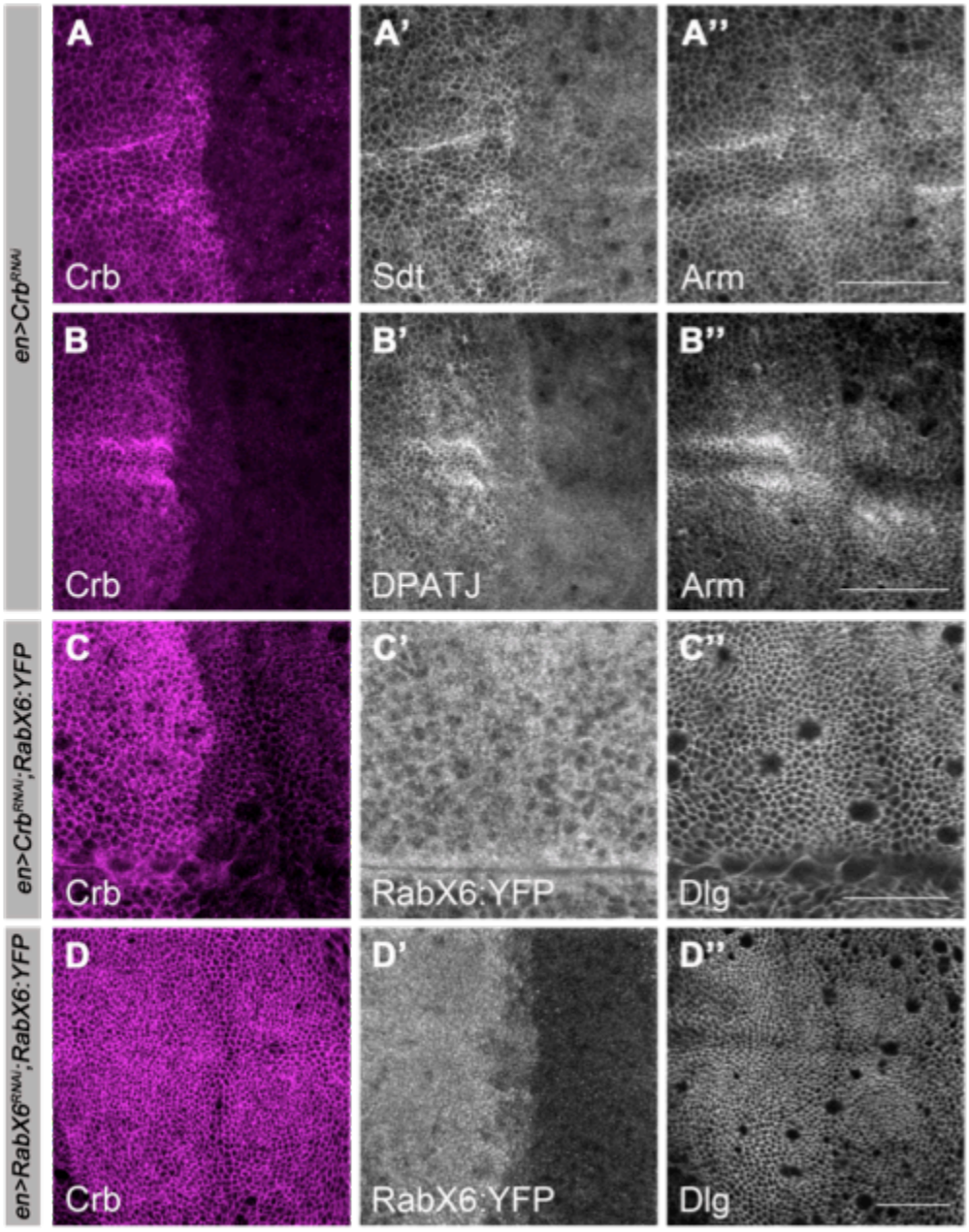

Figure 12: Knocking down RabX6 in wing discs does not affect the localization of Crb and *vice versa*. (A-A'') Third-instar *en>crb*^{RNAi} wing disc pouch stained for Crb, Sdt and Arm, respectively. **(B-B'')** Third-instar *en>crb*^{RNAi} wing disc pouch stained for Crb, DPATJ and Arm, respectively. **(C-C'')** Third-instar *en>crb*^{RNAi}*,RabX6:YFP* wing disc pouch stained for Crb, GFP and Dlg, respectively. **(D-D'')** Third-instar *en>RabX6*^{RNAi}*,RabX6:YFP* wing disc pouch stained for Crb, GFP and Dlg, respectively. Data information: Scale bars, 25 µm (A-D'').

In order to verify these results, the localization of the well-known partners of Crb, Sdt and DPATJ, were analyzed in these wing discs. Knocking down Crb, leads to reduction of Sdt and DPATJ in the wing disc epithelium (Fig. 12 A' and B'). This experiment showed that the reduction of Crb is effective, based

on the effect on its partners. The reverse experiment was also conducted. The localization of the different polarity markers was checked, upon the knockdown of RabX6. Knocking down RabX6:YFP does not affect the polarity of the tissue in the wing discs (Fig. 12 D). It does not affect the localization of the apical marker Crb, and the lateral protein Dlg, respectively (Fig. 6 D and D''). In conclusion, the reduction of Crb and RabX6:YFP does not affect the localization of RabX:YFP and Crb, respectively.

bbg **genetically interacts with** ***crb***

The second gene that was analyzed in the enhancer/suppressor genetic screen was *bbg*. Overexpression of $Crb^{extraTM}$*-GFP* gave a smaller wing phenotype as compared to the control wings (Fig. 13 A-C). The overexpression of $Crb^{extraTM}$*-GFP* in the background of a copy of the deficiency *Df(3L)4543* on the 3rd chromosome, showed enhancement of the smaller wing phenotype that is observed upon the overexpression of $Crb^{extraTM}$*-GFP alone* (Fig. 14 D-F). The deficiency line *Df(3L)4543* includes the genomic region of the gene *bbg*. Knocking down *bbg* simultaneously with the overexpression of $Crb^{extraTM}$*-GFP* remarkably enhanced the smaller wing phenotype obtained upon overexpression of $Crb^{extraTM}$*-GFP* (Fig. 13 D-F). Analysis of the wings of lines heterozygous for bbg^{B211}, a null mutation for *bbg*, in the background of overexpression of $Crb^{extraTM}$*-GFP*, revealed a similar enhancement of the phenotype that was obtained in the experimental analysis of the interaction of $Crb^{extraTM}$*-GFP* overexpression and the *Df(3L)4543* deficiency (Fig. 14 A-C). The enhancement of the overexpression of $Crb^{extraTM}$*-GFP* phenotype that is shown with the *Df(3L)4543* line (Fig. 14 D-F) and the bbg^{B211} heterozygotes (Fig. 14 A-C) is weaker than the one obtained with the *RNAi* knockdown of *bbg* (Fig. 13 D-F). This result is not unexpected as in the Fig. 14 A-F only one copy of *bbg* is missing. Reduction of *bbg* alone showed a smaller wing phenotype compared to the control wings (Fig. 13 G-I). However, flies homozygous for bbg^{B211} showed even smaller wings compared to control (Fig. 13 J-L). Quantification assays were in agreement with the previous observations (Fig. 13 M).

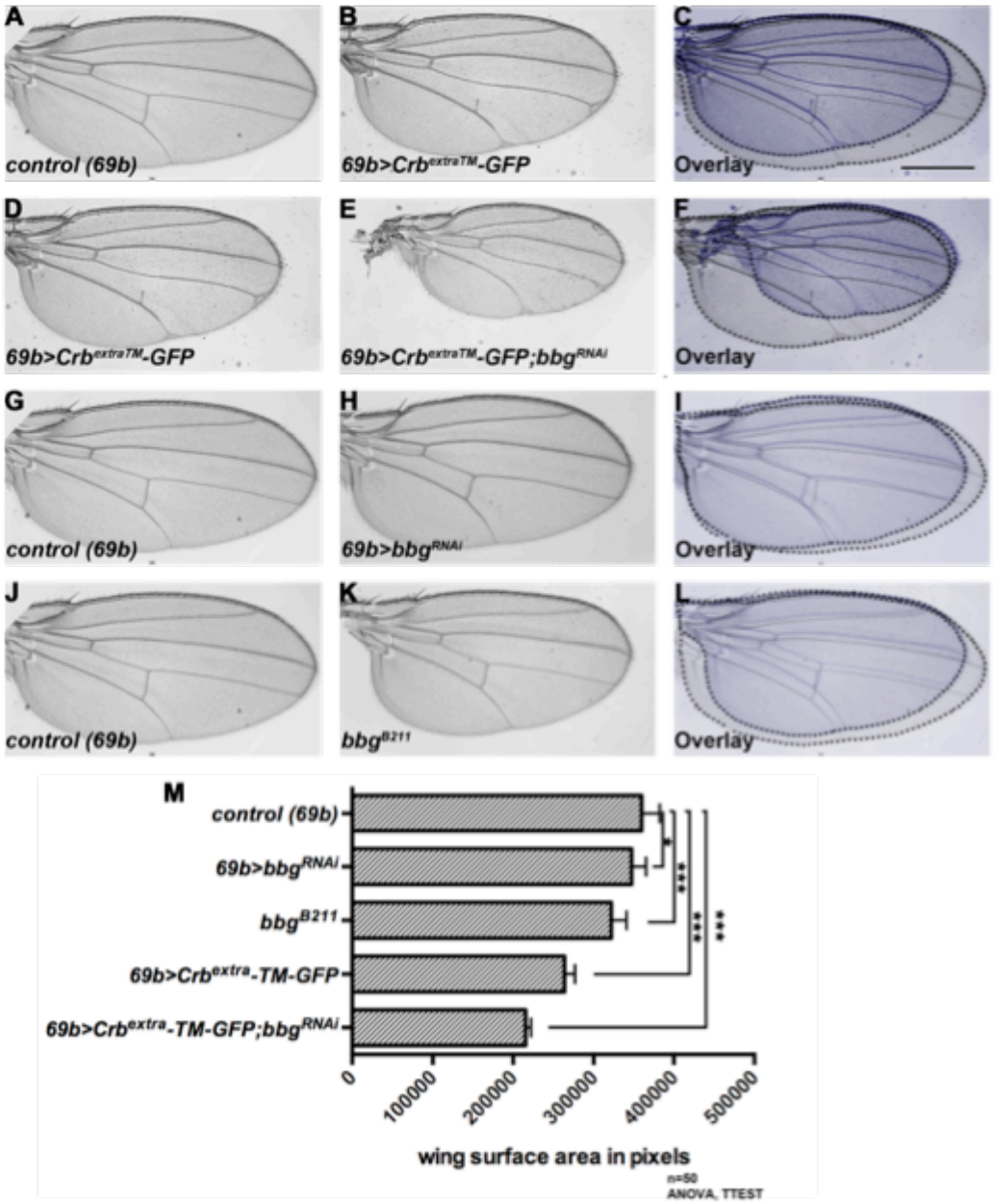

Figure 13: *bbg* genetically interacts with *crb*. (A-C) Control (*69b-Gal4*) wing, Expression of UAS-*Crb^{extra}-TM-GFP* with *69b-Gal4* wing and overlay, respectively. **(D-F)** Expression of UAS-*Crb^{extra}-TM-GFP* with *69b-Gal4* wing, Expression of UAS-*Crb^{extra}-TM-GFP* & *UAS-bbg^{RNAi}* with *69b-Gal4* wing and overlay, respectively. **(G-I)** Control (*69b-Gal4*) wing, Expression of *UAS-bbg^{RNAi}* with *69b-Gal4* wing and overlay, respectively. **(J-L)** Control (*69b-Gal4*) wing, *bbg^{B211}* wing and overlay, respectively. **(M)** Statistical analysis of the size of the wings, measuring the surface area of 50 independent female wings per condition. For the analysis it was used TTEST and ANOVA test. One asterisk indicate $p \leq 0.1$. Three asterisks indicate $p \leq 0.001$. Error bars show standard deviation. Data information: Scale bars, 500 μm (A-L).

Similar to the smaller wing phenotype obtained in the absence of *bbg* (Fig. 13 J-L), the genotype *bbg^{B211}/Df(3L)4543* showed a smaller wing phenotype compared to control wings (Fig. 14 G-I). The reduction in size was

comparable in both cases. Using an alternative driver, the *C765-Gal4*, which is expressed in the wing disc, the smaller wing phenotype obtained by the knockdown of *bbg* was confirmed (Fig. 14 J-L). The above results demonstrate that *bbg* is required for the development on normal sized wings in *Drosophila*.

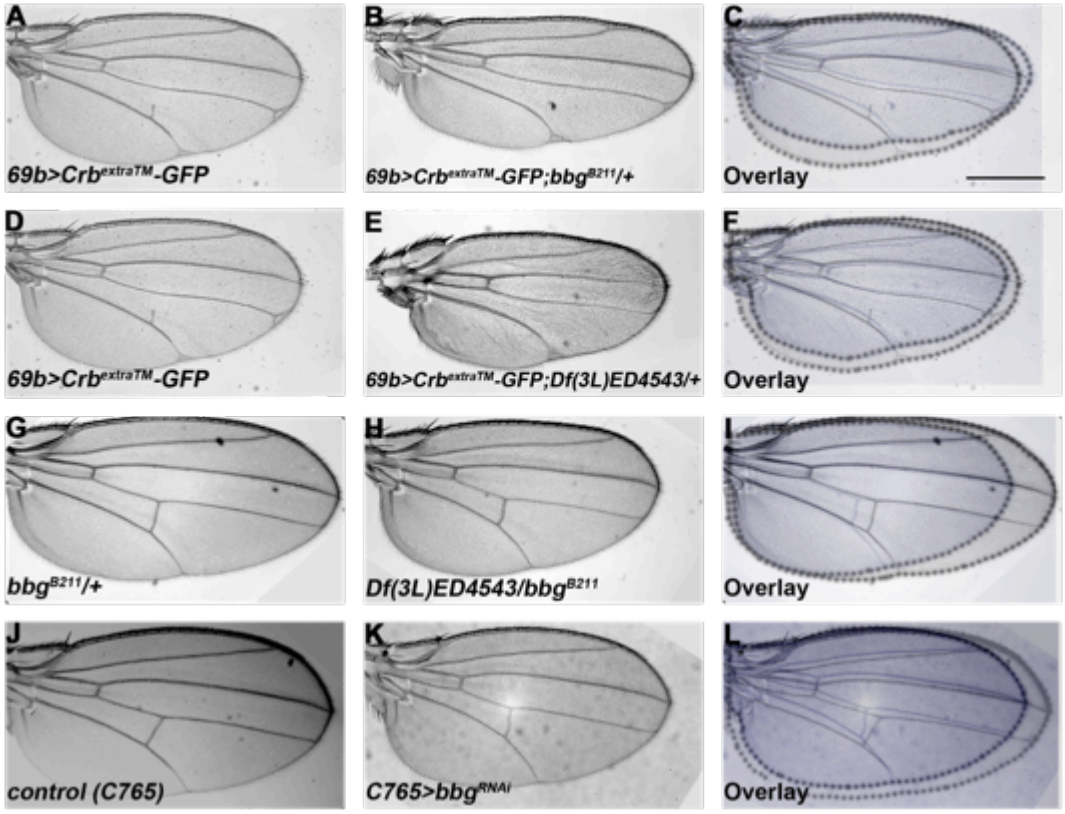

Figure 14: *bbg* genetically interacts with *crb*. (A-C) Expression of UAS-*Crb^{extra}-TM-GFP* with *69b-Gal4* wing, Expression of UAS-*Crb^{extra}-TM-GFP* with *69b-Gal4* in heterozygous *bbg^{B211}*/+ wing and overlay, respectively. **(D-F)** Expression of UAS-*Crb^{extra}-TM-GFP* with *69b-Gal4* wing, Expression of UAS-*Crb^{extra}-TM-GFP* with *69b-Gal4* in heterozygous for the deficiency line *Df(3L)ED4543/+* wing and overlay, respectively. **(G-I)** Heterozygous *bbg^{B211}*/+ wing, *bbg^{B211}/Df(3L)ED4543/+* wing and overlay, respectively. **(J-L)** Control (*C765-Gal4*) wing, *C765>bbg^{RNAi}* wing and overlay, respectively. Data information: Scale bars, 500 µm (A-L).

The *bbg*^{B211} mutation leads to a frame shift mutation and a generation of a premature stop codon

As mentioned above, the *bbg*^{B211} mutant line was published [Kim et al., 2006] and the molecular characterization of the mutation followed. Bbg is a protein with multiple isoforms as most PDZ domain proteins, and the gene encodes several alternative splice variants (Fig. 15 A-B).

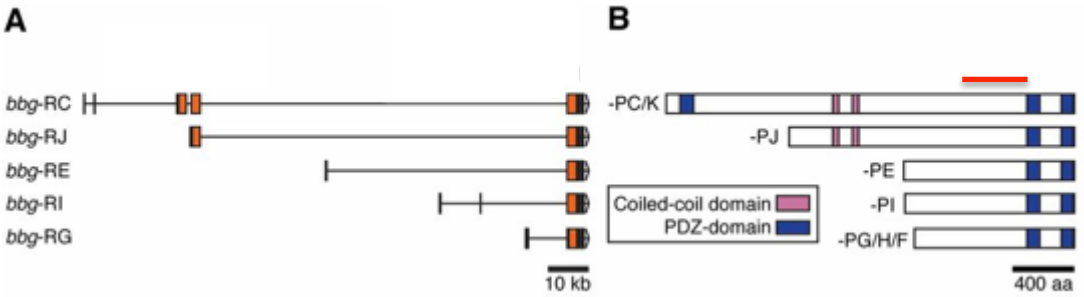

Figure 15: *bbg* alternative transcripts and Bbg isoforms. (A) Diagram of five *bbg* predicted transcripts (adapted from FlyBase); coding exons are in orange. **(B)** Schematic diagram of the eight Bbg protein isoforms, which have either two or three PDZ domains. The red line corresponds to the sequence of the phusion protein for the generation of the antibody. The antigenic region is found within all the predicted protein isoforms of Bbg. (Aranjuez et al., 2012).

In Fig. 16, the protein sequence of the Bbg-PC isoform is shown. The *bbg*^{B211} allele was generated by imprecise excision of *P{GawB}bbg*^{C96}, however the location of the genetic excision was not included in the publication [Kim et al., 2006]. Sequencing with specific primers enabled to conclude that this excision leads to a frame shift mutation leading to a premature stop codon (the excision of the 1191 bases/397 amino acids is marked in red in Fig. 16). The lower given sequence, consisting of 12 amino acids is the one that replaces the red coloured sequence in the *bbg*^{B211} encoded protein. Worthy of mention is that the two of the three PDZ domains (shown in green boxes in Fig. 16) of the protein are encoded by this red sequence that is missing in the mutant protein. The *bbg*^{B211} mutant is antibody-null as predicted, based on the experiments done with the antibody generated in our lab and also confirms that the antibody is specific to Bbg (Fig. 17). The experiments are as described below.

Bbg-PC isoform 5'3':

MASTPKANGTTAKTATINDDYITVVEVDDPTSNPKDRLKKLVKRQSSVAE
DSSFITVLTINEMELLQQRKKEEDVGSGSSPTMEEQIENVTVFRLPGERL
GFGLKFQGGTRSTELVQKLYIQSCAADSPASKVSTSWGNLREGDEIVSID
GRDVRELTRIDCVRGLKDNVAIKLVVRNGHGQKPPSEEDPQQQEHLSITL
NAQPPPPPPVPPRKLVRRQNSKENQAQLLIEKPLTPPPDAEYYLNLLTES
IKAGSESDDTASTISTVIDKFSVGSNYSSDSSLNGHELAKVLQPFTLLEQ
EFLPLEQPLGHPKLLIPGNNYENVEFKTEKVNVYENVELRSPETTPTPKP
RVQLATVEPKKRSIIPMPRKIPTPTKLPIEVTPPRVPILEEPKTPTNNKV
DSPKTPTNELKESPISATKIPKAKFSRAKTEGEIKLHLPAPKQQSPQSKS
RIPIVSTPTAQKTVPKPVSPTMNGTPLSSNIPRLLQKQKSETDLKLNLYR
SKSKESSPRPPLQRANSAEAPERTFIPVLLNGNSKSSNSLESVSSIGSSS
SGNSVRSPKGPKPKPPERVQSLQKTQIPKLQALPTTPPQQIPKLSMQTFK
QSPPTPRSTPVGTPSPTSNREIRFKIQTYESKTQDEDKLPSLFDLVHSQE
NDKDKDRDSDSLKTHNSITALLAAAAAEAADLSRESPPPLVVGKCMKIVD
DTNTTTCYTSSSSGEEDEDDLDASNREYICEDGEKLGPPELINGPGPSEA
YFNMFWHSNMLPTIGEVEEEFSSLEPQSLTNGNLVKSEESKKLPKMEVNA
GGLAQLTDDKIADHDASATRADTRDEVTTNQTQEISSSSSSSVKSQKTTT
TTRVTTTKTSSSSSSSSCSSTVIPDVAFKLQPYEERDDILSEPITTIHEE
RRVLSEQKTLSESRTRDALTGEEQLVTSANSKSSSARFKKISSNDNLLDL
GDEQDMQEQPLTATITQESSLRERLECPQDNQSIDRGTLTLSERGKQLSE
KEGLTTYTECETSEKESYLEGQQVLNGKGGFVSQDENSDQPTYEREVSET
LTIVNDGEKQVTKKLEQNKEIAGKKGAKLLKKTDEERRLEQEAQKLIESY
QKVKKEAEKLYKLELADDDQGFDLSAFEQAEEEDKPEVSEEIKEVKDSQP
VKVDIQIEEEVKTPNQVIGEVKVEDVNKEIKETVQVSQQEIKKEVKVSHQ
ETKETFKSEEKDESNELKIVKEEVKVTHQDLREQIQEIEAVKVVHKEVKV
IKESAKVTTTTSHKQATKEVIISKEDHKNDSALPAVSTTKVEIISPPLED
DLGYVLHKHIIFPQEKVKTAPTPLPKPKPKPPVPTNKPKMPVNLTKPKSA
PPPVPSKRSELSGSGGKPTPTQRRGSLETAQPPKPLERIIVGVEQRDEPE
KPQPIINLASVDLPNVAPNSKQATVETTPVVEMPPDELQFESHQLPDDGE
KEKDLHQESNDLLSGSSSSSVTTPITTPILVSATSSMDSVQSVIEVVNGM
PIISNQQTDDDDIDEVAAYDDGMHLEAEGTKDVRPVQEVTTLTLDREHES
DLGTLSNHHSNISSISGINASSNIPAATLISSSIKKTSTEAATTKPAAPQ
IPGKMELLSSNTGTTTTTTTATHHLHQATTTKQLLVQDYLSYASPPTYSR
LPPDGHEFPPNFSEPLIMHSHPLKVTTELSYEIQKGGKDESSAPPLPKTG
PPATVPRKVYRQDLVINVEPAPSLTRDYQRSLSGGTPRKPSDWRKDEKSE
KSVRDKIAMFSSNNELDAIPPAPATAPISSSFTRKPLNRSSENLLDSCSS
SSAPSLKTRAMSVENLNDVQRQYQLAKQLPQLHVADSMYSLNTATPTPSY
ASLPRRSHGGSYSSGVERRISFSGEGGDAANRKAAITNILEQRRRSLSKL
RGLVIPERPQLLEPILDLPEIKSQVKAASGEDSTDSGLGESHRSTVNRNC
QLGAGGAANNYRSILNTNQRRPLEQQLSQPPAKPPRTSLTPLQPRSMMIP
PPPPPLDQESDTDSVFSHTARVATPPEKFALTRTLSSETNTSIASSNTST
LTSGSSAGSQASCSSLGSTPAVDLTRRVLKSQVINGEAVALSSRKSILAS
AKCR**SAKSRGQEEDNDSTDGEACSLANRRMKPISSYKLQQQQIQLGKQLV**
VDKLINVAAYVELTSDTDDSSRRSDTPAKISAMFIDEERKASFKGDPNQQ
AKVKVEQVKPMVLPMLLPSAKREPLKQQTTAELREKFERSAAAQAQTQNH
SPVIHKVTQKPHHERFSSLDSLASSSSGVSSTTQNVSTTQETATEFGSFS
SLGSNQSLITAQDVQQIVEEADPPLKTPEAFIIVLQRENPESSIGITLAG
GSDYEAKETTIHKILSNTPAAKDGRLKKGDRILAVNGMSMRGLTHRESIS
VLKTPRPEVVLVVTRSESLVVKALTKKRSSLGSLSSLNEKPTELDYERKR
NYHKASRSLDLDLDLVSNEAGESPVATTPSTGSVSPPQPASLHDEDAEAT
IAGIRARRQLSRGDAAKLSTSELLERAAEARNAIAAEIRAQAEDAAASGG
GARCVEIVKDSCGLGFSIEGGFDSPLGNRPLIVKKVFMGGAAQKTNQVRN
CGDEILSINGASTSRMTRVDAWNYMKQLPLGPVKICFA

In the *bbg*^{B211}, replacement of the red sequence with:

5'3': QPKLKPKTTRPStop

Figure 16: The *bbg*^{B211} mutation leads to a frame shift mutation. The upper sequence highlights the protein sequence of the Bbg-PC isoform. *bbg*^{B211} contains a deletion shown in red letters. The underlined-bold sequence corresponds to the sequence that was used for the antibody raising. The green boxes correspond to the three PDZ domains of Bbg-PC. This excision leads to a frame shift mutation and a generation of a premature stop codon. The bottom sequence, consisting of 12 amino acids is the one that replaces the red letter sequence in the *bbg*^{B211} line.

The antibody that was raised against Bbg is specific in western blot and immunostaining

A polyclonal rabbit antibody serum against Bbg was raised in collaboration with the in-house facilities (David Drechsel and Patrick Keller). In Fig. 16 B all the protein isoform for Bbg are shown. The longer isoform consists of three PDZ domains (blue) and two coiled-coil domains (orange). The size of the longer isoform is approximately 288 kDa. The polyclonal antibody was raised against the sequence that is underlined with red (Fig. 16 B). This sequence can be found within all the predicted isoforms of Bbg.

The specificity of the Bbg antibody was analyzed using western blot experiments. As shown in Fig. 17 A, wt (wild-type) and bbg^{B211} samples from adult abdominal tissue were used. The abdominal tissue, which contains the gut, showed high expression of Bbg and was an easy tissue for isolation. In the wt sample, the bands that are marked with an asterisk correspond to the sizes of the predicted isoforms (Fig. 17 A). The bands with smaller size could be the smaller isoforms of the protein that are not yet predicted or the degraded products of the already existing bigger isoforms (Fig. 17 A). In the bbg^{B211} it is evident that all the expected bands are missing. The two bands present could correspond to unspecific products (Fig. 17 A). The tubulin used as a loading control, indicated that there were similar amounts of protein in the *wt* and bbg^{B211} samples.

The antibody is specific as seen in immunostaining, as well (Fig. 17 B). Mutant bbg^{B211} clones were generated in imaginal wing disc tissue. The mutant clones were distinguished as they were demarcated by RFP expression. The advantage of the generation of mosaic clones is that one can analyze the mutant tissue adjacent to the wt tissue. It is evident that the clone area is not stained with the Bbg antibody in contrast to the surrounding wt area, which is specifically stained with the Bbg antibody (Fig. 17 B).

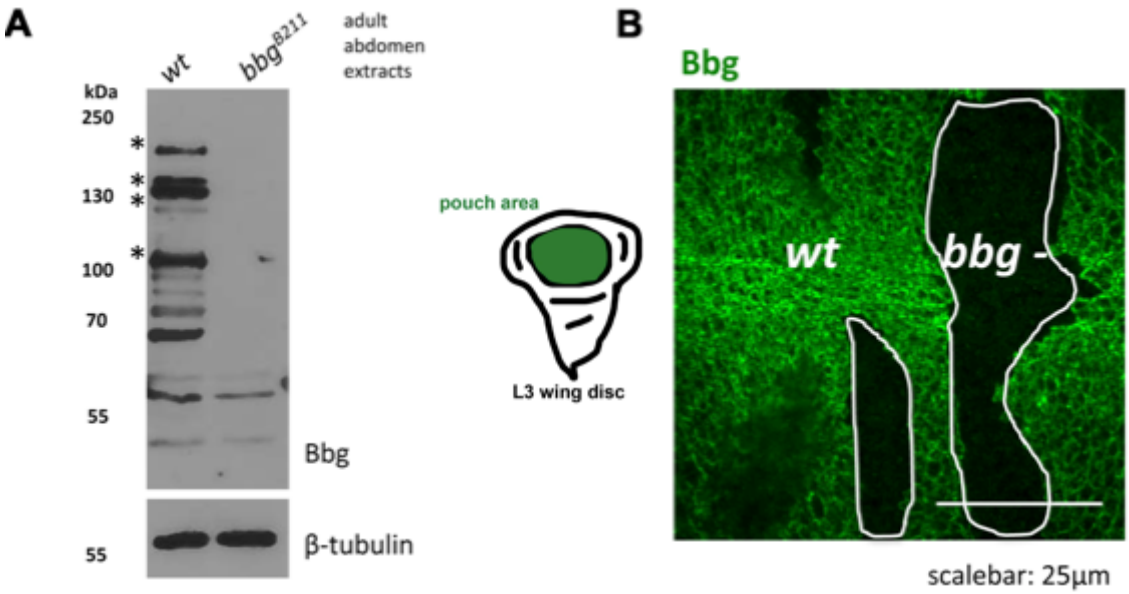

Figure 17: Generation of a polyclonal antibody against Bbg. (A) Representative of the longer protein isoform of Bbg. The red line corresponds to the sequence of the phusion protein for the generation of the antibody. The antigenic region is found within all the predicted protein isoforms of Bbg. **(B)** Western blot of adult abdomen lysates of wt and bbg^{B211} tissues. The asterisks represent the predicted isoforms of Bbg. **(C)** Third-instar bbg^{B211} clones, highlighted in white schemes, *of* wing disc pouch stained for Bbg. In the cartoon is marked with green color the pouch of an imaginal wing disc. The mutant clones are marked with RFP. Scalebar is 25µm (C).

The mRNA of *bbg* is expressed in L3 wing discs, L3 larvae and adult flies

In the study that characterized the *bbg* gene [Kim et al. 2006], it was shown that the *bbg* gene and protein are expressed dynamically throughout development. Bbg encodes multiple isoforms as most PDZ domain proteins, and the gene encodes several alternative splice variants, as it is already mentioned (Fig. 15 A-B). In order to elucidate the expression of the alternative splice variants during *Drosophila* development, primers were used for all the predicted alternative transcripts of *bbg* [Kim et al., 2006]. RNA was isolated from different genotypes as shown in Fig. 18 and cDNA was generated for the analysis of the different alternative transcripts expressed in these various tissue extracts. As shown in Fig. 18, *bbg* mRNA of almost all the predicted alternative transcripts, found to be expressed in L3 wing discs, L3 larvae and adult flies. Differences between samples 1 and 2 are probably due to technical reasons.

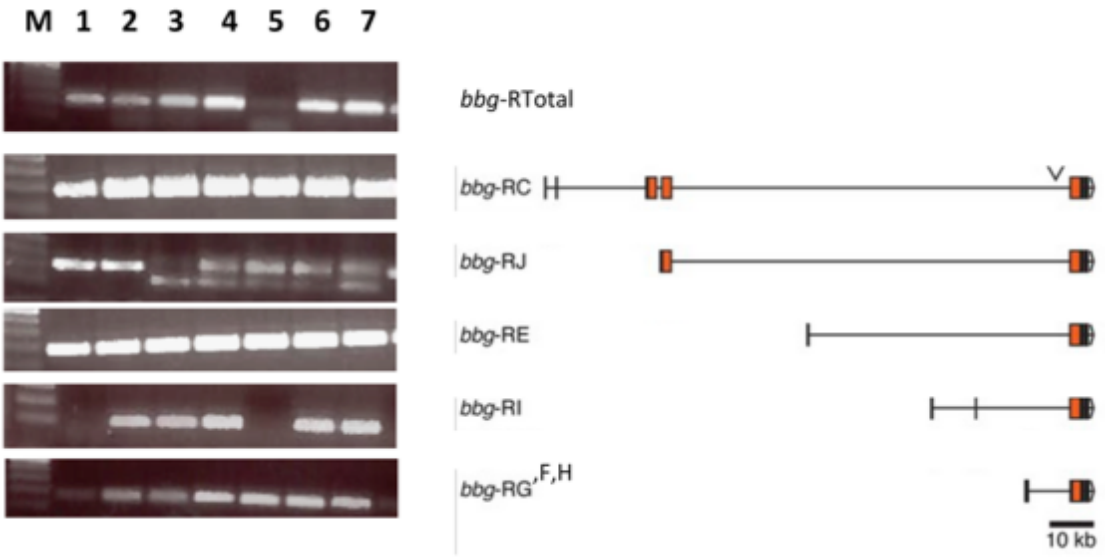

Figure 18: The mRNA of *bbg* is expressed in L3 wing discs, L3 larvae and adult flies. RT-PCR for the alternative mRNA transcripts represented in the right panels. The genotype and the tissue extracts are: (M) Marker, (1) *wt* L3 wing discs, (2) bbg^{B211}/TM3 L3 wing discs, (3) *wt* L3 larvae, (4) bbg^{B211}/TM3 L3 larvae, (5) bbg^{B211} L3 larvae, (6) *wt* adult flies, (7) bbg^{B211}/TM3 adult flies. The Marker is the 100bp from Thermo (SN:1143). RT-PCR, 45 cycles.

Bbg is expressed dynamically throughout embryogenesis in *Drosophila*

As mentioned Bbg is expressed dynamically during embryogenesis [Kim et al., 2006]. Immunofluorescence using the Bbg antibody in embryos, showed where Bbg is localized during embryogenesis (Fig. 19). It found to be expressed ubiquitously at stage 5 and stage 6, with a posterior accumulation in stage 5. It showed a localized expression in the epidermis at stage 12, highlighted the pharynx at stage 12 and the hindgut at stage 15. Finally, Bbg found to be highly enriched in tracheal pits and epidermis at stage 14. In conclusion, the localization of Bbg is dynamic and specific to some organs through embryogenesis.

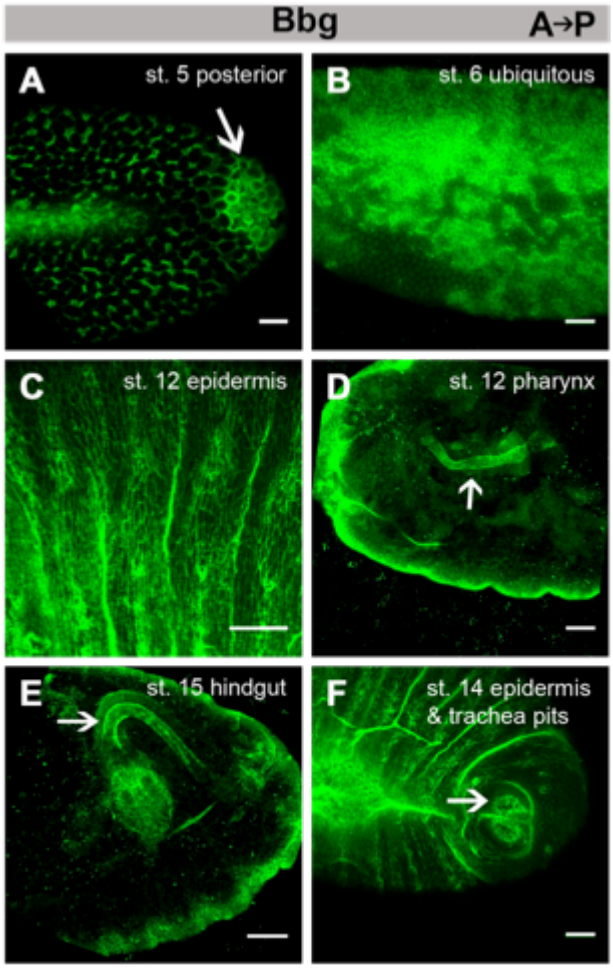

Figure 19: Bbg is expressed dynamically throughout embryogenesis in *Drosophila*. Staining of wt embryos with Bbg. The stages and the tissues are written in the different panels. Anterior is always left. Scale bars, 25 µm.

Checking if Crb colocalizes with Bbg in the epidermis during embryogenesis followed. As shown in Fig. 20 A-A'', Bbg colocalizes with Crb at stage 8. Bbg, which showed a localized expression in epidermis at stage 11 partially colocalizes with Crb, as well (Fig. 20 B-B'').

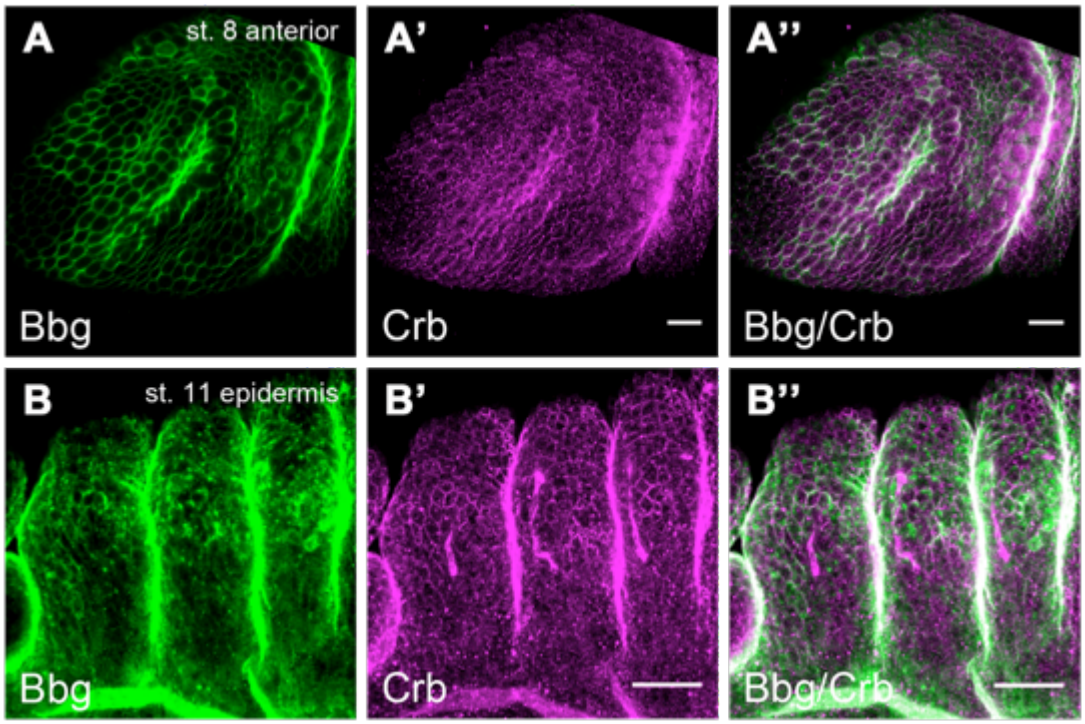

Figure 20: Crb colocalizes with Bbg in epidermis during embryogenesis. (A and B) Staining of wt embryos with Bbg and Crb and overaly, respectively. The stages and the tissues are written in the different panels. Anterior is always left. Scale bars, 25 µm.

The embryogenesis proceeds normally in *bbg*^{B211} mutant embryos

As the *bbg*^{B211} mutation was found to be homozygous viable and fertile embryogenesis was analyzed through all the stages and the localization of Crb was taken as readout of the polarity and integrity of the epithelial tissues. Embryogenesis proceeds normally in the *bbg*^{B211} homozygous flies (Fig. 21). Comparing wt and *bbg*^{B211} embryos at stage 13 no differences were observed in the epidermis and the whole integrity of the tissue (Fig. 21 A and B). Analysis of specific organs showed that the integrity of salivary glands, trachea, hindgut and Malpighian tubules remains unaltered in *bbg*^{B211} mutant embryos (Fig. 21 C-H). Finally the localization of Crb in all the previously mentioned conditions remains unaltered (Fig. 21).

The viability of *bbg*^{B211} was also analyzed carefully. After counting the larvae that hatch in three independent experiments, it was concluded that embryogenesis proceeds normally (~138 *bbg*^{B211} embryos hatch of 150, after three experimental repeats).

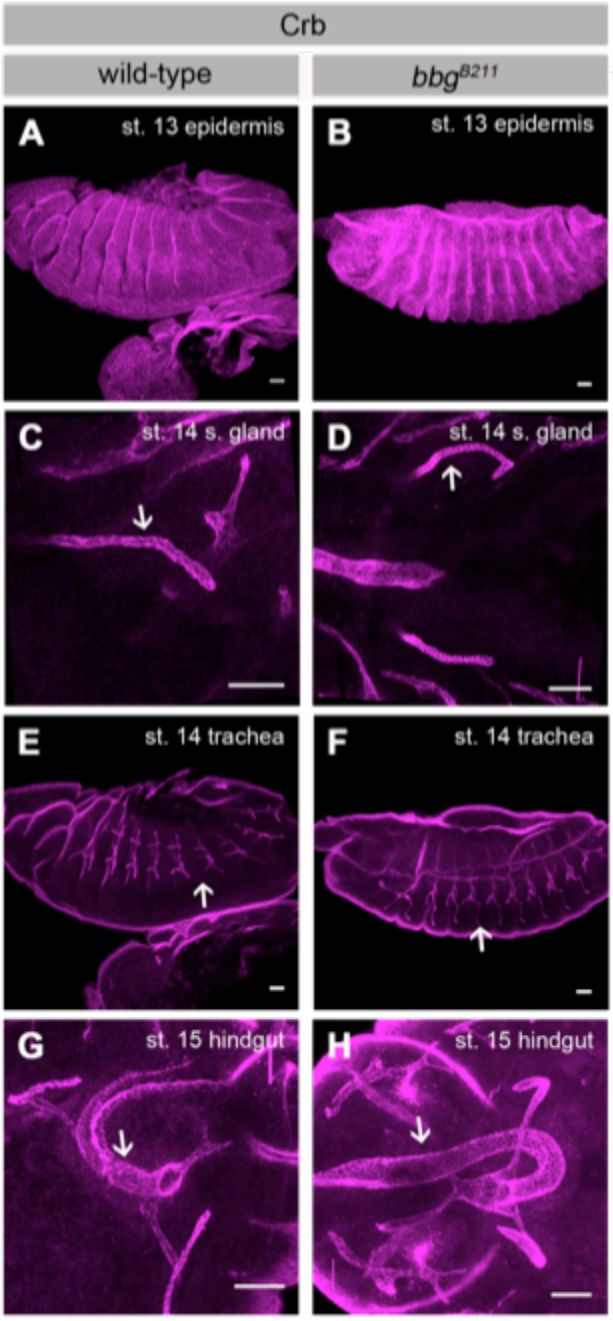

Figure 21: Embryogenesis proceeds normally in *bbg*^{B211} mutant embryos. (A-H) Staining of wt embryos (left panel) and *bbg*^{B211} embryos (right panel) with Crb. The stages and the tissues are written in the different panels. Anterior is always left. Scale bars, 25 µm.

Follicle cells are not affected in the *bbg*^{B211} mutants

The localization of Bbg was checked in the follicle cells, since it is another epithelium tissue with apical Crb localization. As is evident from Fig. 22 A, Bbg is localized on the apical side of the monolayer epithelial tissue of follicle cells throughout stages 5-10 of oogenesis. It is known for a number of

genes that they show similar mRNA and protein localization [Lecuyer et al., 2007]. This is the case for Bbg as the mRNA shows apical follicular localization at stage 8 as well (Fig. 22 B).

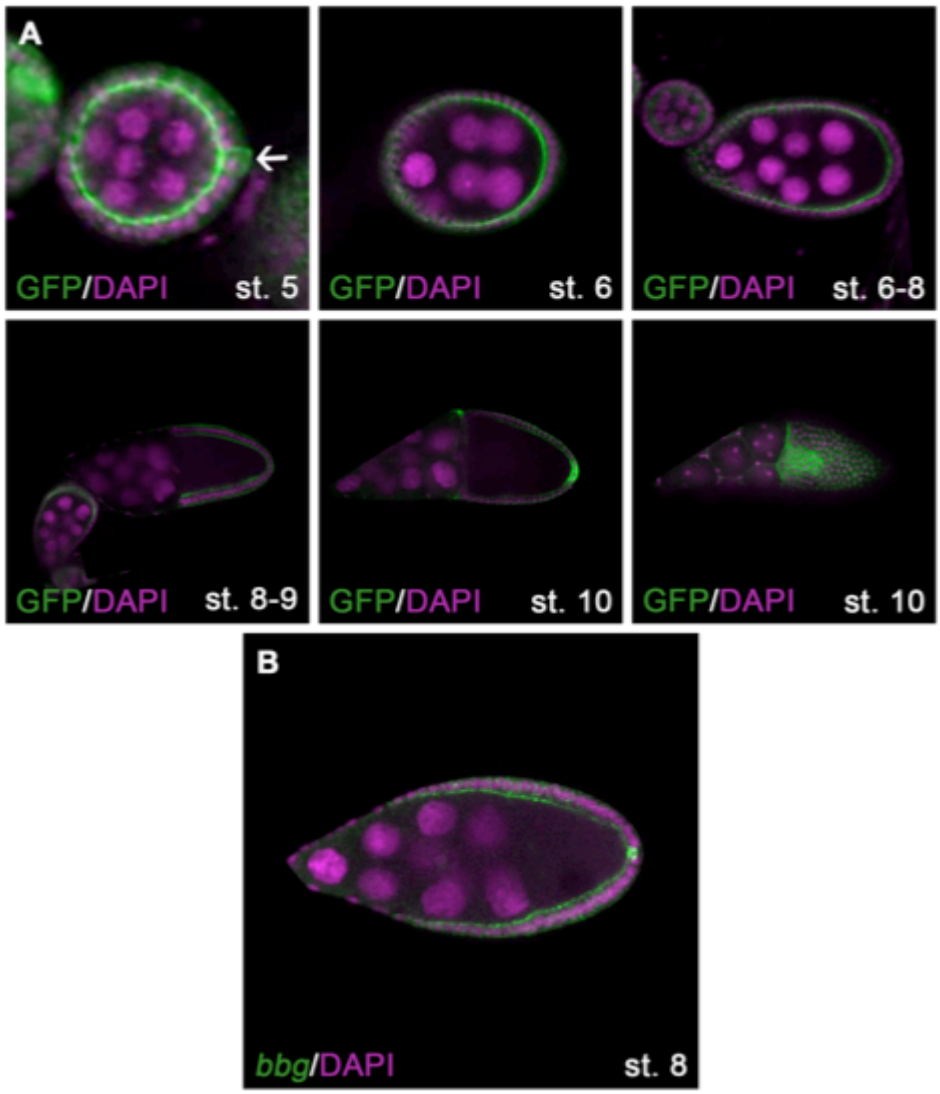

Figure 22: The mRNA and the protein of *bbg* are expressed apically in the follicle cells. (A) Staining of the *Fosmid:Bbg-GFP* follicle cells of GFP and DAPI. Arrow in st. 5 marks the polar cells. The stages are written in the different panels **(B)** *In situ* hybridization of the *Fosmid:Bbg-GFP* follicle, st. 8, made by Helena Jambor [Jambor et al., 2015].

Then the localization of Crb and the integrity of the tissue in the bbg^{B211} were analyzed. Similar to embryogenesis, the integrity of bbg^{B211} follicle cells was not affected. Comparing Fig. 23 A with Fig. 23 B, Crb localization was found to be unaltered. The integrity of the follicular tissue, highlighted with the lateral marker Dlg, was normal, as well (Fig. 23 A' and B').

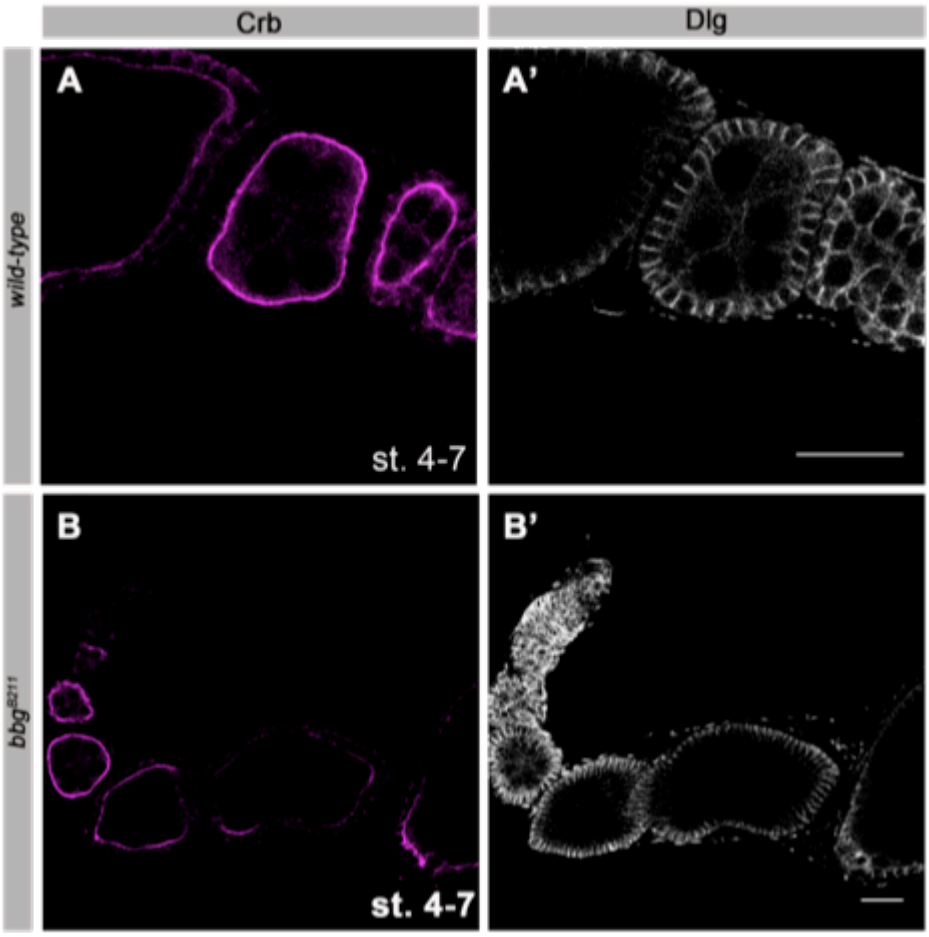

Figure 23: Follicle cells are not affected in the *bbg*^{B211} mutants. (A, A') Staining of wt follicle cells with Crb and Dlg. The stages are written in the different panels. **(B, B')** Staining of *bbg*^{B211} mutant follicle cells with Crb and Dlg. The stages are written in the different panels. Scale bars, 25 µm.

Bbg is localized in the eye imaginal wing disc epithelium and in the adult eye

It was shown previously that Bbg is expressed in developing eyes [Kim et al., 2006]. However, it is not known the exact localization of Bbg in eye imaginal disc and in the adult eyes. Bbg showed expression in the eye discs (Fig. 24) and was localized specifically in the posterior compartment in the cells that surround the differentiated cells (Fig. 24 A-B'''). Crb is expressed in the differentiating cells that give rise to the future photoreceptor cells (Fig. 24 B''). Regarding the anterior compartment of the eye imaginal discs, the proliferative compartment of the disc, Bbg was enriched in the membrane of this proliferative epithelial tissue and colocalized with Crb (Fig. 24 D-D''').

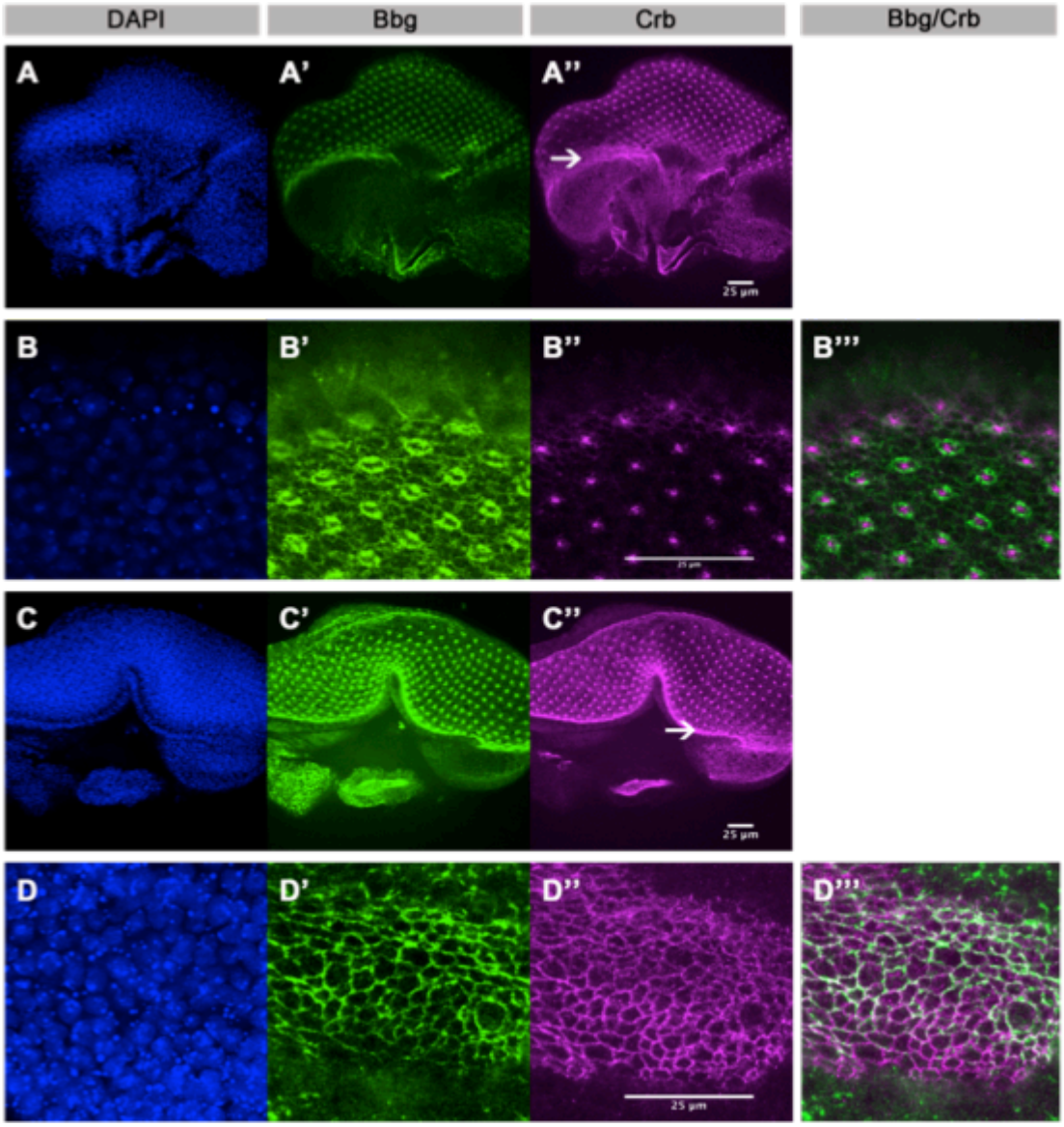

Figure 24: Bbg is localized in the eye imaginal wing disc epithelium. (A-A''') Staining of a third-instar wt eye disc stained with DAPI, Bbg Crb, respectively. The arrow corresponds to the morphogenetic furrow. The region above the arrow is the posterior compartment. The region beneath the arrow is the anterior compartment. **(B-B''')** Zoom in the posterior compartment of same third-instar wt eye disc. **(C-C''')** Staining of a third-instar wt eye disc stained DAPI, Bbg and Crb, respectively. The arrow corresponds to the morphogenetic furrow. **(D-D''')** Zoom in the anterior compartment of same third-instar wt eye disc Data information: Scale bars, 25 µm (A-D''').

The localization of Bbg in the adult eyes was then analyzed. The *Drosophila* eye is composed of about 800 ommatidia, cylindrical, barrel-like structures, containing eight photoreceptor cells in their center that are arranged in a stereotypic manner. Bbg showed expression in the pigment cells in the adult eyes (Fig. 25 A and B). It shows cytoplasmic staining in the pigment cells and does not colocalize with Crb, as Crb is localized in the neighboring photoreceptor cells (Fig. 25 A and B).

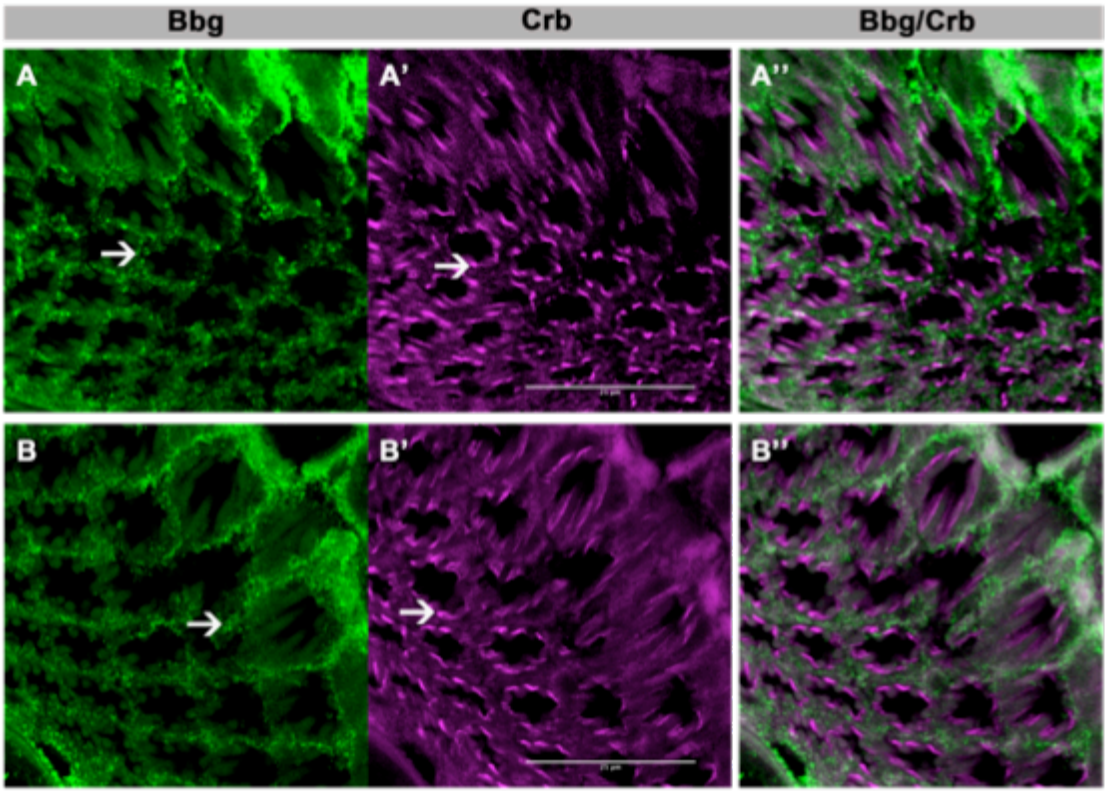

Figure 25: Bbg is expressed in the pigment cells in the adult eyes. (A-B'') Staining of *wt* adult eye sections of the anterior area (thickness: 7µm) with anti-Rabbit-Bbg, anti-rat-Crb and overlay, respectively. Both of the sections are equal. (A, B) arrows: pigment cells, (A', B') arrows: stalk membrane of photoreceptor cells. Scale bars, 25 µm (A-B'').

bbg^{B211} mutant eyes have bigger pigment cells compared to wt

Given Bbg is expressed in the adult eyes, in the pigment cells, the role of Bbg in adult eye morphogenesis was analyzed. Comparing wt with *bbg*^{B211} mutant eyes, it was shown that the pigment cells were bigger in size compared to wt (Fig. 26 A' and C'). The photoreceptor cells remain unaffected in the *bbg*^{B211} eyes (Fig. 26 A, A' and C, C'). This is explained by the fact that Bbg is not expressed in the photoreceptor cells but only in the pigment cells. The length of the rhabdomeres was normal in *bbg*^{B211} eyes (Fig. 26 B and D).

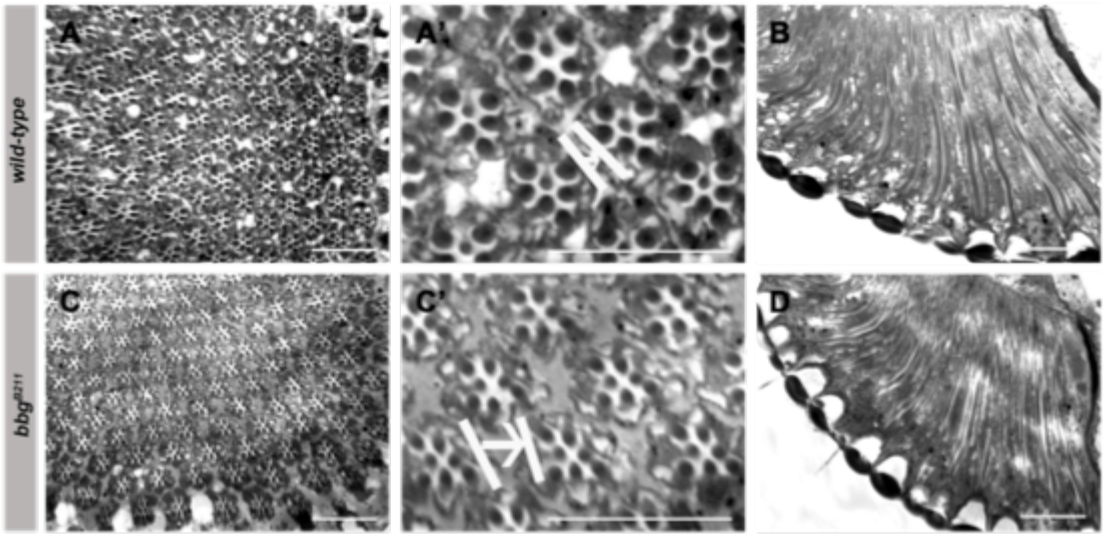

Figure 26: *bbg*^{B211} mutant eyes have bigger pigment cells compared to wt. (A-B) Cross and longitudinal sections of wt retinas, respectively (A') Zoom in from A. **(C-D)** Cross and longitudinal sections of *bbg*^{B211} mutant retinas, respectively. (C') Zoom in from C. The lines separate two different ommatidia. The arrow represents the distance between the two ommatidia, and the size of the pigment cell that is between them. Scale bars, 25 µm (A-D).

Loss of *bbg* in the eye leads to gradual, light-induced retinal degeneration

In *Drosophila*, hereditary retinal degenerations are light dependent in several cases, like in the absence of *crb* [Johnson et al. 2002]. The role of *bbg* in the eye homeostasis was further analyzed after constant light exposure of flies (Fig. 27). When *bbg*^{B211} flies were kept in constant light for seven days, the retina showed degeneration (Fig. 27 A,A' and C, C'). As shown with the arrow, it was not possible to distinguish the seven different photoreceptor cells in several ommatidia, as some of the photoreceptor cells were missing (Fig. 27 C'). This phenotype strictly depends on continuous exposure to light, since in flies kept under standard laboratory conditions, i.e., in artificial low light, no degeneration of photoreceptors occurred (Fig. 27 E and G). The longitudinal sections from the same eyes are represented (Fig. 27 B, D F and H).

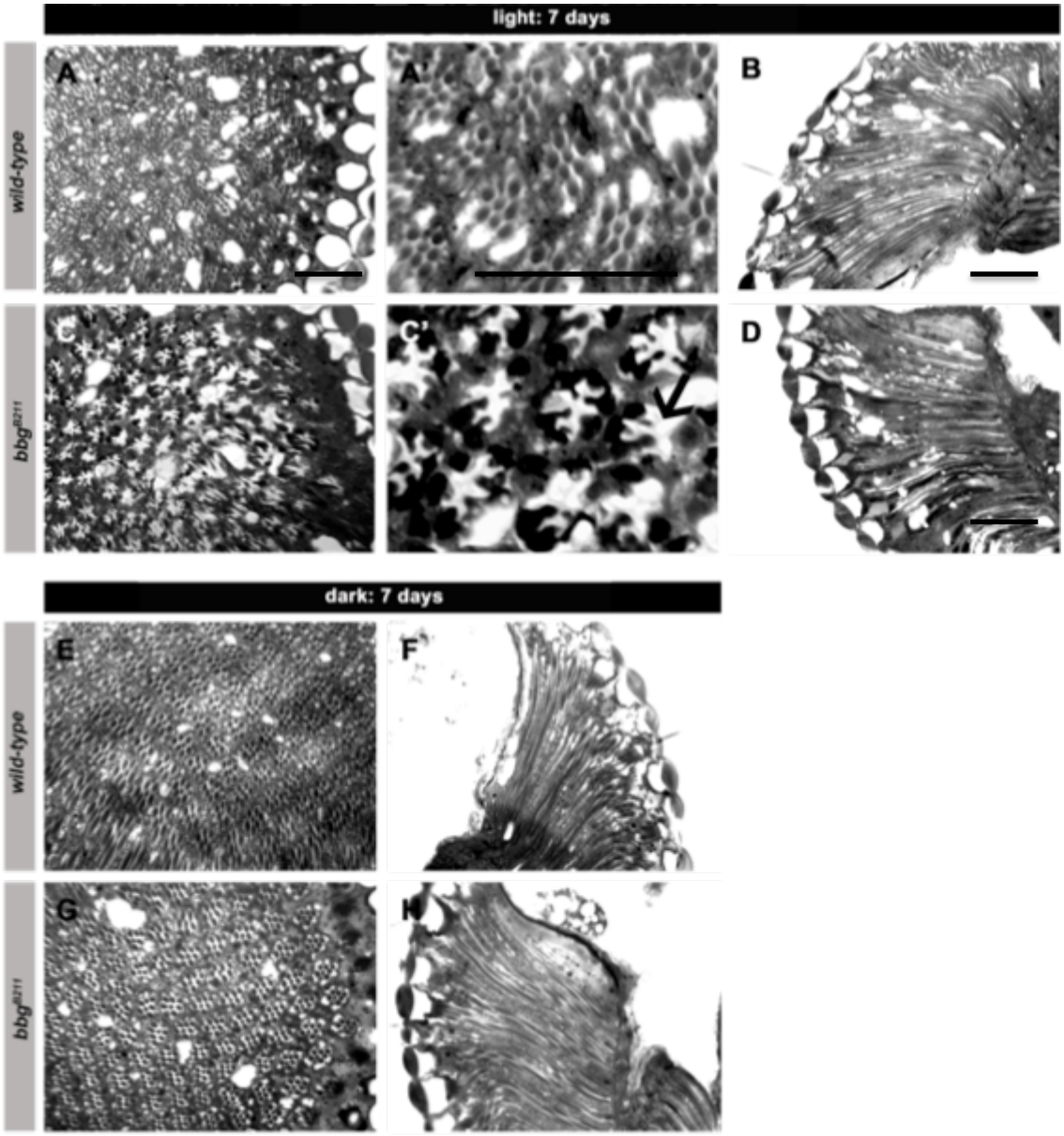

Figure 27: Loss of *bbg* in the eye leads to gradual, light-induced retinal degeneration. Cross and longitudinal sections of wt **(A-B)** and *bbg*^{B211} **(C-D)** retinas after seven days in constant light. The arrow indicates an ommatidium with less than seven photoreceptor cells (C'). A' and C' are magnifications of A and C, respectively. Cross and longitudinal sections of wt **(E-F)** and *bbg*^{B211} **(G-H)** retinas after seven days in constant dark. Scale bars, 25 µm (A-H).

In order to exclude the possibility that *bbg*^{B211} mutant flies contain any other mutations that cause the eye degeneration phenotype, the deficiency line *Df(3L)4543* that includes the *bbg* region was used, to verify the previous light dependent degeneration result. As the deficiency line is homozygous lethal the genotype *Df(3L)4543/bbg*^{B211} was used. When *Df(3L)4543/bbg*^{B211} flies were kept in constant light for seven days, the retina showed degeneration (Fig. 28 A-B'). As shown with the arrows (Fig. 28 B'), the seven

different photoreceptor cells in many of the ommatidia could not be distinguished as with the homozygous line. No degeneration of photoreceptors occurred in flies kept under standard laboratory conditions, i.e., in artificial low light, (Fig. 28 C and D).

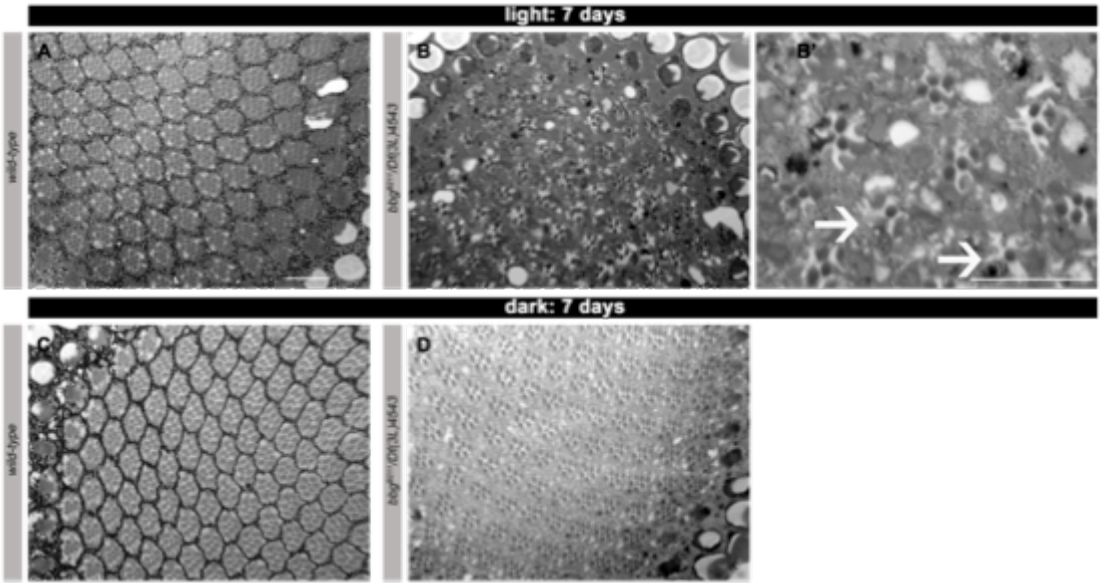

Figure 28: The genotype *Df(3L)4543/bbg^{B211}* shows similar light dependent degeneration of photoreceptor cells similar to the *bbg^{B211}* eyes. Cross sections of wt **(A)** and ***Df(3L)4543/bbg^{B211}*** **(B-B')** retinas after seven days in constant light. The arrows indicate few ommatidia with less than seven photoreceptor cells (B'). The B' is magnification of B. Cross sections of wt **(C)** and *bbg^{B211}* **(D)** retinas after seven days in constant dark. Scale bars, 25 µm (A-D).

The absence of *bbg* or the overexpression of *Crb^{extraTM}-GFP* results in fewer divisions and increased apoptosis in wing discs

Since the absence of *bbg* produces smaller wings (Fig. 13 J-L), it was interesting to determine whether the growth defects started already at an earlier developmental stage and/or if there was any perturbation in the cell cycle progression. Therefore, the growth defects due to the absence of *bbg* at the cellular level were further analyzed. The actual number of the cells of the earlier developmental stage of L3 wing discs and more specifically the pouch area of the discs were analyzed, using the Dlg marker to outline the cell membranes (Fig. 29 B, D, F, G). The comparison was between the control (*69b>GFP*) and *bbg^{B211}* wing discs. The overexpression of *Crb^{extraTM}-GFP* was used as well as it gives smaller wings, similar to the absence of functional Bbg (Fig. 29 C-D). The *69b>GFP* was used as control, in order to exclude the possibility that the phenotype observed upon the overexpression of *Crb^{extraTM}-*

GFP comes from the overexpressed GFP. The overexpression of *Crb*^{extraTM}*-GFP* in the background of *bbg* knockdown and the *bbg* knockdown alone was used as well (Fig. 29 G-I). Upon counting the number of cells in the center of the pouch area (defined by the charachteristic smaller cell size in the DV boundary and the cell line morphology in the AP boundary) and comparing these values in independent samples, it was observed that in the absence of *bbg* there are ~35% fewer cells in the pouch area of the wings relative to the control (Fig. 29 G). Similar results were obtained for the overexpression of *Crb*^{extraTM}*-GFP* (Fig. 29 G). The smaller wing phenotype in the absence of *bbg* occurred from an earlier developmental stage, at least the L3 as the cell number was already decreased.

To determine whether these cells were arrested in the cell cycle or excluded via apoptosis, the number of the mitotic cells in the whole pouch area were counted, using the PH3 (PhosphoHistone3) marker and it was observed that the dividing cells were ~38% fewer in *bbg*^{B211} compared to control (Fig. 29 H. This was the same for all the different genotypes including the overexpression of *Crb*^{extraTM}*-GFP* (Fig. 29 H). TUNEL (Terminal deoxynucleotidyl transferase dUTP nick end labeling) assay showed that apoptosis increases by ~25% upon loss of *bbg* (Fig. 29 I). The overexpression of *Crb*^{extraTM}*-GFP* showed even greate increase in apoptosis (Fig. 29 I).

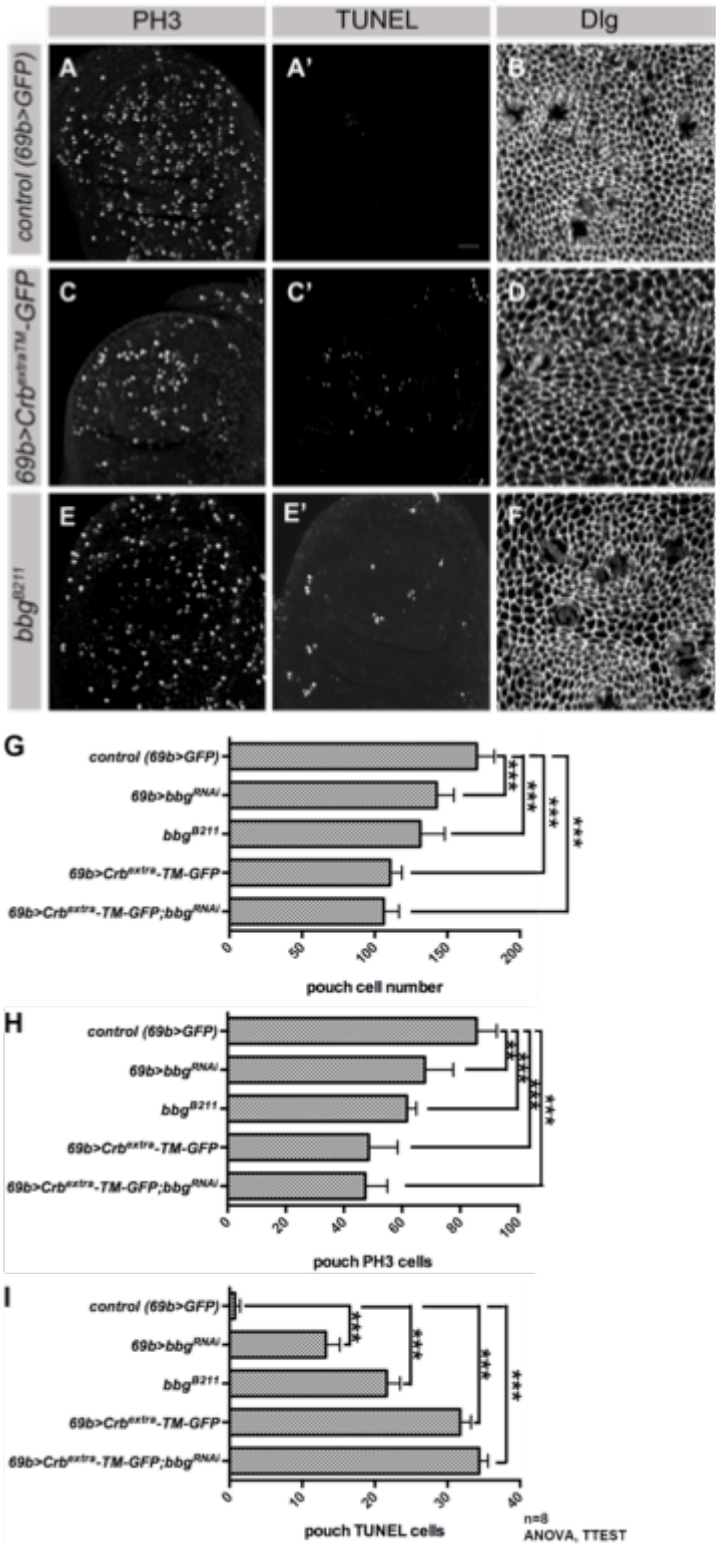

Figure 29: The absence of *bbg* or the overexpression of *Crb^{extraTM}-GFP* results in a slower cell cycle and increased apoptosis in wing discs. (A-B) Third-instar *control (69b>GFP)* wing disc pouch stained with anti-Rabbit-PH3, TUNEL assay and anti-mouse-Dlg, respectively. **(C-D)** Third-instar *69b>Crb^{extra}-TM-GFP* wing disc pouch with anti-Rabbit-PH3, TUNEL assay and anti-mouse-Dlg, respectively. **(E-F)** Third-instar *bbg^{B211}* wing disc pouch stained with anti-Rabbit-PH3, TUNEL assay and anti-mouse-Dlg, respectively. . **(G)** Quantifications of the pouch actual cell number, using eight independent wing discs per condition. **(H)** Quantifications of the pouch PH3 positive cells, using eight independent wing discs per condition **(I)** Quantifications of the pouch TUNEL positive cells, using eight independent wing discs per condition. Data information: Scale bars, 25 μm (A-F). For the analysis (G-I) it was used TTEST and ANOVA test. Two asterisks indicate $p \leq 0.01$. Three asterisks indicate $p \leq 0.001$.Error bars show standard deviation. Scale bars, 25 μm (A-F).

In the absence of *bbg* or in the overexpression of *Crb*^{extraTM}*-GFP*, less mitotic cells were observed. Therefore, fluorescence-activated cell sorter (FACS) analysis was conducted in order to distinguish the cell cycle stages and to analyze the possibility of cell cycle arrest. In order to characterize the normal relationship of cell growth to cell cycle progression, wt discs were dissociated into single cells and FACS analysis was used to collect data for cell numbers (similar in all cases) and cellular DNA content (fluorescent intensity of the Hoechst nuclear marker). As shown in Fig. 30, the two different peaks (marked with arrows) help to distinguish at least the G0/1, S and G2 phases of the cell cycle. The same analysis was conducted in the absence of *bbg* (Fig. 30 A) or in the overexpression of *Crb*^{extraTM}*-GFP* (Fig. 30 B). In conclusion, upon loss of *bbg*, the cell cycle progressed normally compared to wt. This was the same conclusion for the overexpression of *Crb*^{extraTM}*-GFP* as well.

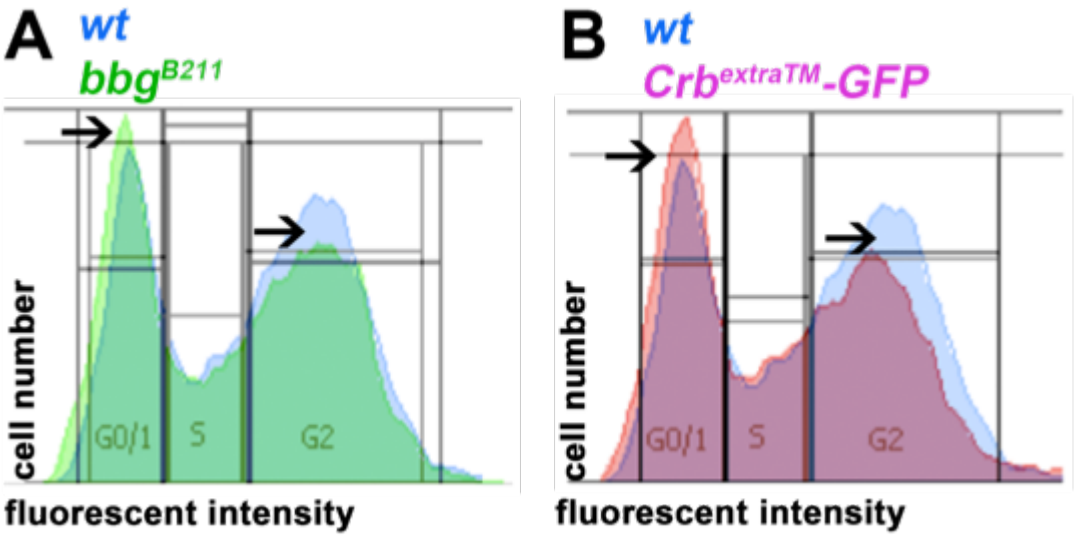

Figure 30: Neither loss of *bbg*, nor overexpression of *Crb*^{extraTM}*-GFP*, affects the cell cycle progression. (A) FACS analysis of wt and *bbg*^{B211} cells of 20 L3 wing discs per condition. **(B)** FACS analysis of wt and overexpression of *Crb*^{extraTM}*-GFP* cells of 20 L3 wing discs per condition. FACS analysis of L3 wing disc cells, showing similar cell cycle phasing between wt and *bbg*^{B211} or wt and overexpression of *Crb*^{extraTM}*-GFP*. Histograms display DNA content/fluorescent intensity (x, fluorescent intensity of the Hoechst nuclear marker) and cell numbers (y). The arrows indicate the G0/1 and G2 phases. Between them there are the cells in S phase.

Given the cell cycle/division and apoptosis are linked to the size of the cells (dividing cells increase their size and apoptosis causes shrinkage of the

cell), this parameter was analyzed as well. Clones of overexpression of *Crb*^{extraTM}*-GFP* revealed cells with ~35% larger apical surface area in comparison to the adjacent wt cells (Fig. 31 A, A'). Similar observations were obtained from *bbg*^{B211} clones, as the *bbg*^{B211} mutant cells have ~30% larger apical surface area in comparison to the adjacent wt cells (Fig. 31 B, B').

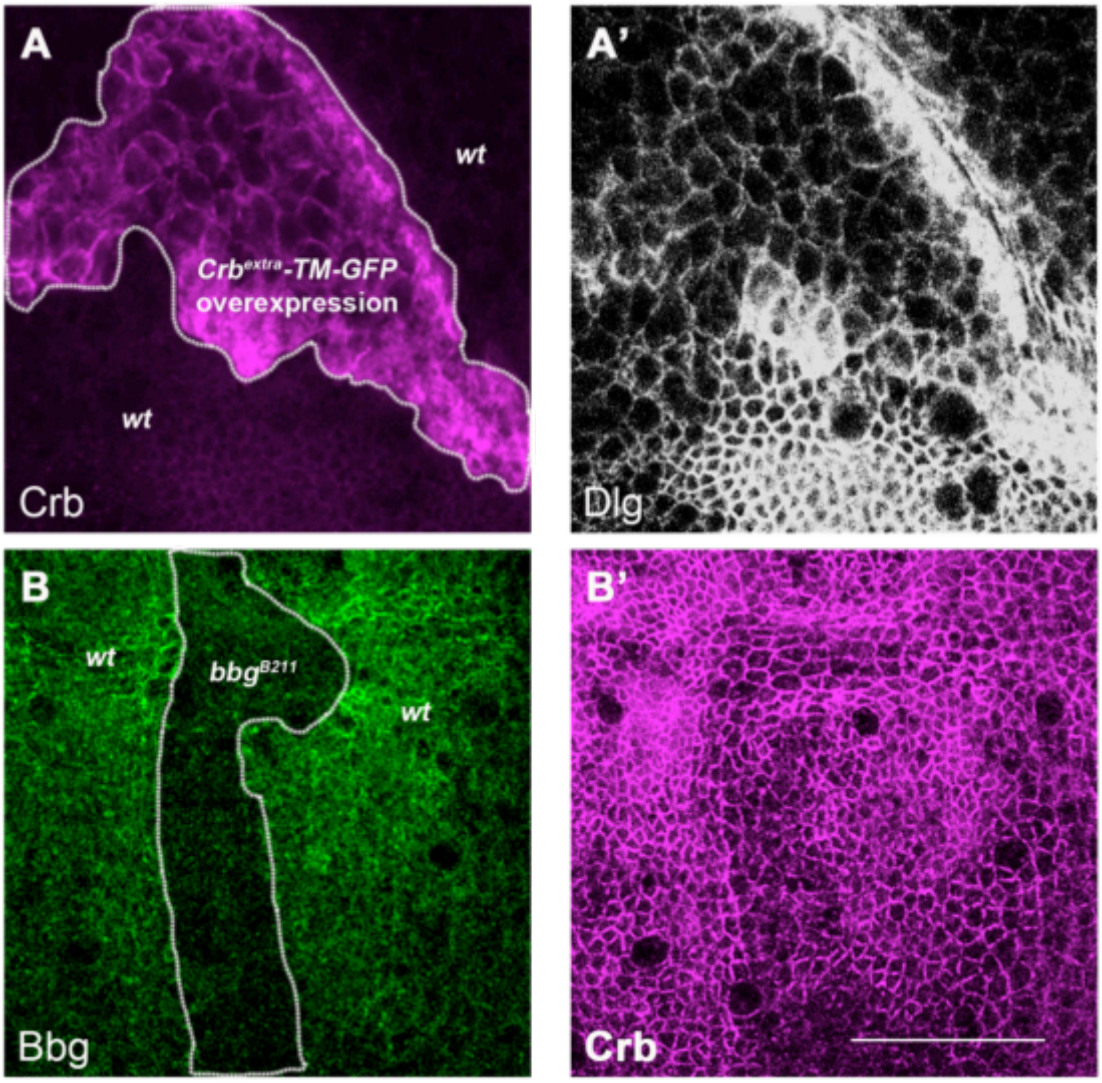

Figure 31: Cell size either upon overexpression of *Crb*^{extra}*-TM-GFP* or *bbg*^{B211}, in L3 imaginal wing discs. (A-A') Third-instar *wt* wing disc pouch stained with Crb and Dlg, respectively. White outlining depicts an overexpression of *Crb*^{extra}*-TM-GFP* clone. **(B-B')** Third-instar wt wing disc pouch stained with Bbg and Crb, respectively. White outlining depicts a *bbg*^{B211} mutant clone. Scale bars, 25 μm (A-B).

In order to analyze further the *bbg*^{B211} larger cell phenotype, the size and the shape of wt and *bbg*^{B211} mutant wing disc cells were tracked. The cells were bigger and elongated upon loss of *bbg*, in comparison to wt tissue (Fig. 32 A-B'). As the cell cycle progressed normally in *bbg*^{B211} wing discs, live-imaging experiments were also conducted in order to visualize the

divisions that cells undergo in real-time, in the wing discs. Comparing wt with *bbg*^{B211} mutant wing discs in a specific time window of six hourss it was observed that the discs upon loss of *bbg* divide ~25% less (from three independent *bbg*^{B211} mutant discs, Movies are not shown). The divisions of the cells can be tracked with the cells that increase their size. Taken together, our results showed that the absence of *bbg* was responsible for fewer divisions as well as for increased apoptosis in wing discs and these two events are not mutually exclusive. These results suggest that *bbg* plays an essential role in regulating the normal cell cycle rate/division of the wing disc cells. This is true for the overexpression of *Crb*^{extraTM}*-GFP* as well.

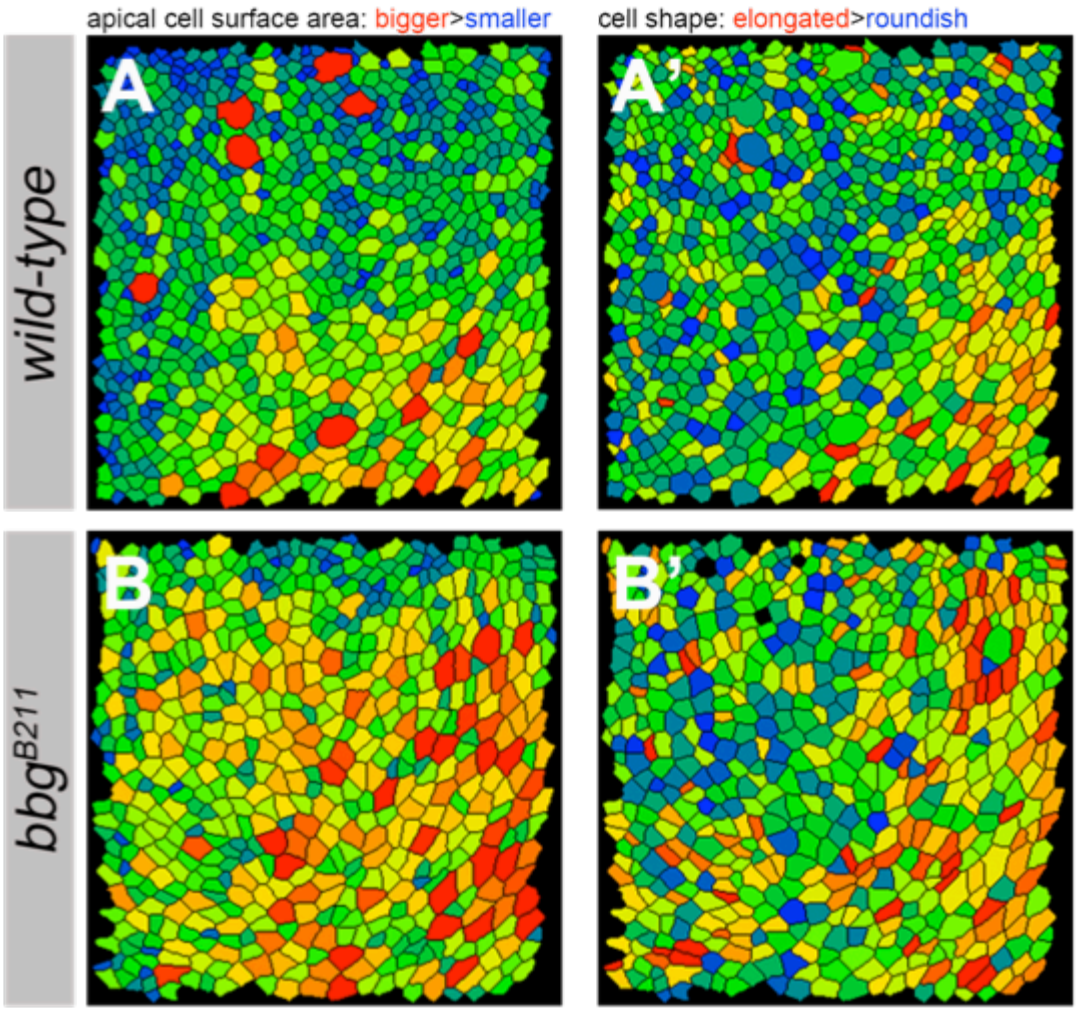

Figure 32: The cells are bigger and more elongated in *bbg*^{B211} wing discs. Using Packing Analyzer program to quantify the size and the shape of the cells in (A, A') wt (E-Cadherin: GFP) and (B, B') *bbg*^{B211} mutant (E-Cadherin: GFP) wing discs. All figures are analyzed from the same area of the wing discs: Dorsal-Anterior area of the pouch. Aknowledgments to Natalie Dye for aquaring the movies and providing the packing analyzer program.

Epithelial cells of the wing disc pouch divide less in *bbg*^{B211} mutants

In order to verify whether the epithelial cells of the wing disc pouch divide less in *bbg*^{B211} mutants compared to wt (Fig. 29 E-F), a subset of cells of the pouch were marked via overexpressing GFP in clones. The overexpression of GFP is helpful for the tracking of a small cluster of dividing cells either in wt or in *bbg*^{B211} wing discs. *GFP* clones were generated in *bbg*^{B211} mutant wing discs and this would allow comparison of the size of the clones with GFP clones in wt discs (Fig. 33). Three independent time points of inducing the clone formation (24h, 48h and 72h induction of clones after egg laying, left, middle and right panel respectively) were used. Upon comparison of the clones of wt and *bbg*^{B211} mutant (overexpression of *GFP* in both cases), it was evident that the size of the *bbg*^{B211} clones were ~40% less (hs after 24h) (Fig. 33 G) and ~53% less (Fig. 33 H) (compare Fig. 33 B, D, F to A, C, E). Notably, the only one clone upon overexpression of *GFP* in *bbg*^{B211} after 72h was in the peripodial membrane and not in the monolayer epithelium tissue (maybe due to apoptosis) of the wing disc (Fig. 33 F, F', the Dlg staining indicates that the cells are bigger in size, therefore highlights the peripodial membrane). Therefore the size of the *GFP* clones in *bbg*^{B211} was not measured after 72h of hs. In conclusion, *bbg*^{B211} mutant wing disc cells divide less or the cells are eliminated via apoptosis. These two events are not mutually exclusive.

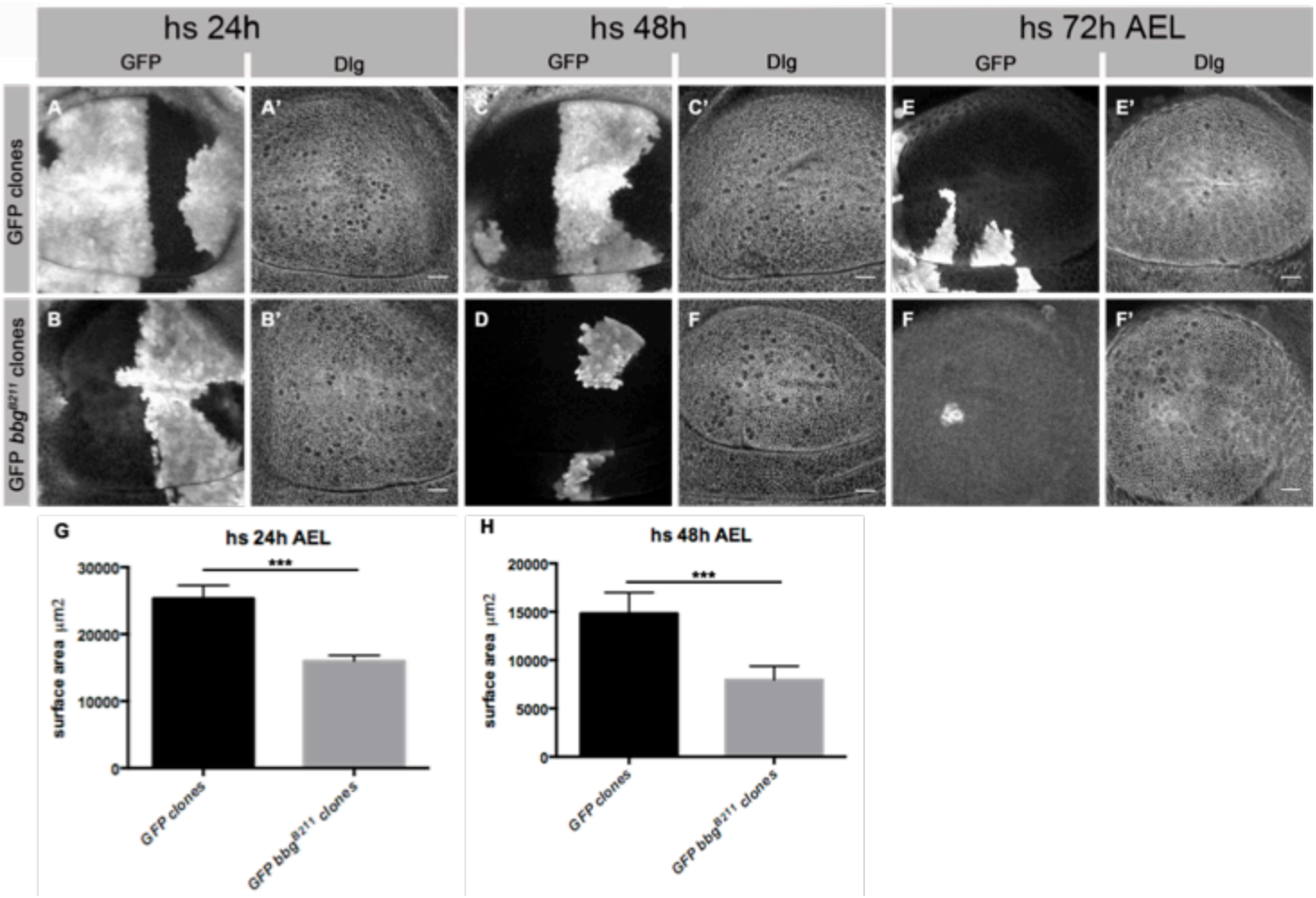

Figure 33: Epithelial cells of the wing disc pouch divide less in *bbg*^{B211} mutants. Generation of overexpression GFP clones in wt wing discs **(A, C, E)**, and *bbg*^{B211} **(B, D, F)** in three independent times points (hs after 24h AEL left panel, 48h AEL middle panel and 96h AEL right panel) and stained GFP and Dlg, respectively. Scale bars, 25 µm. **(G, H)** Statistical analysis of measuring the size of the clones in the pouch area of overexpression of GFP, in wt and *bbg*^{B211} wing discs after 24 of hs **(G)** and 48h **(H)** using 10 independent discs/condition. For the analysis (G-H) it was used TTEST and ANOVA test. Three asterisks indicates $p \leq 0.001$. Error bars show standard deviation.

Bbg is expressed in the apical cortex in the wing disc epithelium

Since the absence of *bbg* gives smaller wings, the localization of Bbg in the precursor tissue of the adult wing, i.e., the wing disc, was analyzed. Immunofluorescence experiments showed that Bbg is expressed apically in the cortex of the cells (Fig. 34 A, A'). The cell cortex, also known as the actincortex or actomyosin cortex, is a specialized layer of cytoplasmic proteins on the inner face of the plasma membrane of the cell periphery (Fig. 34 D). It functions as a modulator of plasma membrane behavior and cell surface

properties. It was observed that Bbg is highly enriched along the A-P boundary of the disc, like a cable phenocopying the localization of actin (arrows in Fig. 34 A') [Major and Irvine., 2005]. Bbg partially colocalizes with Crb, especially in the edges of the polygonal structured cells (Fig. 34 B-B''). Notably, Bbg is enriched in the sub-apical region where Crb is localized (Fig. 34 C-C'').

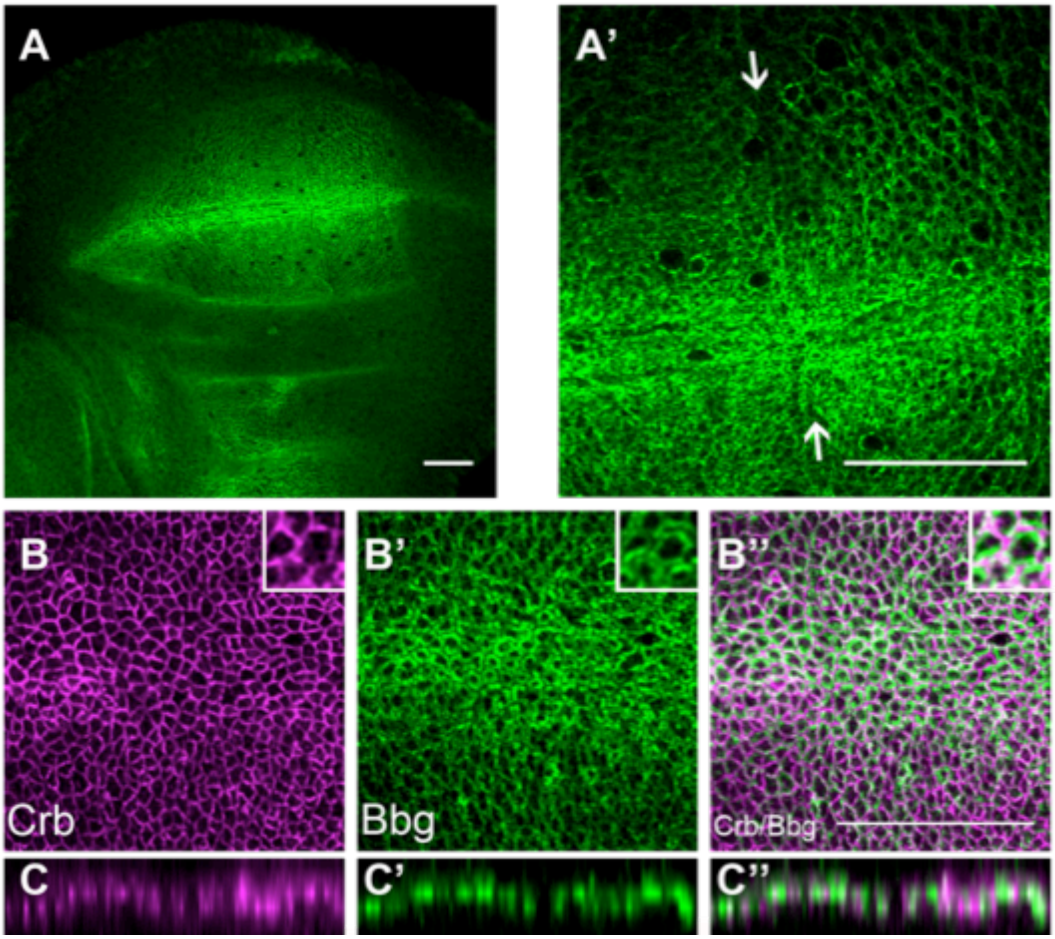

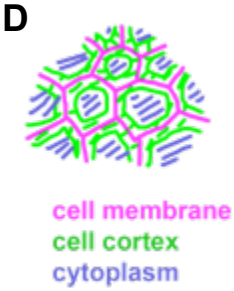

Figure 34: Bbg is expressed in the apical cortex in the wing disc epithelium. (A) Third-instar wt wing disc stained with Bbg. (A') magnification of the pouch area of the wing in figure A. **(B-B'')** Third-instar wt wing disc pouch stained with Bbg, Crb and overlay, respectively. Small boxes in the top right corners: zoom in specifically of 5-6 cells in the same pouch areas, respectively. **(C-C'')** xz position of the central area of the wing disc from the figure B-B''. **(D)** Cartoon representing the cortical area of the cell. Data information: Scale bars, 25 μm (A-C'').

Bbg acts as scaffolding molecule as it is required for the proper localization of apical proteins in wing discs

As loss of *bbg* enhances the wing phenotype obtained upon the overexpression of the apical protein $Crb^{extraTM}$-*GFP* and because Bbg is expressed in the same area as Crb in wing discs (Fig. 34 C''), the epithelial integrity and the localization of the polarity markers of the epithelial sheet of wing disc were checked upon loss of *bbg*. Notably, the apical protein Crb was mislocalized from the apical membrane in bbg^{B211} wing discs (Fig. 35 A and C), while the lateral polarity marker Dlg remained unaffected (Fig. 35 A'' and C''). Comparison of xz sections between wt and bbg^{B211} wing discs showed that Crb expanded laterally whereas Dlg retains its lateral localization (Fig. 35 B and D). The localization of Bbg was apical in the wing disc epithelium (Fig. 34 C'). This localization of Bbg is in the same plane as Crb and this is consistent with the observation that loss of *bbg* correlates with mislocalization of Crb (Fig. 35 A, B, C and D). Similarly Bbg was not expressed laterally; the localization of the lateral marker Dlg was not altered upon Bbg's loss (Fig. 35 B'' and D'').

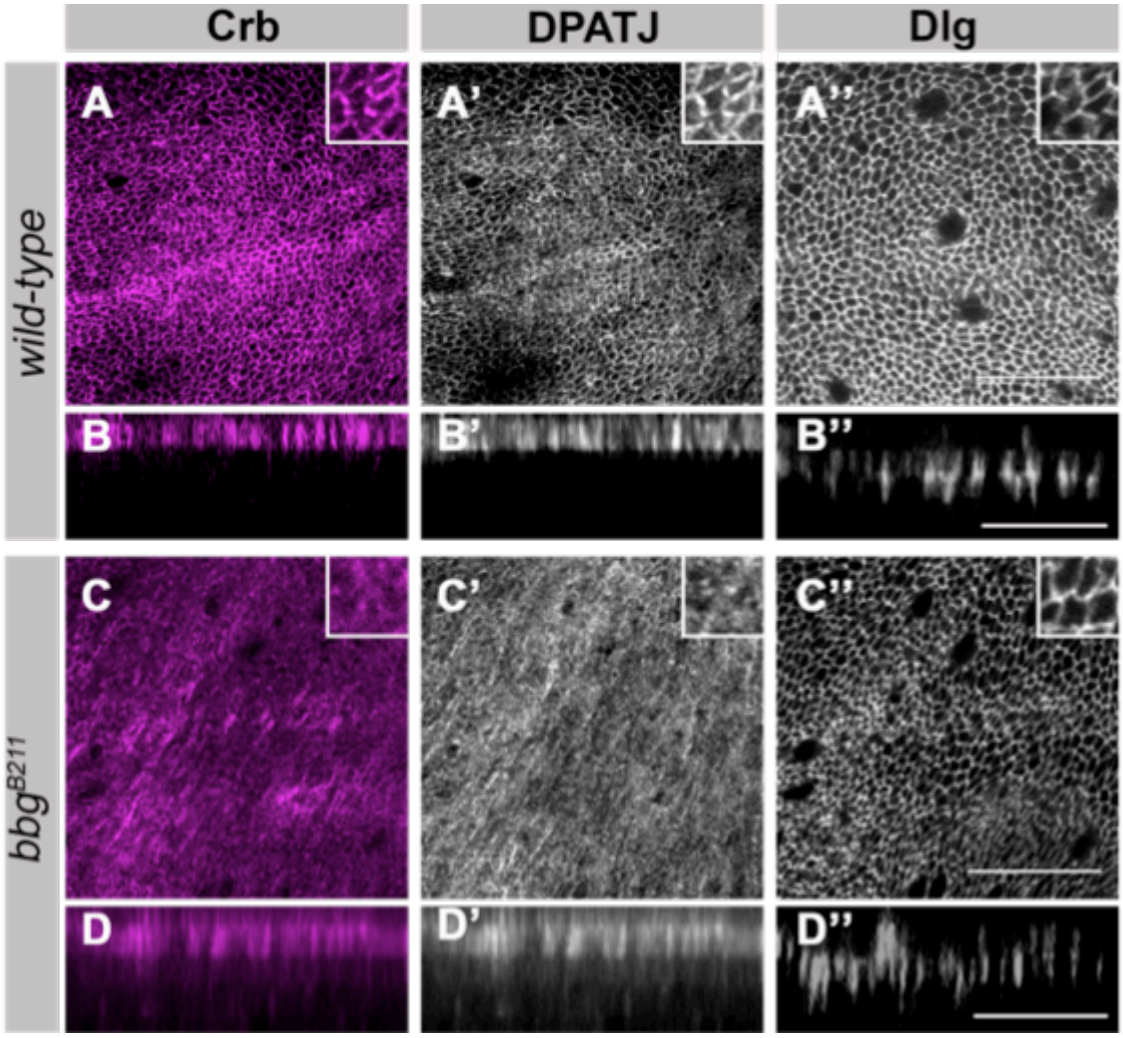

Figure 35: Loss of *bbg* affects the localization of Crb and DPATJ in L3 imaginal wing discs. (A-A'') Third-instar wt wing disc pouch stained with Crb, DPATJ and Dlg, respectively. **(B-B'')** xz position of the central area of figure A. **(C-C'')** Third-instar bbg^{B211} mutant wing disc pouch stained with Crb, DPATJ and Dlg, respectively. **(D-D'')** xz position of the central area of Figure C. Scale bars, 25 µm (A-D''). Small boxes in the top right corners: zoom in specifically of 5-6 cells in the same pouch areas, respectively.

In order to verify the previous result, mutant clones for *bbg* were generated. The absence of *bbg* led to reduction of Crb (Fig. 36 A and A'). Moreover, as shown in Fig. 36 A'' in order to quantify this result, 10 independent clone areas from 10 independent wing discs were analyzed and the intensity of fluorescence of overall Crb inside the clone was measured. The negative control was 10 independent wt tissue areas with the same size as the mutant clones exactly adjacent to the mutant clone. The counting clones were either near to the ventral or the dorsal compartment of the wing disc. Quantification showed reduction of the fluorescence intensity of Crb inside the bbg^{B211} clone (Fig. 36 A'').

The localization of Bbg in the absence of Crb was then checked. Mutant clones for *crb* were generated and it was found that the absence of Crb promotes decrease in the levels of overall Bbg, as well (Fig. 36 B and B'). In order to quantify this result, a similar quantification protocol as above was followed. 10 independent clone areas from 10 independent wing discs were analyzed as above and the fluorescence intensity of Bbg inside the clone was measured (Fig. 36 B''). The negative control was 10 independent wt tissue areas with the same size as the mutant clones exactly adjacent to the mutant clone. Clones that were counted were either near to the ventral or the dorsal compartment of the wing disc. Quantification showed reduction of the fluorescence intensity of Bbg inside the crb^{11A22} clone (Fig. 36 B''). In conclusion, generation of mutant clones either for *bbg* or *crb*, leads to reduction of Crb and Bbg in wing discs, respectively.

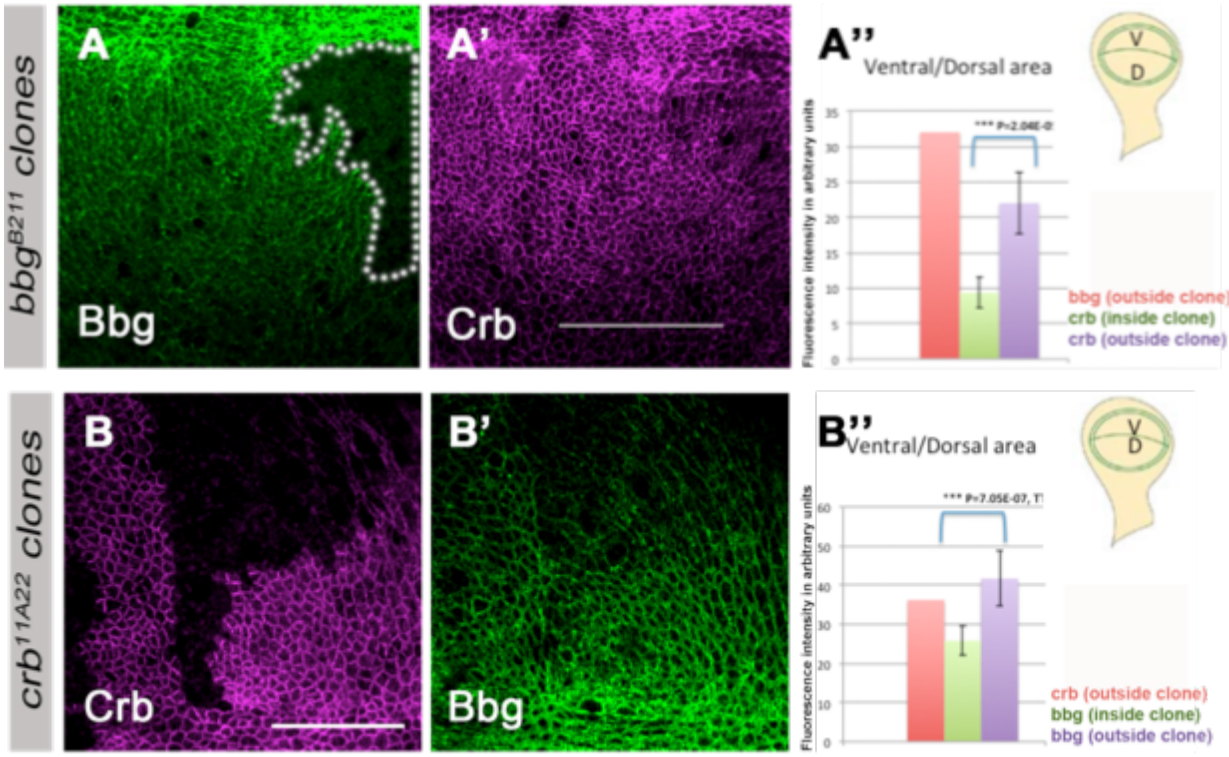

Figure 36: Loss of *bbg* or *crb* leads to reduction of Crb and Bbg in wing discs, respectively. (A,A') Third-instar bbg^{B211} clones, highlighted in white schemes, stained Bbg and Crb, respectively. **(A'')** Statistical analysis of 10 independent clone areas from 10 independent wing discs and then measurement of the intensity of the fluorescence of Crb inside and outside the clone. **(B, B')** Third-instar crb^{11A22} clones stained for Crb and Bbg, respectively. **(B'')** Statistical analysis of 10 independent clone areas from 10 independent wing discs and then measurement of the intensity of the fluorescence of Bbg inside and outside the clone. Data information: Scale bars, 25 μm (A,A',B and B'). For the statistical analysis it was used TTEST. Three asterisks indicate $p \leq 0.001$.

To further elucidate this reduction of Crb in *bbg*^{B211} wing discs, the localization of the apical proteins DPATJ, Bazooka (Baz) and aPKC was studied. Similar to Crb, the well-characterized partner of Crb, DPATJ [Bulgakova and Knust, 2009] was also mislocalized from the apical membrane in *bbg*^{B211} wing discs (Fig. 35 A' and C'). Comparison of xz sections between wt and *bbg*^{B211} wing discs showed that DPATJ is expanded laterally (Fig. 35 B' and D') whereas Dlg retains its lateral localization (Fig. 35 B'' and D''). The localization of both the proteins Baz and aPKC was perturbed in the *bbg*^{B211} wing discs (Fig. 37 A-B and D-E). Despite the perturbation of localization of the apical polarity markers, the localization of the more lateral adherens junction marker DE-cadherin remained unaltered in *bbg*^{B211} wing discs (Fig. 37 C and F). All these results suggest that Bbg is responsible for the proper localization and stabilization of only the apical proteins in the epithelium tissue of the wing disc.

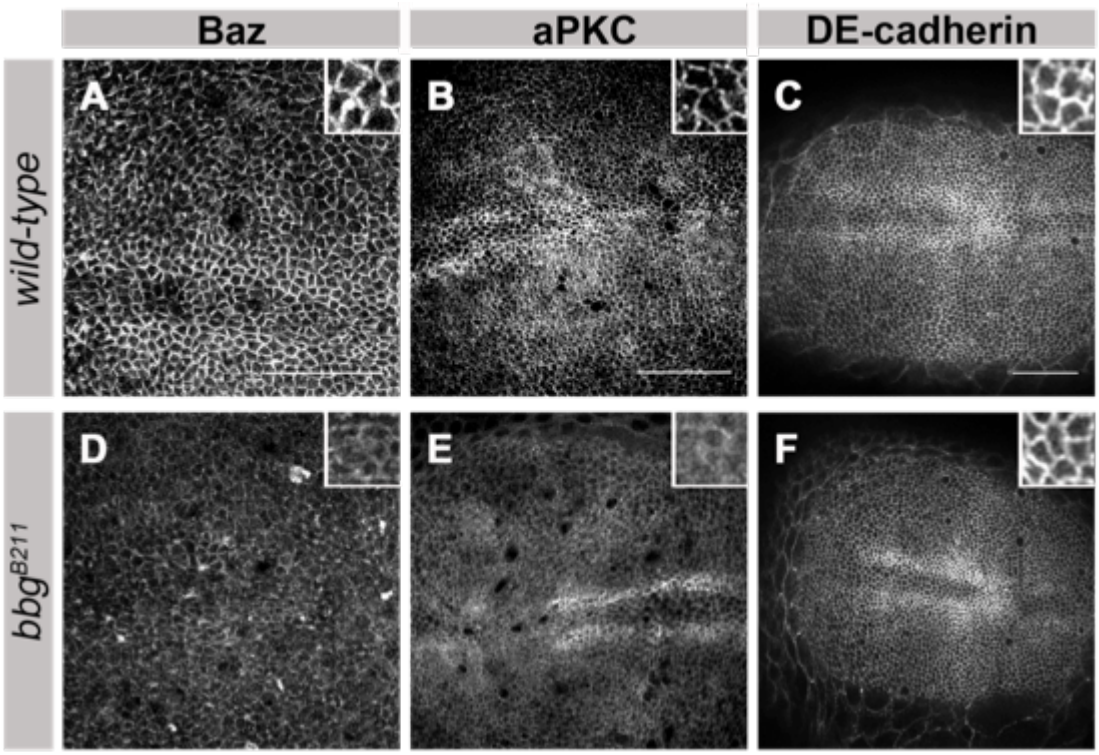

Figure 37: Loss of *bbg* affects the localization of the apical proteins Baz and aPKC (in L3 imaginal wing discs. (A-C) Third-instar wt wing disc pouches stained with Baz, aPKC and DE-cadherin, respectively. **(D-F)** Third-instar *bbg*^{B211} wing disc pouches stained with Baz, aPKC and DE-cadherin, respectively. The magnification of the white box of the left panel is shown on the right of the figure. Data information: Scale bars, 25 μm (A-F).

Localization of Bbg is not affected upon overexpression of *Crb^{extra}-TM-GFP* in wing discs

The genetic screen showed an interaction between the overexpression of *Crb^{extraTM}-GFP* and *bbg*. Since *bbg* encodes a cytoplasmic protein and *Crb^{extraTM}-GFP* is a membrane bound protein, the localization of Bbg upon overexpression of *Crb^{extraTM}-GFP* in wing discs was carefully analyzed (Fig. 38). As shown by the two different approaches, 1) overexpression of *Crb^{extraTM}-GFP* in the posterior compartment (Fig. 38 A-B'') and 2) generation of clones overexpressing *Crb^{extraTM}-GFP* (Fig. 38 C-D'), the localization of Bbg remains unaltered in both cases. The same effect is seen for Dlg, as well (Fig. 38 A-B'').

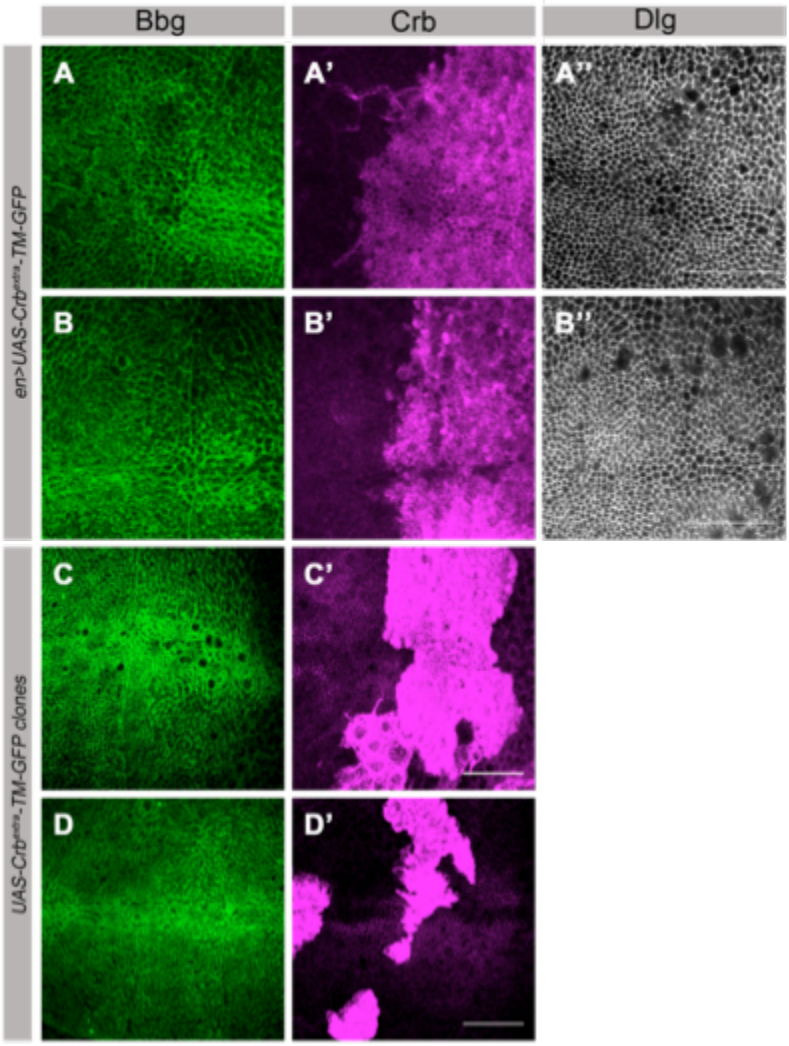

Figure 38: The localization of Bbg is not affected after overexpression of *Crb^{extra}-TM-GFP* in wing discs. (A-B'') Overexpression of *Crb^{extraTM}-GFP* posteriorly in wing discs and staining with Bbg, Crb and Dlg, respectively. **(C-D')** Generation of clones of overexpression of *Crb^{extraTM}-GFP* in wing discs and staining with Bbg and Crb, respectively. Scale bars, 25 µm.

Adherens and septate junction proteins are not affected in *bbg*^{B211} wing discs

DE-cadherin is as an adherens junction marker that is not affected in *bbg*^{B211} mutant wing discs (Fig. 37 C and F). Armadillo, which is the homologue of β-catenin, as another adherens junction marker was also analyzed in the *bbg*^{B211} mutant discs (Fig. 39 A and B). Similar to DE-cadherin (Fig. 37 A and B), the localization of Armadillo was not affected in the *bbg*^{B211} wing discs (Fig. 39 A and B). Since the septate junction marker of the pouch, Dlg remained unaltered (Fig. 35 B and C), the localization of another septate junction marker, Coracle was also analyzed (Fig. 39 C and D). The localization of Coracle is not changed in *bbg*^{B211} wing discs (Fig. 39 C).

Among the several adherens junction proteins that were tested, the atypical cadherin protein Dachsous was affected in the *bbg*^{B211} wing discs (Fig. 39 E and F). Dachsous antibody was used that was more enriched in the anterior notum adjacent to the pouch area of the wing disc, due to technical reasons. However, it is known that Dachsous is expressed ubiquitously at the apical junctions in the whole wing disc [Brittle et al., 2012]. The absence of *bbg* caused a disruption in the localization of Dachsous (Fig. 39 E and F). Given that Dachsous is implicated in the Fat-Dachsous signaling pathway [Ambegaonkar et al., 2012], the analysis of the localization of the proteins Fat and Dachs followed. However the quality of the antibodies against Fat and Dachs were not high enough to analyze the localization of the proteins in the wing discs.

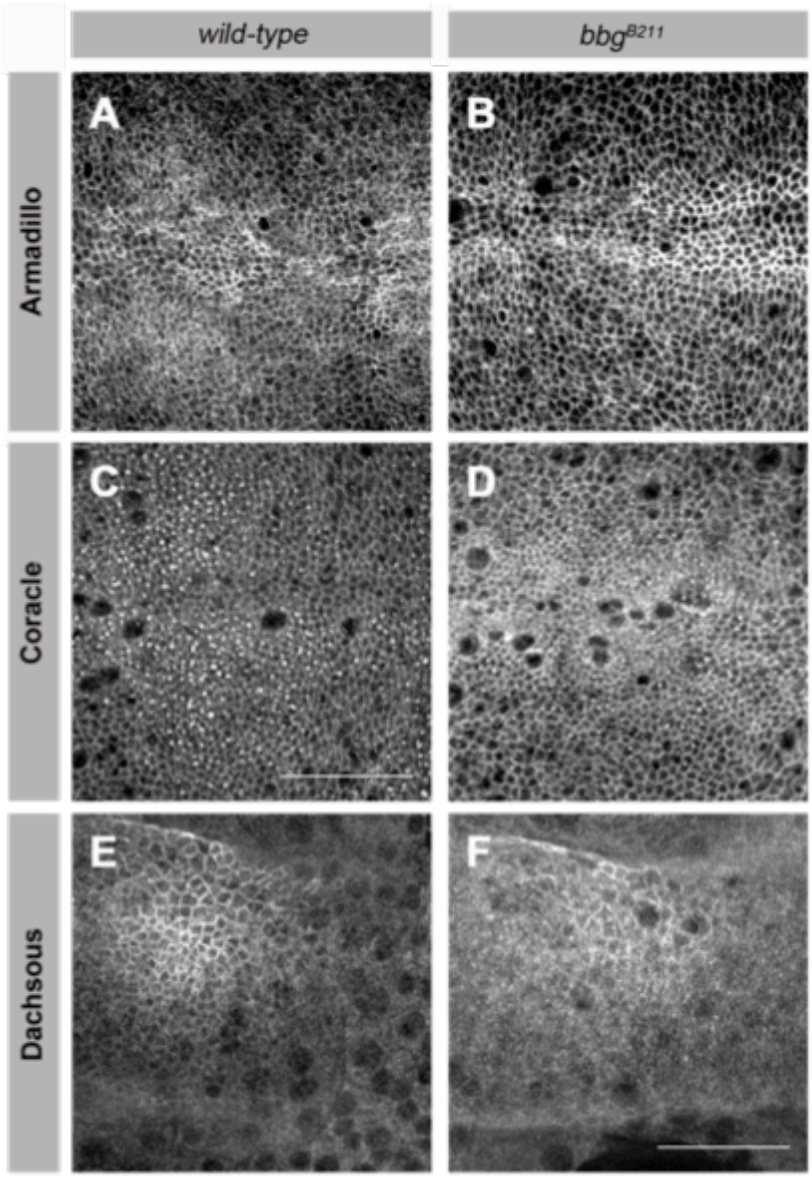

Figure 39: The polarity adherens and septate junction proteins are not affected in the *bbg*^{B211} wing discs. Third-instar wt **(A, C, E)** and *bbg*^{B211} **(B, D, F)** wing disc pouch stained with Armadillo, Coracle Dachsous, respectively. Scale bars, 25 µm.

The integrity of the epithelial sheet, except from the septate junctions, remains unaffected in *bbg*^{B211} mutant wing discs

In *bbg*^{B211} wing discs, localization of apical polarity proteins were found to be affected (like: Crb, DPATJ, Baz and aPKC), although most of the lateral proteins were not (like: DE-cadherin, Armadillo, Dlg and Coracle). In order to study the tissue integrity and to have a detailed analysis of the different membranous structures such as the microvilli and junctions EM (Electron

Microscopy) was used. The central area of the pouch was used as the sample. It was ensured that all the sections were in the same position in wt and *bbg*^{B211} wing discs. In Figure 40 A the structure of the wt epithelial sheet is represented (apical side of the tissue is aligned upwards). In this figure the different membranous structures of the cell such as the microvilli (arrow) and the nucleus (arrowhead) are shown (Fig. 40 A). Only the apical and lateral structures of the cells are represented in this image. In a higher magnification of Fig. 40 A, the adherens junctions of wt cells can be recognized (arrow in Fig. 40 A'). The septate junctions can be recognized more laterally (arrow Fig. 40 A''). The septate junctions have a specific ladder-like structure. The integrity of the microvilli, and adherens junctions were not affected in the *bbg*^{B211} wing disc tissue and look similar to the wt tissue (Fig. 40 B, B'). Another interesting observation was that the ladder-like structure of the septate junctions was affected in the *bbg*^{B211} (compare Fig. 40 B'' and A'').

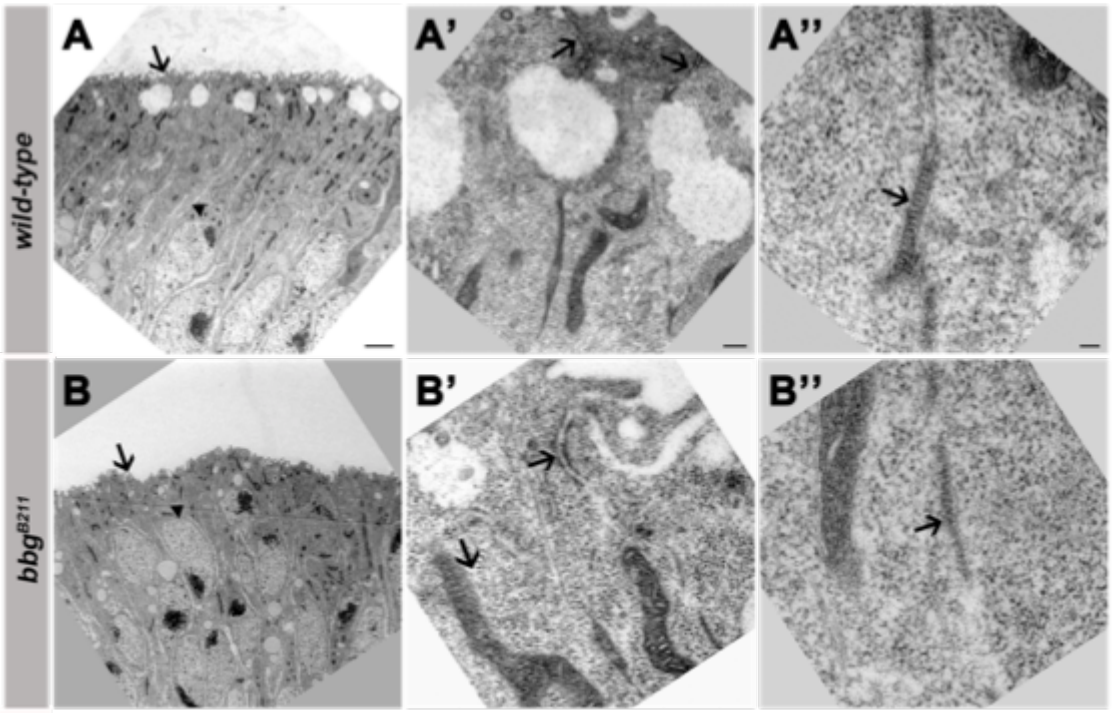

Figure 40: The integrity of the epithelial sheet, except from the septate junctions, remains unaffected in *bbg*^{B211}. (A-A'') wt wing disc section from the central pouch area. The arrow marks the microvilli and the arrowhead the nucleus of one cell in **A.** Apical is always up. **(A')** Maginification of A, arrows: adherens junctions. **(A'')** higher magnification of A, arrow: septate junction. **(B-B'')** *bbg*^{B211} wing disc section from the pouch area. The arrow marks the microvilli and the arrowhead the nucleus of one cell in **B**. Apical is always up. **(B')** Maginification of B, arrow: adherens junction. **(B'')** higher magnification of B, arrow: septate junction. Scalebars: 2000nm (A, B), 300nm (A', B'), 100nm (A'', B'').

Bbg directly interacts with Crb, independently of Sdt and DPATJ

In *bbg*^{B211} wing discs, Crb was mislocalized in the epithelial tissue (Fig. 35 C and A) and Bbg was reduced from the apical cortex (Fig. 36 B-B''). This lead to the analysis of the interaction between Bbg and Crb in *crb*^{11A22} clones. The intriguing question was if Bbg interacts with the core complex of Crumbs, consisting of Crb, Sdt and DPATJ. Indeed, using *Drosophila* abdomen tissue from adult females (4 days old) and an Sdt antibody for immunoprecipitation experiments, it was confirmed that Sdt was in the same complex with Crb and DPATJ but not with Bbg (Fig. 41 A). Using a Bbg antibody for immunoprecipitation, Bbg was immunoprecipitated together with Crb but not with Sdt and DPATJ (Fig 41 B). In conclusion, these two immunoprecipitation experiments show that in the adult abdominal tissues Crb and Bbg are in the same complex and act independent of the Crb core complex that includes Crb, Sdt and DPATJ (Fig 41 C).

To provide further evidence for a direct interaction between Crb and Bbg, a recombinant His-tag protein including the C-terminus part of Bbg was generated (396 amino acids, including the stop codon of Bbg, recombinant-Bbg: approxiamtely 40 kDa). The His tag is in the N-terminus of the recombinant-Bbg protein. The His-Bbg protein contained two of the three PDZ domains that are found within all the predicted protein isoforms (Fig. 41 D, Fig. 15 B). The constructs GST-Crb^{intra} and GST-Crb$^{intra\Delta ERLI}$ (Fig 41 D) were also used [Lin, PhD thesis 2015]. The Crb-intra motif–ERLI is the PDZ-binding motif that directly interacts with the unique PDZ domain of Sdt in the Crb core complex (Fig. 41 D) [Bachmann et al., 2001, Hong et al., 2001]. Using a His antibody for pull-down and a purified version of His-Sdt^{RF} and the GST-Crb^{intra} (Fig. 41 E), it was verified that GST-Crb^{intra} directly interacts with His-Sdt^{RF} [Lin, PhD thesis, 2015]. The GST-Crb$^{intra\Delta ERLI}$, lacking the last four amino acids, is not capable of interaction with PDZ domains. The proteins His-Bbg, GST-Crb^{intra}, GST-Crb$^{intra\Delta ERLI}$ and GST were expressed in bacteria. A His antibody used for pull-down revealed an interaction between His-Bbg and GST-Crb^{intra} (Fig. 41 F). His-Bbg does not interact with GST-Crb$^{intra\Delta ERLI}$ or GST alone (Fig. 41 F). In conclusion, the His-Bbg directly interacts with the PDZ-binding motif of Crb, *in vitro*.

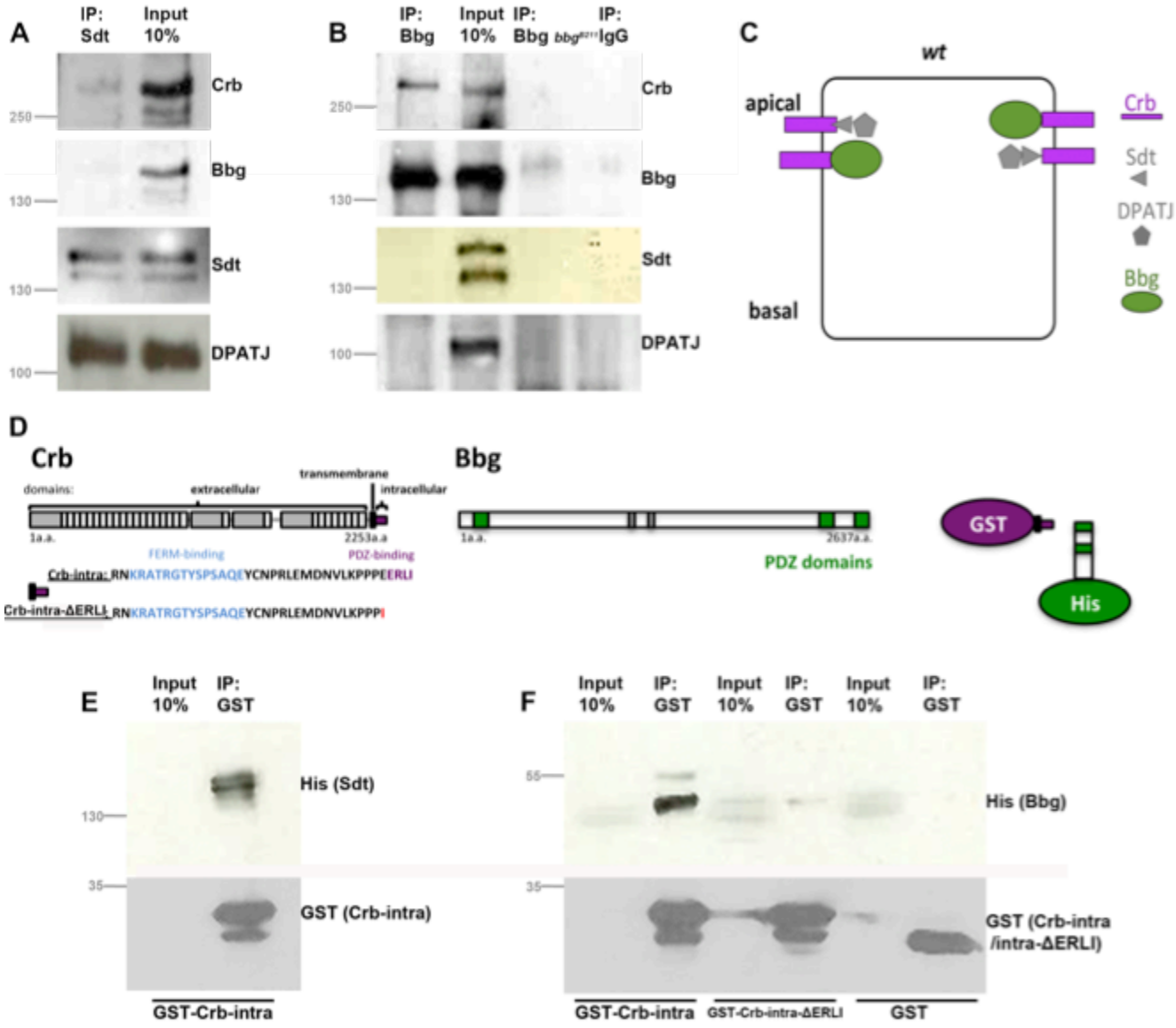

Figure 41: Bbg directly interacts with Crb, independently of Sdt and DPATJ. (A) Crb, DPATJ but not Bbg are immunoprecipitated with a-Sdt antibody from extracts of *wild-type* adult abdomens. **(B)** Crb, but not Sdt and DPATJ are immunoprecipitated with a-Bbg antibody from extracts of *wild-type* adult abdomens. None of the above proteins are immunoprecipitated with a-Bbg antibody from extracts of bbg^{B211} adult abdomens. None of the above proteins are immunoprecipitated with a-IgG antibody from extracts of *wild-type* adult abdomens, too. **(C)** Schematic drawing of a wing disc epithelial cells with the 2 independent complexes between Crb-Sdt-DPATJ and Crb-Bbg. **(D)** Schematic drawing of Crb-intra, Crb-ΔERLI and truncated Bbg. The His tag is in the C-terminus of the recombinant-Bbg protein. **(E)** *In vitro*, pull down experiment: Sdt purified protein is pulled-down with a-GST antibody detecting Crb-intra, meaning that Crb physically interacts with Sdt. **(F)** *In vitro*, pull down experiment: truncated Bbg purified protein is pulled-down with a-GST antibody detecting only Crb-intra, but not with a-GST antibody detecting Crb-ΔERLI or GST, meaning that Crb physically interacts with Bbg, too.

Notch signaling seems not to be affected in *bbg*^{B211} mutant wing discs

Bbg was localized in the apical cortex of the wing disc epithelium. Next it was investigated if the localization of the apical signaling proteins Notch and Delta [Sasaki et al., 2007] was affected in the absence of *bbg*. Notch, the receptor of the pathway was not affected in *bbg*^{B211} discs (Fig. 42 A-B'). This was also the case with the ligand of Notch signaling pathway, Delta (Fig. 42 C-D'). The two target genes of the Notch pathway, Wingless and Cut were then checked for. Wingless is expressed in a diffused manner along the Dorsal-Ventral boundary in the pouch of the wing discs and was not altered in the *bbg*^{B211} (Fig. 42 E-F'). Cut is expressed in the nucleus of the cells along the DV boundary and the expression levels were not altered in the *bbg*^{B211}, as well (Fig. 42 G-H').

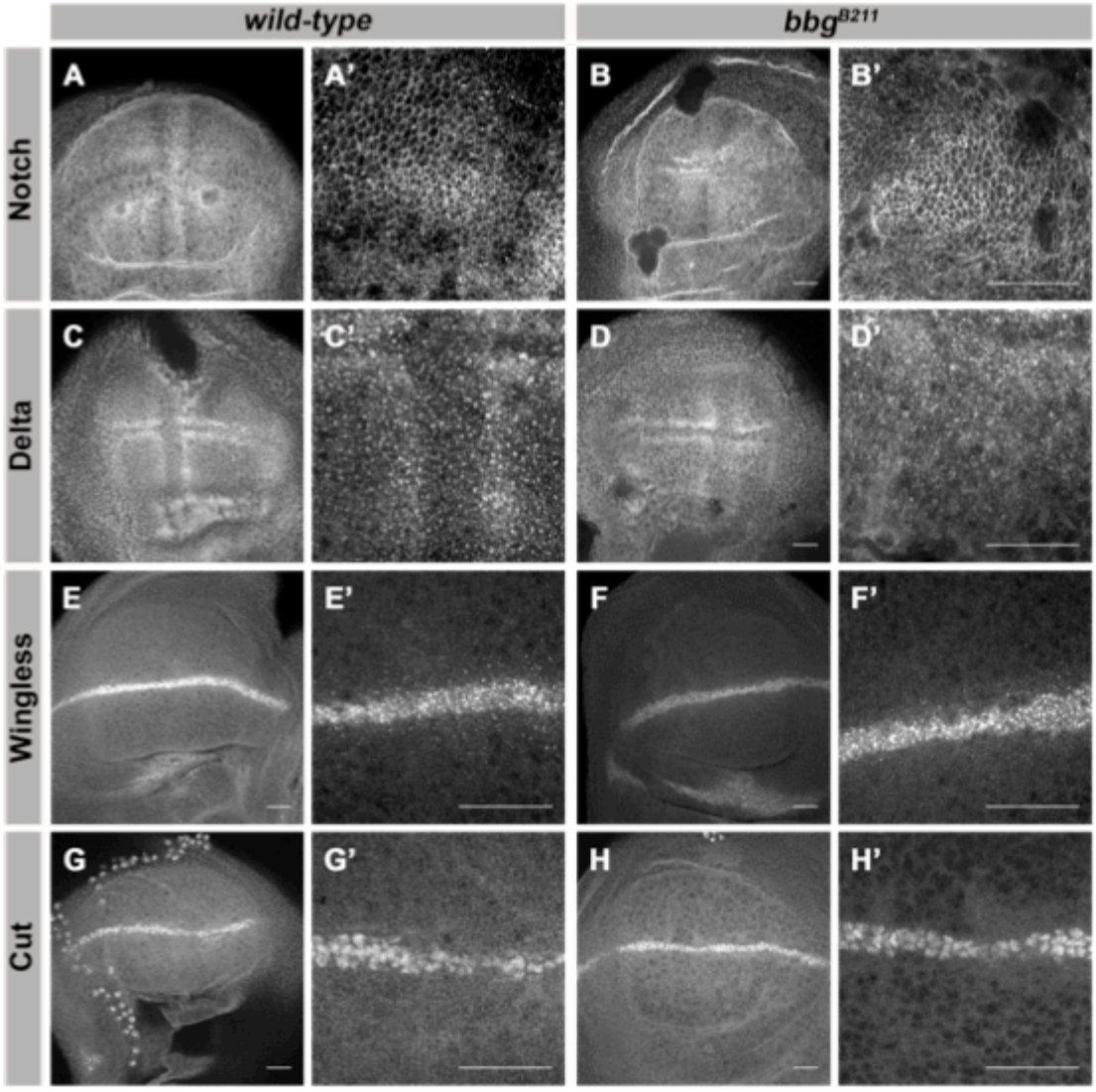

Figure 42: Notch signaling seems not to be affected in *bbg*^{B211} mutant wing discs Third-instar wt (left panels) and *bbg*^{B211} (right panel) wing disc pouch stained with **(A-B')** Notch, **(C-D')** Delta, **(E-F')** Wingless and **(G-H')** Cut, respectively. Scale bars, 25 µm.

Identification of Bbg interactors using Mass Spectrometry

To determine how Bbg regulates the localization of apical determinants (Fig. 35-37) in the wing disc epithelium and eventually the tissue growth (Fig. 13 J-L), and to identify interactors of Bbg, a mass spectrometry (MS) screen was conducted. The screen was done using wt wing disc lysate. This lysate was incubated with the Bbg antibody for immunoprecipitation and then the whole sample was loaded onto a gel. IgG was used as the negative control in this experiment. The gel was then sequentially fragmented into four pieces and analyzed with MS in order to identify possible regulators of Bbg (collaboration with Anna Shevchenko) (Fig. 43 A). After three experimental

repeats 186 hits were obtained as putative interactors of Bbg (Fig. 43 B, Appendix). The MS data showed 17 hits as interactors of IgG only (Fig. 43 B, Appendix) and 61 hits that overlap in both lists, as interactors for both anti-Rabbit-Bbg and anti-Rabbit-IgG (Fig. 43 B, Appendix). In order to find specific hits obtained, several criteria were applied such as, 1) the protein threshold to be at least 99%, 2) the minimum peptides to be at least two, 3) the presence of expression in wing discs, 4) any possible function of the protein in wing development and 5) characterized proteins. Some genes that regulate cell polarity and/or tissue growth were also chosen independent of the MS screen. With this procedure the hits were minimized to 15 (Table 1). As shown in Table 1, the proteins were categorized into three independent categories, based on their function, from cell polarity/growth to cell cycle control.

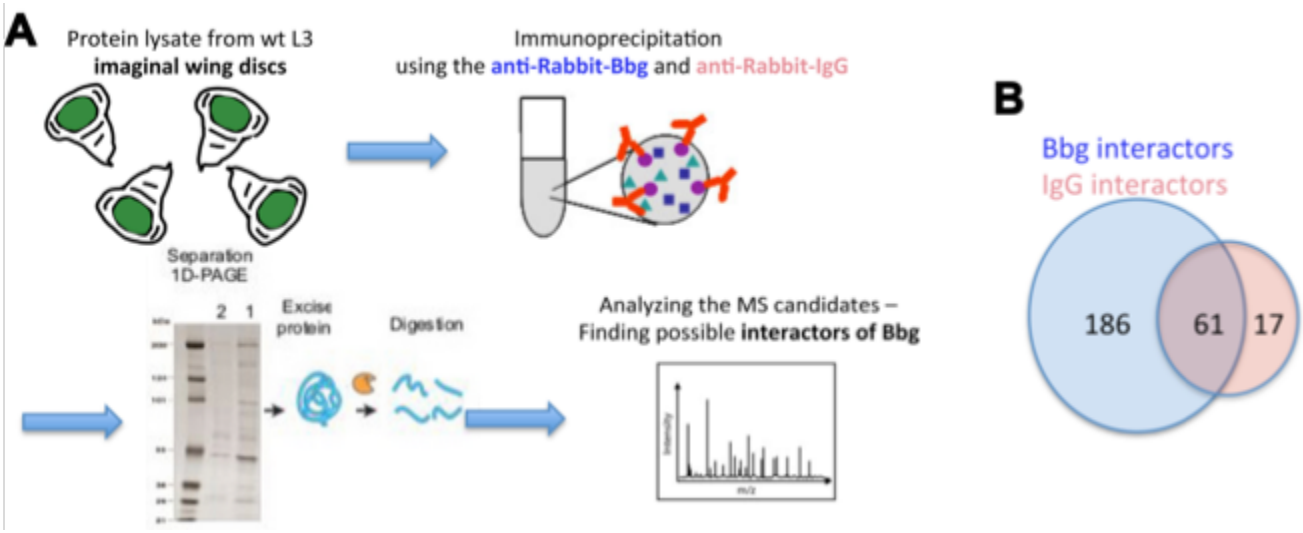

Figure 43: Mass Spectrometry analysis after IPs with anti-Rabbit-Bbg and anti-Rabbit-IgG, in order to identify interactors of Bbg. (A) Schematic representation of the MS procedure after immunoprecipitation with the Bbg and IgG. **(B)** Identification of the MS interactors of Bbg, IgG and the overlapping after 3 experimental repeats.

category	name of protein	main domain/-s	main function/-s
1	Spaghetti squash	Myosin heavy chain binding, Calcium ion binding	Myosin II filament assembly
	*** β spectrin**	Actin binding	Cytoskeletal binding
	Echinoid	Immunoglobulin 2, Fibronectin III	Homophilic cell adhesion
	*** Polychaetoid**	PDZ, SH3	Apical protein localization
	*** Canoe**	PDZ, Ras-association	RAS GTPase binding, embryonic morphogenesis
	Crumbs	EGF-like, Laminin G	Establishment and maintenance of cell polarity
	Stardust	SH3 domain, PDZ domain	Establishment and maintenance of cell polarity
	Atypical Protein Kinase C	PB1, Protein kinase C	Establishment and maintenance of cell poalrity
	Bazooka	PDZ domain	Establishment and maintenance of cell polarity
	*** LethalGiantLarvae**	Lgl-like, WD40	Cellular biogenesis, Larval development
2	Wingless	Wnt, Wnt protein	Wing extension
	*** Toucan**	Kinase binding	Wing morphogenesis
	*** WNK homolog**	Serine/threonine kinase	Wing disc development, regulator of Wnt signaling
3	*** Mud**	DNA binding	Mitotic spindle orientation
	*** Bub3**	WD40	Mitotic spindle assembly

Table 1: Possible interactors of Bbg identified. Table of categorized MS candidates – possible interactors of Bbg. The candidates were categorized in three independent categories regarding to their function: 1. Cytoskeletal organization/ tissue polarity and growth, 2. Wing morphogenesis and 3. Cell cycle control. The **MS candidates** are indicated in **bold with an asterisk**.

Genetic interactions between *bbg* and possible interactors

In order to understand the relationship between these 15 most interesting candidates and *bbg* (Table 1), a genetic screen was conducted with double knock down of both genes (one of these 15 candidate genes and *bbg*) in order to identify any interesting genetic interaction based on the size of the wings. Knocking down *bbg* shows a smaller wing phenotype compared to the wt wing size (Fig. 13 J-L). The following question was if the knocking down of the candidates would give a wing phenotype and if the double knock down of the interesting candidates one at a time with *bbg* showed any genetic interaction. Two independent Gal4 drivers specific for the wing were used to express the *RNAi* constructs, *engrailed (en)-Gal4* and *69b-Gal4*. Interestingly, the double knock down of *bbg* and seven of the candidate genes showed enhancement of the wing phenotype in comparison to that obtained upon knocking down the genes alone: *crumbs (crb), spaghetti squash (sqh),*

canoe (cno), lethal giant larvae (lgl), atypical Protein Kinase C (aPKC), Echinoid (Ed) and *mud* (Fig. 44 A-G and Table 2). In some cases, it was not possible to study the genetic interactions between *bbg* and the potential interacting partner, as knocking down some of the candidates' alone showed lethality (~100%) (Fig. 44 B3, D6, E6 and F6). Importantly, knocking down *bbg* and *sqh* at the same time with *69b-Gal4*, showed 90% lethality (Fig. 44 B 7). Knocking down *bbg* and *ed* showed lethality, although the percentage was not counted. In conclusion *bbg* genetically interacts with *crb, sqh, cno, lgl, aPKC, ed* and *mud* (Table 2).

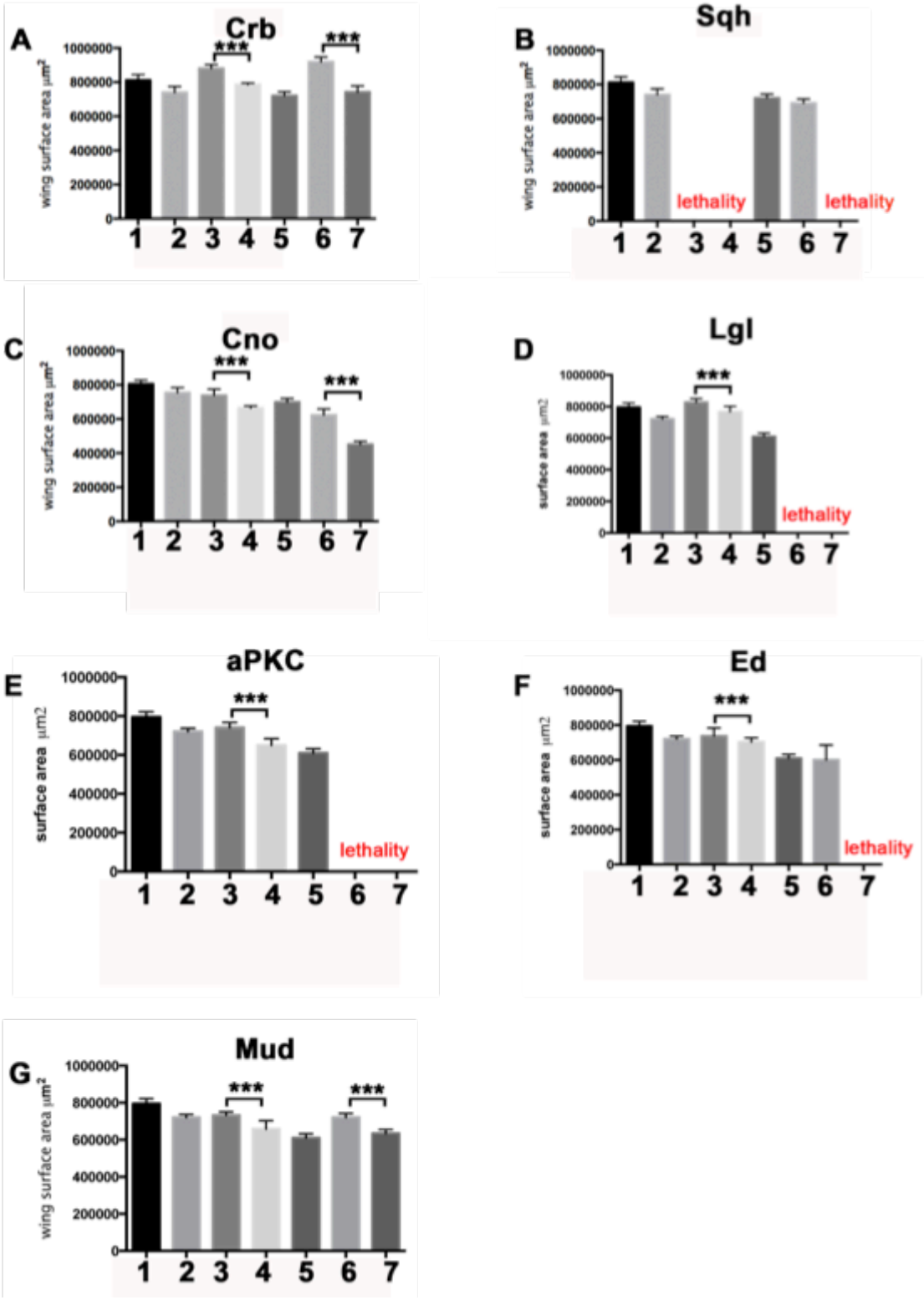

Figure 44: Genetic interactions between *bbg* with *crb, sqh, cno, lgl, aPKC, ed* and *mud*. Statistical analysis of measuring the surface area of 15 adult wings per condition. **(1)** *wt*, **(2)** *en>bbg*^{RNAi}, **(3)** *en>Xgene*^{RNAi}, **(4)** *en> bbg*^{RNAi}*;Xgene*^{RNAi}, **(5)** *69b>bbg*^{RNAi}, **(6)** *69b>Xgene*^{RNAi}, **(7)** *69b> bbg*^{RNAi}*;Xgene*^{RNAi}. For the analysis TTEST and ANOVA test was used. Three asterisks indicate $p \leq 0.001$. Error bars show standard deviation.

category	name of protein	main domain/-s	main function/-s
1	Crb	EGF-like, Laminin G	Establishment and maintenance of cell polarity
	Sqh	Myosin heavy chain binding, Calcium ion binding	Myosin II filament assembly
	Cno	PDZ, Ras-association	RAS GTPase binding, embryonic morphogenesis
	Lgl	Lgl-like, WD40	Cellular biogenesis, Larval development
	aPKC	PB1, Protein kinase C	Establishment and maintenance of cell poalrity
	Ed	Immunoglobulin 2, Fibronectin III	Homophilic cell adhesion
3	Mud	DNA binding	Mitotic spindle orientation

Table 2: Genetic interactors/enhancers of *bbg*. Table of Genetic interactors/enhancers of *bbg*. The candidates were categorized in two independent categories regarding to their function: 1. Cyotskeletal organization/ tissue polarity and growth, and 3. Cell cycle control. (based on Table 1).

However, the other eight genes (from Table 1) did not show any genetic interactions with *bbg* with this assay (Fig. 45 A-I). These included *bazooka (baz), stardust (sdt), βspectrin (βspec), polychaetoid (pyd), toucan (toc), WNKhomolog (wnk), bub3 and wingless (wg)*, respectively (Fig. 45 A-I). In some cases, it was not possible to study the genetic interactions between *bbg* and the potential candidate using the *69b-Gal4* drivers, as knocking down some of the candidates' alone showed lethality (~100%) (Fig. 45 B, G-I).

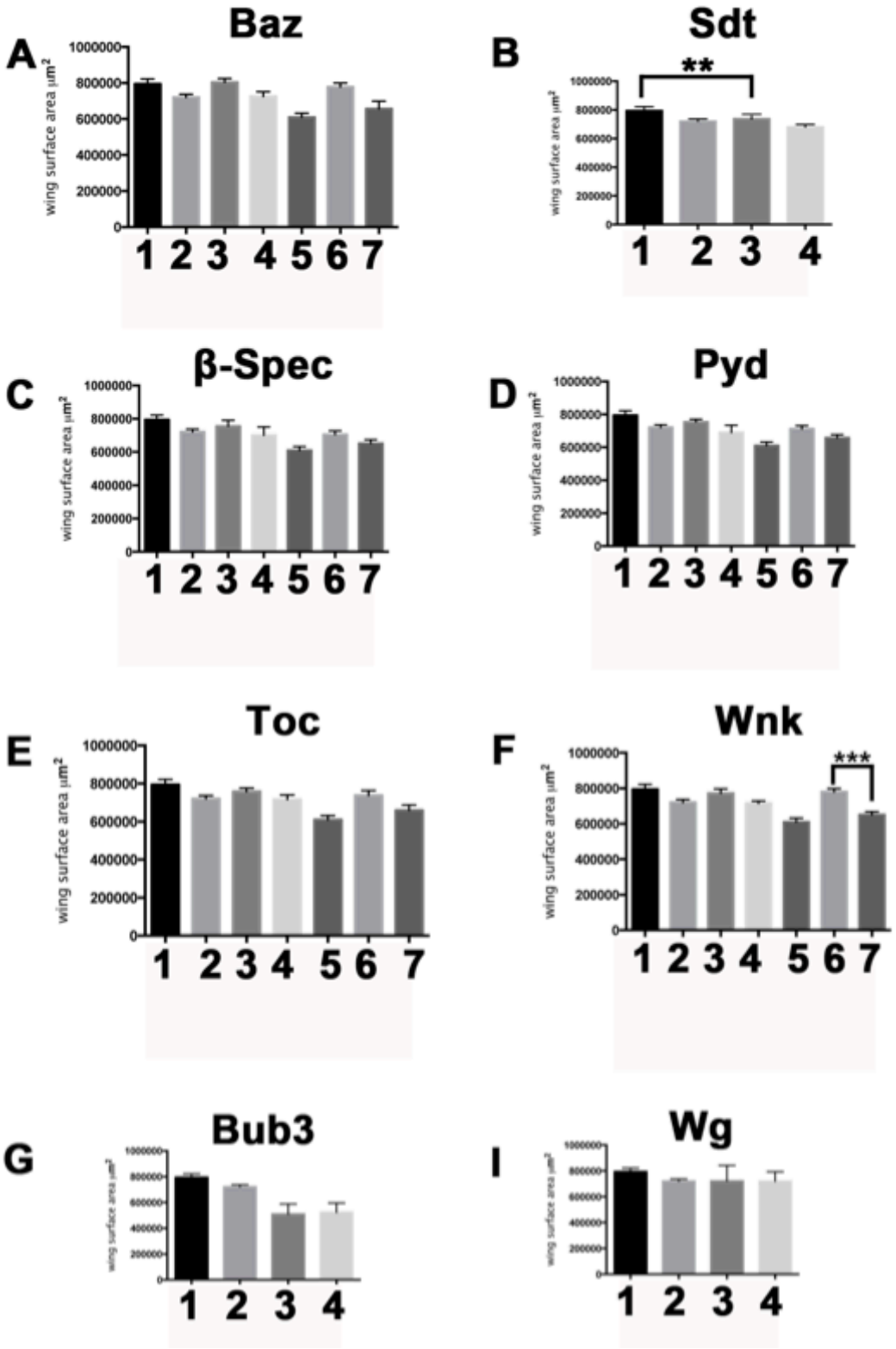

Figure 45: The genes baz, sdt, βspec, pyd, toc, wnk, bub3 and wg do not interact with *bbg*. Statistical analysis of measuring the surface area of 15 adult wings per condition. **(1)** *wt*, **(2)** *en>bbg*^{RNAi}, **(3)** *en>Xgene*^{RNAi}, **(4)** *en> bbg*^{RNAi}*;Xgene*^{RNAi}, **(5)** *69b>bbg*^{RNAi}, **(6)** *69b>Xgene*^{RNAi}, **(7)** *69b> bbg*^{RNAi}*;Xgene*^{RNAi}. For the analysis TTEST and ANOVA test was used. Two asterisks indicate $p \leq 0.01$. Three asterisks indicate $p \leq 0.001$. Error bars show standard deviation.

crb and *bbg* compensate each other geneticaly

As shown in figure 44 A, the simultaneous knock down of *bbg* and *crb* resulted in a smaller wing phenotype. This is in contrast to the overgrowth phenotype of the knock down of *crb* (Fig. 44 A). It was previously known that knock down of *crb* produces an overgrowth wing phenotype [Robinson et al., 2010, Grzeschik et al., 2010, Ling et al., 2010, Chen et al., 2010]; (Fig. 44 A and 46 A-C). Put together, the wing size is the biggest in the knock down of *crb*, it gets smaller with the simultaneous knock down of *crb* and *bbg* and smallest in the knock down of *bbg* alone (Fig. 44 A and 46A-F). Probably *crb* and *bbg* compensate each other. The genetic interaction between *bbg* and *crb* is also mentioned in this paragraph because in ~50% of the cases the simultaneous knock down of *crb* and *bbg* produced flies with deformed wing (Fig. 46 G).

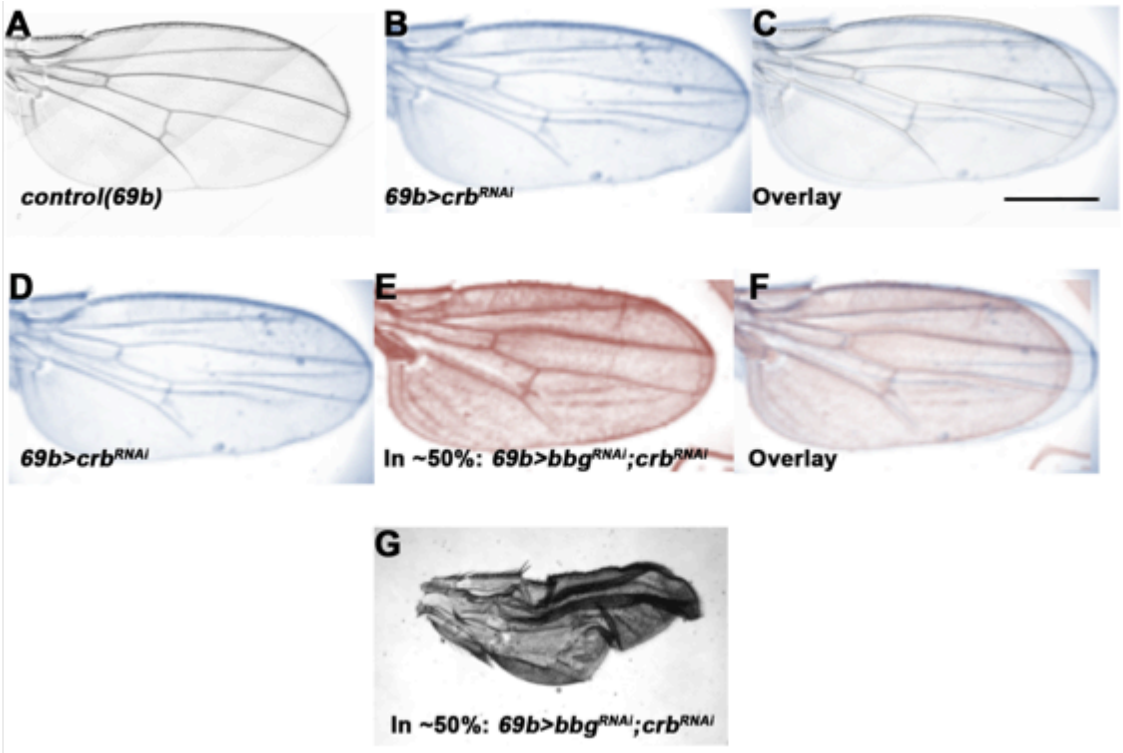

Figure 46: *crb* and *bbg* compensate each other geneticaly (A-C) Adult wing phenotypes of control, *69b>crb*^{RNAi} and overlay, respectively. **(D-G)** Adult wing phenotypes of *69b>crb*^{RNAi}, *69b>crb*^{RNAi}*;bbg*^{RNAi} and overlay, respectively. **(G)** Extreme wing phenotype of *69b>crb*^{RNAi}*;bbg*^{RNAi}. Scale bars, 500 µm.

Bbg stabilizes Sqh in the apical cortex of the wing discs

Given that *bbg* strongly interacts with *sqh* genetically, knocking down *bbg* and *sqh* at the same time with *69b-Gal4*, showed 90% lethality (Fig. 44 B 7) The interaction between *bbg* and *sqh* was further analyzed. When knocking down *bbg* and *sqh* at the same time, the development was normal up to late pupal stage but the flies never hatched from the pupal case. *sqh* (*non-muscle myosin II*) encodes an actin-binding protein that has actin cross-linking and contractile properties and is regulated by the phosphorylation of its light and heavy chains. Myosin molecules can walk along, propel the sliding of or produce tension on actin filaments [Manzanares et al., 2009].

Immunostaining analysis showed that Sqh [Sqh:GFP] localizes to the apical cortex in L3 wing discs and colocalizes with Bbg (Fig. 47 A-B''). Notably, in bbg^{B211} wing discs, Sqh localization was affected (compare Fig. 47 C' to A'). Western blot analysis of wing disc extracts showed almost ~ 50% reduction of Sqh in bbg^{B211} (Fig. 47 D). Next sqh^{RNAi} was expressed under the control of *en-Gal4* in wing discs, to check the localization of Bbg and analyze tissue integrity (Fig. 47 E-E''). In order to distinguish the anterior (A) and the posterior (P) compartment the marker Ptc, which is expressed in the A-P boundary, was used (Fig. 47 E''). The localization of Crb and Bbg was not affected (Fig. 47 E, E'). Interestingly the cells had a larger apical surface area in the P compartment, where *sqh* was knocked down (Fig. 47 E), phenocopying the bbg^{B211} phenotype (Fig. 31 B-B'). However, Dlg remained unaltered upon the double knock down of *bbg* and *sqh* in wing discs (Fig. 47 F-F''). These results suggest that Bbg stabilizes Sqh in the apical cortex of the monolayer epithelial sheet of wing discs.

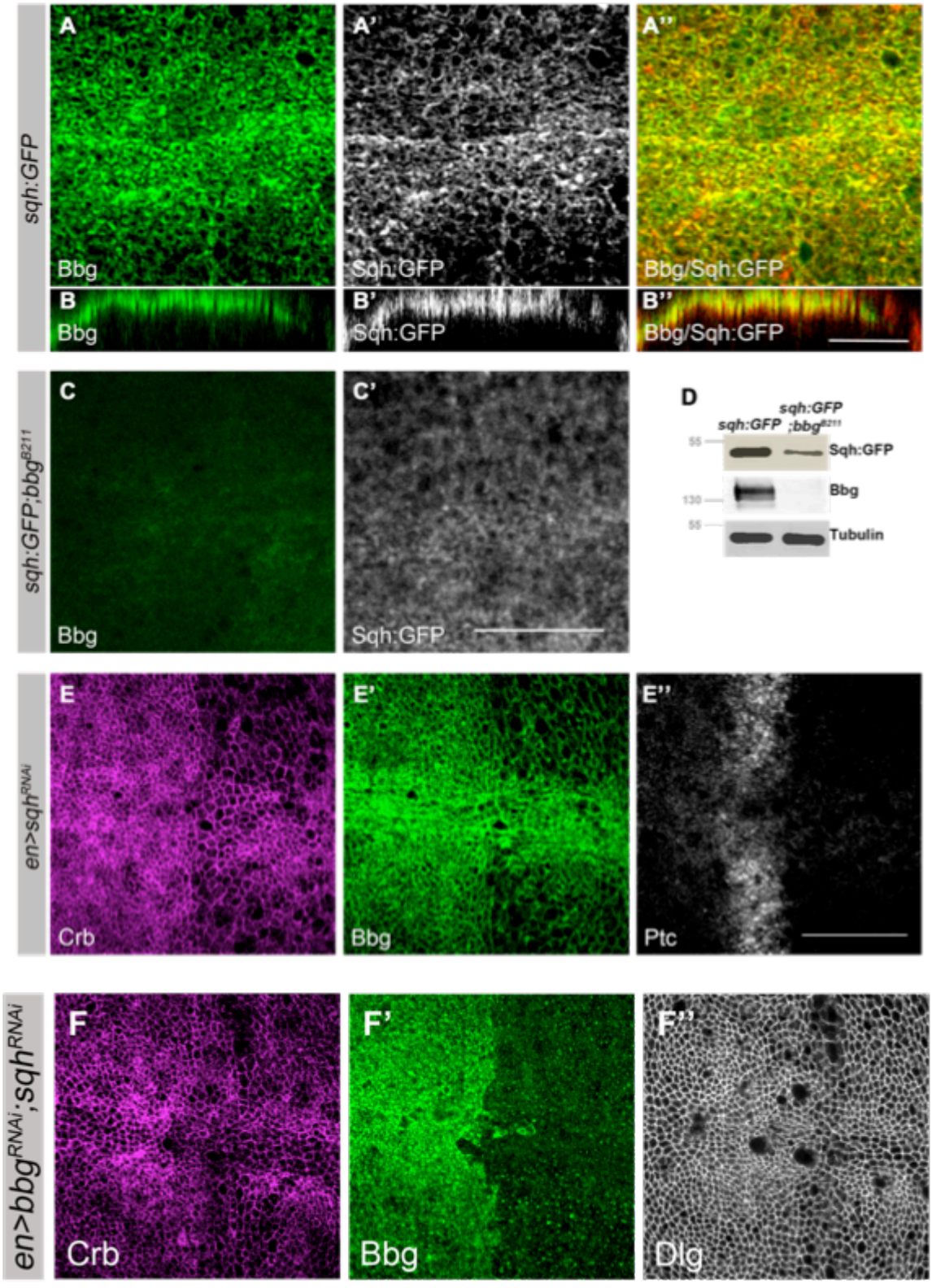

Figure 47: *bbg* regulates Sqh cytoskeletal organization (A-A'') Third-instar *sqh:GFP* wing disc pouch stained with Bbg, GFP and overlay, respectively. **(B-B'')** xz position of the central area of (A). **(C-C')** Third-instar *sqh:GFP;bbg*^{B211} wing disc pouch stained with Bbg andante-mouse-GFP, respectively. **(D)** Western blots from third-instar *sqh:GFP* and *sqh:GFP;bbg*^{B211} *Drosophila* wing discs with GFP, Bbg and Tubulin as a loading control demonstrating an reduction of Sqh:GFP in *sqh:GFP;bbg*^{B211}. **(E-E'')** Third-instar *en>sqh*^{RNAi} wing disc pouch stained with Crb, Bbg and Ptc, respectively **(F-F'')** Third-instar *en>bbg*^{RNAi}*;sqh*^{RNAi} wing disc pouch stained with Crb, Bbg and Dlg respectively. Scale bars, 25 µm.

Bbg is in the same complex with Sqh in wing discs

To identify how Bbg regulates the stability of Sqh in the apical cortex of the wing discs, immunoprecipitation with a GFP antibody (corresponds to Sqh:GFP) was performed using wing disc lysate. Bbg was pulled down in this experiment (Fig. 48, left two lanes). However, Sqh:GFP was not detected in the input (Fig. 48 left lane). This might be due to the small quantity of the protein in the wing disc extract. This experiment needs to be repeated. As a negative control the wt tissue was used. Here, the GFP antibody (corresponds to Sqh:GFP) did not pull down Bbg (Fig. 48, right two panels). In conclusion, Bbg forms a complex with Sqh in order to stabilize Sqh in the apical cortex of the monolayer epithelial sheet of wing discs.

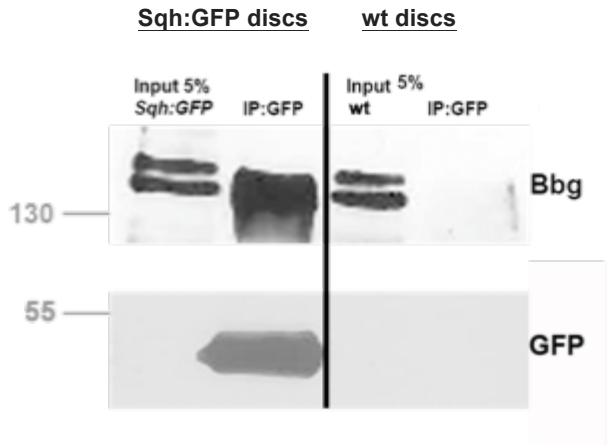

Figure 48: Bbg is in the same complex with Sqh in wing discs. Bbg is immunoprecipitated with a GFP-antibody from extracts of *Sqh:GFP* wing discs (two left lanes). However, Bbg is not immunoprecipitated with a GFP-antibody from extracts of wt wing discs (two right lanes).

Discussion

Several observations link cytoskeletal organization to tissue growth. Our results support that a gene namely *bbg* regulates wing tissue growth through regulation of the cytoskeletal organization. *bbg* and *crb* genetically interact as the absence of *bbg* upon overexpression of $Crb^{extraTM}$-*GFP* regulate wing tissue growth. Bbg has a novel localization in the apical cortex of the wing disc cells and stabilizes the actin-binding motor protein, Sqh in the apical cortex of the wing disc epithelium. Bbg acts as a scaffolding molecule, stabilizing apical proteins like Crb in the sub-apical region, too. The referring results of this thesis can be discussed in four different sections: role of overexpression of $Crb^{extraTM}$-*GFP* in tissue growth (I) and role of *bbg* in eye development (II), in different epithelia tissues (III), and tissue growth (IV) in *Drosophila*.

The role of the overexpression of $Crb^{extraTM}$-*GFP* in tissue growth

As shown by Linda Nemetschke overexpression of $Crb^{extraTM}$-*GFP* results in smaller wings (Fig. 13 A-C). It is already known that overexpression of Crb^{intra}/Crb^{full} or absence of *crb* results in overgrowth wing phenotypes and this is linked to Hippo signaling pathway [Robinson et al., 2010, Ling, Chen et al., 2010]. This opposing phenotypes regarding the wing size observed, either from $Crb^{extraTM}$-*GFP* or Crb^{intra} overexpression, should be due to different functions of the extracellular and the intracellular domain of Crb, although this is not clear yet. Another possibility could be that overexpression of $Crb^{extraTM}$-*GFP* directly affects the localization and/or the activity of endogenous Crb (including Crb^{intra}). It is already known that Crb^{extra} can directly interact with each other in *cis* and *trans* [Zou et al., 2012, Fletcher et al., 2012, Letizia et al., 2013]. It has been also reported that overexpression of $Crb^{extraTM}$-*GFP* in the wing discs leads to mislocalization of endogenous Crb (that includes Crb^{intra}) [Hafezi et al., 2012].

Whether overexpression of $Crb^{extraTM}$-*GFP* affects directly the Hippo signaling pathway is not clear yet. One possibility is that $Crb^{extraTM}$-*GFP* interacts with an upstream component of the Hippo signaling pathway, like the

atypical cadherin Fat, a protein with an extracellular domain, too [Halder and Johnson, 2011]. In conclusion, overexpression of *Crb^{extraTM}-GFP* could directly affect the levels of endogenous Crb or interacts with another upstream component of the Hippo pathway (e.g. Fat, Kibra, or Expanded) and directly or indirectly perturbs the Hippo signaling pathway. The interaction between *Crb^{extraTM}-GFP* and Kibra or Expanded is also supported with the genetic interaction between the Hippo upsteream components (*expanded* and *kibra*) and the overexpression of *Crb^{extraTM}-GFP* (Fig. 8).

The role of *bbg* in eye development

Given that Bbg was expressed specifically and dynamically during retina development, the function of the gene was analyzed. The pigment cells were larger in size in the absence of *bbg* (Fig. 26 A' to C'). Maybe the pigment cells are larger because they loose their mechanical structure and the cytoskeletal organization, a possible scenario that would be interesting to study further. Another interesting observation was, that when flies carried *bbg^{B211}* eyes were kept in constant light for seven days, the retina showed a gradual degeneration phenotype (Fig. 27 C', arrow). The degeneration phenotype, taking place in *bbg^{B211}* flies was not 100% severe. In some cases five or six rhabdomeres were counted, instead of seven (normal) (Fig. 27 C', arrow). This result needs further analysis using electron microscopy and quantification of the severity of the phenotype of *bbg^{B211}* flies. The exact mechanism that Bbg, which is expressed in pigment cells, affects the integrity of the retina remains elusive. Whether or not the pigment cells play crucial role in the homeostasis of photoreceptor cells is not clear yet. In vertebrates, the pigment epithelium plays essential role in the renewal of rhodopsin and defects in the pigment epithelium leads to degeneration of photoreceptor cells [Marmorstein et al., 1998]. More specifically, a feature of the pigment epithelium is the apical distribution of Sodium pump α subunit protein (also known as Na^+K^+ATPase), in order to maintain the balance of NA^+ and K^+ in the subretinal space [Marmorstein et al., 1998]. A yeast two-hybrid screen was conducted for possible interactors of Bbg [Kim, PhD thesis 2006]. One of

the most probable interactors of the second PDZ domain of Bbg was the Na^+K^+ATPase, which is a transmembrane protein that catalyzes hydrolysis of ATP coupled with the exchange of Na^+ and K^+ ions across the plasma membrane (from Flybase). Thus, maybe the link between retina development and Bbg is the interaction of Bbg with the Na^+K^+ATPase and the exchange of Na^+ and K^+ ions across the plasma membrane. This is an interesting project that needs further analysis in the future.

The role of *bbg* in different epithelia tissues

Embryogenesis proceeds normally in the absence of *bbg* and the localization of Crb remains unaltered as readout of the embryonic epithelial tissue integrity (Fig. 21). Probably this is due to a redundancy between *bbg* and another gene or signaling pathway that is still unknown. In a sensitized background perturbing together *bbg* with a possible interactor of *bbg* should show a phenotype during embryogenesis. This possible interactor should be a membrane protein or a membrane linked protein as Bbg, is expressed in epidermis or adjusts to epidermis at stage 12 (Fig. 19 C). Baz and Pyd are expressed in the epidermis during embryogenesis and both of them are PDZ domain proteins like Bbg [Mckinley et al., 2012; Choi et al., 2011]. It was mentioned in the introduction that PDZ domains can interact with each other. However, based on the fact that *bbg* produces multiple isoforms, *bbg* should also be pleiotropic in function without a crucial role during embryogenesis.

Given that *bbg* regulates the migration of border cells during oogenesis [Aranjuez G et al., 2012], it was also analyzed the role of Bbg in this stage. It was identified that *bbg* mRNA and protein was localized apically in the epithelium sheet of the follicle cells (Fig. 22 A-B). This is not surprising as several genes show similar mRNA and protein localization, like *crb* [Tepass et al., 1990]. Bbg was highly expressed in the posterior polar cells (Fig. 22 A st. 5, arrow). This is probably due to the fact that *bbg* affects migration of the posterior border cells [Aranjuez G et al., 2012]. Border cells migrate as a cohesive cluster of six to ten cells during late oogenesis in a highly regulated process [Montell 2003]. Migrating cells display morphological changes

induced by dynamic rearrangement of actin filaments providing the necessary force for movement [Ridley 2011]. The interaction of Bbg with Sqh, an actin binding protein, as shown in wing discs (Fig. 47-48) also be important for border cell migration, and it would be interesting to analyze of this relationship in the future.

The absence of *bbg* from the wing disc epithelium affects only the localization of some apical proteins (Fig. 35-37). Bbg could act as a scaffolding molecule stabilizing protein complexes, and this assumption is supported by several findings. Bbg is a PDZ domain protein. It is well known that most PDZ domain proteins act as scaffolding molecules [Cunningham et al. 2010]. Bbg has the properties to act as a scaffolding molecule, as it has multiple alternative splice variants and is a large molecule, with the largest isoform to be approximately 280 kDa. The localization of Bbg is also strictly apical in the wing disc epithelium, like Crb, *D*PATJ, aPKC Baz and all of them are affected (Fig. 35-37). Bbg is not expressed laterally; therefore the localization of the lateral proteins *D*E-cadherin and Dlg is not altered (Fig. 35 A'' and C'', 37 C and F). Thus, several lines of evidence support a role for Bbg as a scaffolding molecule in the stabilization of apical protein complexes.

A question that is raised regarding the interaction between Bbg and Crb is how Bbg, a cytoplasmic protein interacts with the intracellular domain of Crb, since *bbg* genetically interacts with $Crb^{extraTM}$*-GFP*. One explanation could be that overexpression of $Crb^{extraTM}$*-GFP* directly affects the localization and/or the activity of endogenous Crb (including Crb^{intra}). In that scenario, the interaction between Crb^{intra} and Bbg would be perturbed indirectly, upon the overexpression *of* $Crb^{extraTM}$*-GFP*. However the localization of Bbg is not affected after overexpression of $Crb^{extraTM}$*-GFP* in wing discs (Fig. 38). In the future it would be worth to analyze the localization of Bbg in the absence of Crb^{intra}, using the fosmid line for almost endogenous expression of Crb^{extra} in *crb* mutant background.

Analyzing further the epithelial tissue of the wing disc, the structure of microvilli and the adherens junctions remained unaltered in the absence of *bbg*, shown by electron microscopy (Fig. 40 A, A', B and B'). However the septate junction ladder-like structure was disrupted in the absence of *bbg* (Fig. 40 A'' and B''). EM cross-sections images reveal that, septate junctions

display characteristic electron-dense ladder-like structures of 10–20 nm width called septa [Tepas et. al., 2001]. When a septate junction is viewed at right angles to the long axis of the septa, each septum extends across the intercellular space between adjacent cell membranes producing the ladder-like structure [Hand and Gobel, 1971]. Some of the main components of the septate junctions are Na^+K^+ATPase, Neurexin, Coracle, Yurt, Dlg and Pyd [Ganot et al., 2014]. It is worth to mention that it is already reported that Bbg affects and perturbs the smooth septate juntions of the adult midgut [Bonnay et al. 2013]. In this thesis it is shown that the septate junction markers Coracle and Dlg remain unaltered in bbg^{B211} wing discs (Fig. 35 A'' and C'', 39 C and D). One possibility is that indeed the structure of the junctions is affected in the bbg^{B211}. However, the disruption of the septate junctions maybe is not strong enough to destabilize the localization of Dlg and Coracle or the immunostaining, as a technique, is not sensitive enough to detect the disruption of the septate junctions. Another explanation could be that the septate junctions of the wing disc epithelium in the absence of *bbg* are not affected and this result is an artifact, due to technical reasons, e.g. fixation time of the tissue. In the future it would be worth trying different time points of fixation in bbg^{B211} tissue followed by analysis of the structure of the septate junctions by EM.

The role of *bbg* in tissue growth

Multicellular organisms need to control their size throughout development and adult life in the face of challenges such as rapid growth during development [Conlon and Raff 1999]. Unraveling the mechanisms that regulate tissue growth in epithelial tissues in order to generate organs of the correct size and proportion remains a crucial goal of developmental biology. One suitable epithelial tissue, as it is already mentioned, is the proliferative monolayer epithelial sheet of the imaginal wing disc, which will give rise to the adult wing in *Drosophila* [Aegerter-Wilmsen et al., 2007]. The Hippo signaling pathway regulates tissue growth in wing development [Halder and Johnson 2011]. There are several observations that link tissue growth/Hippo signaling

with the actin cytoskeletal organization. Some of the proteins that regulate the actin cytoskeleton are the Capping proteins, and the myosins Sqh and Dachs.

It was recently reported that induction of extra F-actin formation by loss of Capping proteins A or B induced strong overgrowth in *Drosophila* imaginal discs through modulating the activity of the Hippo pathway [Sansores-Garcia et al., 2011]. It was also published that Sqh regulates wing growth through the Hippo signaling pathway [Rauskolb et al., 2014]. Reminding that Sqh results in assembly of bipolar actin filaments binding F-actin to generate contractility [Niederman and Pollard., 1975]. Specifically, direct activation of Sqh activity by expression of Sqh^{E20E21} (containing phosphomimetic Ser to Glu mutations at regulatory sites of Sqh, Jordan and Karess, 1997) could also increase tissue growth, induce *ex-lacZ* expression and decrease Yki phosphorylation. A positive F-actin regulator, Zyxin (Zyx) presumably undergoes conformational change when interacting with an upstream Hippo pathway component, Dachs [Rauskolb et al., 2011]. This conformational change facilitates binding between Zyx and Warts, another component of the Hippo signaling pathway [Rauskolb et al., 2011].

It has been published that the actin binding protein Dachs can regulate tissue growth through proper cell division orientation. More specifically *dachs* mutant wings are smaller in size with larger cells in the imaginal wing discs [Mao et al., 2011]. It has been also shown that Dachs constricts cell–cell junctions to change the geometry of cell shapes at the apical surface, and that cell shape then determine the orientation of the mitotic spindle. Whether or not the smaller wing phenotype, which we also observed by the absence of *bbg*, is due to the Hippo signaling pathway, the organization of the actin cytoskeleton, the orientation of cell divisions or the combination of them, is not clear yet. All the previous observations forced us to ask whether *bbg*, a gene that affects tissue growth is linked to actin cytoskeletal organization.

To determine how Bbg regulates the tissue growth (Fig. 13 J-L), a mass spectrometry (MS) screen was conducted in order to identify interactors of Bbg. In the MS data there were identified several myosins (Appendix). Therefore it was decided to future analyze Sqh, as it regulates tissue growth. Bbg is in the same complex with Sqh and stabilizes Sqh in the apical cortex. This is verified from the observation that Bbg and Sqh genetically interact with

each other (Fig. 44 B). Bbg colocilizes with Sqh in the apical cortex of the wing discs (Fig. 47 A-B''). Bbg affects the localization and the levels of Sqh (Fig. 47 C-D). Immunoprecipitation experiments showed that Bbg is in the same complex with Sqh in wing discs (Fig. 48). It was also identified that RNAi-mediated knockdown of *bbg* disrupted border cell migration during *Drosophila* oogenesis [Aranjuez et al., 2012]. This disruption of the migration of the border cell could be translated in a cytoskeletal defect, as border cells migration requires dynamic cytoskeleton and adhesion changes. Finally, from Flybase it is also reported that a possible interactor of Bbg could be the Dynactin 1 (Dynein binding protein) [Chang et al., 2013]. Dyneins are also motor proteins like myosins and cooperate each other in order to regulate the stability of the cytoskeleton. All the previous observations support the idea that, *bbg* is a novel regulator of the actin cytoskeleton that stabilizes apical proteins and Sqh in order to regulate wing tissue growth.

Regarding the interaction between Bbg and the actin cytoskeleton, it was also observed that the localization of Dachsous (Ds) was affected in the absence of *bbg* (Fig. 39 E and F). Fat (Ft) and Ds are both large, atypical transmembrane cadherins with novel cytoplasmic domains [Clark et al., 1995]. Both *ft* and *ds* mutants were first described having overgrowth phenotypes owned to their distinct importance in the Hippo signaling pathway [Staley and Irvine, 2012]. Ft and Ds were discovered to be necessary for planar polarity (PCP) establishment [Adler et al., 1998]. One important effector of Ds and Ft is the atypical myosin Dachs, which is thought to bind to the Ds intracellular domain and becomes planar polarized towards the distal side of the cell [Brittle et al., 2012]. The interaction between Dachs and Ds is speculated to occur via the myosin head domain of Dachs [Brittle et al., 2012]. Ds is mislocalized or reduced in the absence of *bbg* and this could be explained through an interaction of Bbg with any component of the PCP pathway. Given that *bbg* regulates wing growth, it could also perturb the Hippo signaling pathway, as Ft-Ds does [Gotoh et al., 2015]. In general, it would be interesting to analyze the interaction between Ft-Ds, Bbg and Hippo signaling pathway in imaginal wing discs in the future.

In general, to identify which aspects of the growth phenotype occurred from loss of *bbg*, analyzed at the cellular level the *bbg* wing growth defects in

the wing discs (Fig. 29-33). One possibility is that the cells are excluded from the tissue even in earlier developmental stages, when apoptosis is more evident and is difficult to detect (like L1 or L2) [Milan et al., 1996]. The larger cell phenotype seems to be more a global effect of the smaller wing phenotype. Larger cells were observed in wing discs upon overexpression of *Crb*^{extra}*TM-GFP*, *bbg*^{B211} mutant or knocking down *sqh* (Fig. 31, 32 and 47 E-E''). All previous conditions gave rise to the same phenotype: smaller wings. Probably the cells become larger as an output of the misregulation of their cytoskeletal organization. As it is already mentioned in the absence of *dachs* the cells are larger, leading to defects in the orientation of cell divisions and eventually to smaller adult wings [Mao et al., 2011]. It could be also hypothesized that the smaller wing phenotype observed in the absence of *bbg* is due to a defect in the proper orientation of the mitotic spindle. This possibility can be tested in the future in *bbg*^{B211} mutant wings using live-imaging and mitotic spindle markers of the cells.

Model proposal

Overall, in *bbg*^{B211} mutant cells, mislocalization and reduction of Sqh was observed. Therefore, it can be hypothesized (Fig. 49) that actin stabilization is affected in the apical domain, where Bbg is normally localized. This model can explain the larger cell phenotype in the absence of *bbg*. Actin destabilization or reduction could also explain why the cell cycle progression is slower and apoptosis is increased, without being mutually exclusive (Fig. 29). Bbg is also required for the proper localization of apical proteins like Crb in wing disc epithelium. Crb and Sqh can regulate tissue growth through the Hippo signaling pathway [Tepass, 2012; Rauskolb et al., 2014]. Here is demonstrated that Bbg regulates wing tissue growth, acting as a scaffolding molecule, through the proper localization of apical components of the cells like Crb and the cytoskeletal component Sqh.

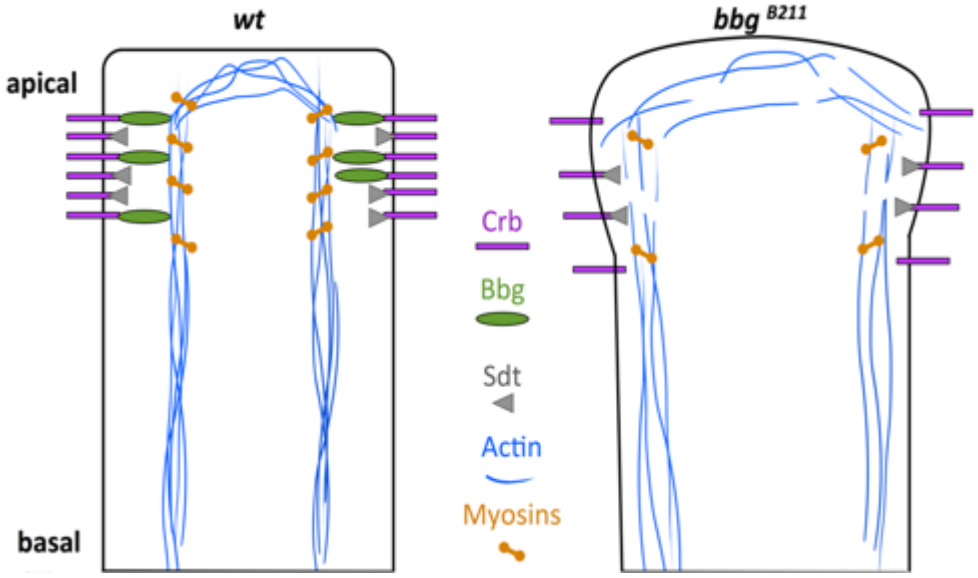

Figure 49: Schematic model showing that *bbg* regulates tissue growth through cytoskeletal organization
In wild-type wing disc cells (left) there are 2 independent complexes between Crb-Sdt-DPATJ and Crb-Bbg. Both of them are apically localized. The actin cytoskeleton is organized tightly with the myosin stabilizing the actin. In the *bbg*^{B211} wing disc cells (right), the apical polarity proteins, like Crb, are reduced from the apical membrane and are more diffused laterally (as it is shown in Fig. 35). Because, in the *bbg*^{B211} cells it was observed mislocalization and reduction of Sqh, it is concluded that the actin stabilization is affected in the apical domain, where Bbg is normally localized. And with this can be explained the larger cell phenotype. The cell cycle progression should be affected or apoptosis is going on, or combination of both of them (as it is noticed in Fig. 29 and live imaging).

Materials and Methods

Genetics

The *bbg*^{B211} null allele was described previously [Kim et al., 2006] and was gifted from Gabrielle Boulianne. *FRT80B.bbg*^{B211}*/TM6B* was generated through recombination with *FRT80B:nls-RFP*. *FRT82B.crb*^{11A22}*/TM6B* stock, was generated in the lab. The *UAS-Crb*^{extra}*-TM-GFP* was described previously [Pellikka et al., 2002] and was gifted from Ulrich Tepass. The Is(2)UAS-crb30.12e, P[w+ UAS-crbmini] (1022 in Knust stock collection) was used. All flies were raised at 25^{0}C. MARCM and flip-out clones were generated by crossing ywhsflp*;;FRT82B/TM6B*, *ywhsflp;;FRT80B/TM6B* and *ywhsflp;actin.FRT.STOP.FRT.Gal4-UAS-GFP* (from S. Eaton) with *FRT82B.crb*^{11A22}*/TM6B*, *FRT80B.bbg*^{B211}*/TM6B* and *UAS-Crb*^{extra}*-TM-GFP* respectively. For wing disc clones, 37^{0}C heat shock was performed for 2h (MARCM clones) and 1.5 h (flip-out clones) on 1st instar larvae. RNAi lines used were, *UAS-bbg*^{RNAi}(III), *UAS-bbg*^{RNAi}(II) (VDRC: 15974 and15975, respectively), *UAS-sqh*^{RNAi} (VDRC: 7917), *UAS-crb*^{RNAi} (VDRC: 39177), and *UAS-cno*^{RNAi} (gift from Christian Klämbt). These were driven exclusively in the whole wing disc using *69b-Gal4* and *C765-Gal4* and in posterior compartment using *engrailed-Gal4(hen)* obtained from S. Eaton. The fosmid line *Flyfos030100, fTRG 527, Bbg(CG9598):tag* was used. The Cadherin:EGFP(II), gift from S. Eaton was also used. Deficieny lines used were *Df(3L)ED4543/TM6C* (8073), *Df(3R)ED5664/TM3* (24137), *Df(2L)BSC107/CyO* (8673), *ex*^{1}*/CyO* (295) and *sqh:GFP* (57145) flies from Bloomington Stock Center (http://flystocks.bio.indiana.edu/), too.

Adult wing mounting and imaging

The left wings from female flies were dissected in PBS and mounted in Euparal MTNG medium (6372B). Images were obtained in a Zeiss Axionplan2 imaging microscope using a 5X lens and were processed using Fiji.

Antibody generation and purification

Using adult *Drosophila* cDNA as a template, a 0.67 kb of the portion of *bbg-PC* cDNA clone was amplified by PCR. This represents 224 amino acids (Fig. 16 bold-underlined sequence). The sequence of the forward primer used was: 5′-ATGTCGACGCAGTGCCAAGAGTCGAGGTCA-3′. The reverse primer was: 5′-GTGTCGACTCTTTAGTGGAGGATCAGCCTC-3′. The PCR product was subcloned into the plasmid pCR2.1-TOPO (Invitrogen), and then digested with SalI (restriction sites included in the primers) for subcloning into pGEX-4T-1$(His)_6$C (bases on the Amersham vector pGEX-4T-1, modified to include a 6xHis tag at the terminus.) Recombinant protein was expressed under standard conditions for expression (500 μM IPTG, 37°C, 4 h) using the BL21DE3 expression strain (Novagen) and the His tagged protein was purified by a pull-down using Ni-NTA Agarose beads (Invitrogen) according to the manufacturer's instructions. This process yielded more than 100 mg of soluble, highly pure protein. Recombinant protein containing a GST-tag was injected into female New Zealand White rabbits (2.5 - 3.0 kg). For immunization 0.2 mg of recombinant protein in 0.6 ml PBS was mixed with an equal volume of Complete Freund's Adjuvant. The resulting emulsion was injected at multiple sites intra-cutaneously, intra-muscularly, and sub-cutaneously. For subsequent boosts, 0.2 mg of recombinant protein in 0.6 ml PBS was mixed with an equal volume of Incomplete Freund's Adjuvant. Boosts were done on day 28, day 56, and day 84. Small volume bleeds for testing were harvested on day 38 and day 66. The final bleed was harvested after 94 days. Serum was prepared by centrifugation of the coagulated blood. The serum (Bbg-GST) was coupled to HiTrap NHS-activated HP column, followed by serum re-circulation using an Ismatec Reglo Digital peristaltic pump. The serum was passed twice over the column at 0.5 ml/min. After washing and elution steps the antibody was concentrated in an Amicon Ultra 30K followed by buffer exchange to PBS pH 7.8 on Zeba Spin Desalting Columns 40 K (10 ml). The final concentration of the antibody was 5.64 mg/ml.

Construction of the His-Bbg Expression Plasmid and Purification of the recombinant protein

The Bbg protein was purified similarly to the protein for the antibody facility. The only difference is that the region of the *bbg-PC* cDNA that was amplified was 1191 bp using the primers Forward: AATAATAACCATGGGTCATAAGGTCACCCAGAAGCCG and Reversed: AATAATAAGCGGCCGCTTTCATCTAGGCGAAACAAATCTT and was cloned to the vector: pETMM-11. The other steps are similar to the previous paragraph.

Antibodies

Antibodies were used at the following concentrations for immunofluorescence (IF) or westernblot (WB): Rabbit anti-Bbg (1:1000; IF and WB; generated as described above), rat anti-Crb 2.8 (1:1000; IF and WB; Tepass et al., 1990), Rabbit anti-Crb-intra (1:1000; IF; generated in our lab, 2662), Rabbit anti-Sdt (1:1000; IF and WB; Berger et al., 2007), Rabbit anti-DPATJ (1:1000; IF and WB; Richard et al., 2006a), Rabbit anti-aPKC (1:1000; IF; C-20 Santa Cruz), Rabbit anti-Baz (1:1000; IF;ed from A. Wodarz), mouse anti-Armadillo (1:1000; IF; DSHB N2 7A1), mouse anti-Coracle (1:1000; IF; DSHB C566.9), mouse anti-Wingless (1:100; IF; DSHB 4D4), mouse anti-Cut (1:50; IF; DSHB 2B10), mouse anti-Notch (1:1000; IF; DSHB C458.2H), mouse anti-Delta (1:1000; IF; DSHB C594.9B), mouse anti-Dachsous (1:1000; IF; gift from S. Eaton), Rabbit anti-Yorkie (1:1000; IF; gift from D. Pan), mouse anti-Lamin C (1:1000; IF; DSHB LC28.26), Rabbit anti-SAS (1:500; IF; gift from D. Cavener), mouse anti-Patched (1:100; IF; DSHB apa1), mouse anti-Dlg (1:1000; IF; DSHB 4F3), mouse anti-DE-cadherin (1:1000; IF; DSHB rr1), Rabbit anti-PH3 (1:1000; IF; Millipore 06-570), Rabbit anti-IgG (1:1000; WB; Santa Cruz Biotechnology, Inc.), mouse anti-His (1:1000; WB; Qiagen 34660), mouse anti-GST (1:1000; WB; Sigma 1160), rat anti-tubulin (1:3000; WB; AbD Serotec), Rabbit anti-GFP (1:1000; IF; Invitrogen). Secondary antibodies labeled with Alexa dyes (1:1000; IF; Invitrogen). Secondary antibodies labeled with HRP (1:5000; WB; Santa Cruz).

RT-PCR for all the predicted isoforms of *bbg*

The isolation of RNA from *Drosophila* L3 wing discs, larvae and adult tissue was done using the standard protocol (https://dgrc.bio.indiana.edu/include/file/CGB-TR-200610.pdf). For the PCR Hot Star Taq polymerase from Qiagen was used. The primers that were used for the detection of the different *bbg* isoforms are as described in Bonnay et al., 2013. Below are the sequences of the primers, as described in Bonnay et al. 2013:

mRNA isoform	Forward	Reverse
Bbg-RC	5′-AAGAGAACCAGGCTCAGTTGCTCA-3′	5′-AGGAGTAATTGGAGCCCACGGAAA-3′
Bbg-RE	5′-GCGGGTGTAGCTGAAAGTGGAAA-3′	5′-AAGCAGTTCGTCTCTGTAGGCGAT-3′
Bbg-RF,G, H	5′-ACCTTCGAGTGCAAACAGAAAGCA-3′	5′-TTCTCTCTAACCGCTGATCCGCTT-3′
Bbg-J	5′-TCGGAACTGATCGAACCTGTCTCT-3′	5′-GTCCACCGGCGTTTACTTCCATTT-3′
Bbg-I	5′-TGCTCAGAATTAATCGCTACAGGG-3′	5′-GCGTTAATGCCGCTAATGCTGCTT-3′
Bbg-total	5′-TTCCACCCAATTTCAGCGAACCAC-3′	5′-TAAACTGGGTGCTGGCTCTACGTT-3′

Seuquencing of the bbg^{B211} allele

The isolation of RNA from *Drosophila* adult tissue was done using the standard protocol (https://dgrc.bio.indiana.edu/include/file/CGB-TR-200610.pdf). For the PCR Phusion polymerase from NEB was used. The primers that was used are listed:

Bbg-PC F: CAGCGGCAATATCAGTTGGC

Bbg-PC R: CTCATCGCGCGAGTTTTCAG

Bbg-PC F: CAGCGGCAATATCAGTTGGC

Gal900 R: TTAGCCATTGGAGCCTGGTG

Immunoprecipitation

Drosophila abdomens were collected on dry ice and mashed with a pestle before the addition of lysis buffer (50mM Tris, pH 8, 0.5% Triton X-100, 150mM NaCl, 1µg/ml µg/ml leupeptin, 250 µg/ml PefaBloc, 2 µg/ml aprotinin, and 1 µg/ml pepstatin). The lysate was left on ice for 30 min and then clarified

by centrifugation. 1 mg total protein was used per IP. Antibody was added to the lysate and incubated at 4°C rotating for 2 h. Then, 50 µl protein G agarose (GE Healthcare) per IP was added to the lysate antibody mixture and left to rotate again at 4°C O/N. The beads were then washed with lysis buffer six times and then boiled with loading buffer for 5 min at 100°C and analyzed by conventional SDS-PAGE.

Preparation of 3rd instar wing discs and WB

20 L3 (staging: collection of larval crawling to the vials) wing discs were prepared for SDS page by washing in PBS, drying and then mashing in 50µl 2xSDS loading buffer (100mM Tris pH6.8, 4% SDS, 0.2% Bromophenol Blue, 20% glycerol, 2% beta-mercaptoethanol) using a 1.5ml Eppendorf tube and pestle. Samples were boiled, clarified by centrifugation and run on 8% SDS PAGE gels. Proteins were transferred to Nitrocellulose membrane 0.45µm (GE Healthcare), and then probed using the antibodies referred to above.

Fixation of 3rd instar wing discs for EM

Wing discs (staging: collection of larval crawling to the vials) were incubated at 2h in 4% PFA/ 2,5% glutaraldehyde in 0,1M phosphate buffer, pH 7.4 at RT, followed by post fixation for 1h in 1,5% potassium Ferrocyanide/1% osmium tetroxide in 0,1M phosphate buffer, pH 7.4. Then they were stained with 1% tannic acid in 0,1M phosphate buffer, pH 7.4 for 45min. they were then dehydrated stepwise by washes with serial dilutions of ethanol and then incubated with propylene oxide for 30min These wing discs are then infiltrated with Durcupan and embed in pure Durcupan. Following of polymerization for 24h at 60^0C(!!). They were then cut into 70nm thin sections, for EM. Leica Ultracut UCT. Finally the discs were imaged (EM) using Morgani 268 TEM (from FEI), 80kV, Tungsten filament with CCD camera (SIS/Olympus).

Adult retina fixation for preparation of semi-thin sections

Fly heads were collected and cut in half. They were then fixed for 20min with 25% glutaraldehyde in 0.1M phosphate buffer, pH 7.2 at RT. 3-4x washes with 0.1M phosphate buffer, pH 7.2, followed this. These tissues were then fixed for 30 min in 1% osmium tetroxide/ 2% glutaraldehyde in 0.1M phosphate buffer pH 7.4 at 4^0C. Followed by 3-4x washes with 0.1M phosphate buffer, pH 7.2. They were fixed for 1h with 2% osmium tetroxide in 0.1M phosphate buffer pH 7.4 at 4^0C, washed 3x with distilled water. They were dehydrated in serial dilutions of ethanol of 50, 70, 90 and 96% for 5min on ice. They were then given 2x washes in 100% EtOH for 10min at RT and incubated in 2x 100% acetone for 10min at RT. This was followed by infiltration in 1:1 Durcupan/ Acetone over night at 4^0C. Then they were infiltrated for 3-4h in pure Durcupan and the retinas were then finally embedded and orientated in molds. The medium was left to polymerize for 24h at 60^0C. The molds were then cut into 1µm thick sections for light microscopy.

Immunofluorescence and Microscopy

Wing discs, eye discs, adult retinas, embryos and ovaries were prepared for IF according to standard protocols [Sullivan, W., et al., 2000]. 3rd instar discs (staging: collection of larval crawling to the vials) were fixed in 4% PFA for 20 min. Primary antibodies were incubated overnight at 4ºC. Tissues were washed with PBT, incubated in secondary antibodies (in block) for 2 hr at room temperature, then washed with PBT and mounted in Vectashield medium (Vector laboratories). The only exceptions are ovaries and embryos, which were post fixed in 100% Ethanol overnight at -20^0C. Images were acquired using a Zeiss LSM 700 inverted confocal microscope using 25X and 63X lenses and processed using Fiji. All images shown are representatives of the results obtained from several independent experiments (between 6 and 8 individual wing discs and other tissues collections and staining per genotype).

Flow Cytometry

Wing discs were dissected according to the protocol described from Cruz and Edgar 2008. 20 wing discs were dissociated into single cells using a solution containing trypsin and Hoechst 33342 diluted in PBS for 1.5 h in R/T. The samples were directly sorted using FACS. The flow cytometry was performed on a 5-laser - BD FACSAria IIIu sorter (BD Bioscience), and analyzed using the FACS Diva software (BD Bioscience, v8.0) and the flow cytometry modeling software ModFit LT. Gates were applied as follows: a P1 gate was set on a SSC/FSC dot-plot, to identify live cells based on size and shape. The P1 fraction was restricted, by setting a P2 gate on a SSC/GFP (exponential, blue laser, 488 nm). The P3 gate was generated on a BV2421-W/BV421-H (linear, UV laser, 375nm) dot blot to discriminate (maybe filter or demarcate would be a better word?) singlets and to visualize the DNA content using the Hoechst 33342 dye. Out of the P3 population a histogram for counts/BV421-A (linear, UV laser, 375 nm) was generated to analyze the cell cycle. Each 100,000 events from P2 were acquired to analyze the cell cycle of the different samples and genotypes. Voltage parameters were set based on wild type controls.

EdU staining in wing discs

The EdU kit from Invitrogen was used. The manufacturer order described in http://www.litmusscientific.com/sites/default/files/reviews/ Invitrogen-Click-iT %20EdU%20Imaging%20Kits%20(C10337).pdf, was used. More specifically, 3rd instar wing discs (staging: collection of larval crawling to the vials) were fixed in 4% PFA for 20 min. Primary antibodies were incubated overnight at 4ºC. Discs were washed with PBT, incubated in secondary antibodies (in block) for 2 hr at room temperature. Afterwards discs were incubated in the TUNEL mix (according to the manufacturer), incubated in 37^{0}C for 1hr, then washed with PBT and mounted in Vectashield medium (Vector laboratories).

TUNEL assay

TUNEL assays were performed using the Roche *in situ* cell death detection kit (fluorescein, Catalog number 1 684 795). In brief, wing discs were fixed with 4% PFA for 20 min and washed with PBT (PBS, 0.1% Triton X-100). Then the discs were transferred to a reaction buffer for 10 min, and then to a working-strength reaction buffer containing terminal deoxynucleotide transferase. The discs were incubated with the enzyme at 37°C for 1 h. Finally the discs were rinsed in three changes of PBT. They were then immunoreacted with antibodies or directly imaged using a confocal microscope.

Appendix

Number	Bbg Interactors
1	paramyosin [Drosophila melanogaster].
2	myofilin, isoform B [Drosophila melanogaster]
3	myosin light chain 2, isoform A [Drosophila melanogaster]
4	tropomyosin 2, isoform B [Drosophila melanogaster]
5	tropomyosin II [Drosophila melanogaster].
6	myosin alkali light chain 1, isoform B [Drosophila melanogaster]
7	myosin heavy chain, isoform D [Drosophila melanogaster]
8	actin 57B, isoform A [Drosophila melanogaster]
9	zipper, isoform C [Drosophila melanogaster]
10	alpha-spectrin [Drosophila melanogaster]
11	beta-spectrin [Drosophila melanogaster]
12	larval serum protein 1 gamma [Drosophila melanogaster]
13	beta-Tubulin at 56D, isoform B [Drosophila melanogaster]
14	Rab 6 [Drosophila melanogaster].
15	sarco/endoplasmic reticulum-type Ca-2+-ATPase [Drosophila
16	Flotillin-1, isoform A [Drosophila melanogaster]
17	ATPsyn-beta [Drosophila yakuba]
18	Ecdysone-inducible gene L3, isoform A [Drosophila melanogaster]
19	alpha-Tubulin at 84B [Drosophila melanogaster]
20	Na pump alpha subunit, isoform A [Drosophila melanogaster]
21	GM25183 [Drosophila sechellia]
22	ptip [Drosophila melanogaster]
23	stress-sensitive B, isoform A [Drosophila melanogaster]
24	porin, isoform A [Drosophila melanogaster]
25	alpha actinin, isoform C [Drosophila melanogaster]
26	glyceraldehyde 3 phosphate dehydrogenase 1, isoform A [Drosophila melanogaster]
27	GF13537 [Drosophila ananassae]
28	elongation factor 1alpha48D, isoform A [Drosophila melanogaster]
29	GA13897 [Drosophila pseudoobscura pseudoobscura]
30	ribosomal protein S3A, isoform A [Drosophila melanogaster]
31	squid, isoform A [Drosophila melanogaster]
32	RecName: Full=Alcohol dehydrogenase.
33	heat shock protein cognate 4, isoform A [Drosophila melanogaster]
34	GG17854 [Drosophila erecta]
35	RE30552p [Drosophila melanogaster]
36	ribosomal protein L9 [Drosophila melanogaster]
37	vacuolar protein sorting 13, isoform A [Drosophila melanogaster]
38	pyruvate kinase, isoform B [Drosophila melanogaster]
39	hrp48.1 [Drosophila melanogaster].
40	bent, isoform F [Drosophila melanogaster]
41	ribosomal protein S3 [Drosophila melanogaster]

42	heat shock protein 83, isoform A [Drosophila melanogaster]
43	Ecdysome [Drosophila melanogaster]
44	GG15836 [Drosophila erecta]
45	GG16295 [Drosophila erecta]
46	fat body protein 1 [Drosophila melanogaster].
47	GG10475 [Drosophila erecta]
48	ribosomal protein S4, isoform A [Drosophila melanogaster]
49	protein phosphatase 2A 65 kDa regulatory subunit [Drosophila melanogaster]
50	clathrin heavy chain, isoform A [Drosophila melanogaster]
51	stubarista [Drosophila yakuba]
52	arginine kinase, isoform E [Drosophila melanogaster]
53	GG17216 [Drosophila erecta]
54	CG8888 [Drosophila melanogaster]
55	Rtnl1, isoform H [Drosophila melanogaster]
56	larval serum protein 1 beta [Drosophila melanogaster]
57	GE23400 [Drosophila yakuba]
58	retinoid- and fatty acid-binding glycoprotein [Drosophila melanogaster]
59	GM12194 [Drosophila sechellia]
60	GM18393 [Drosophila sechellia]
61	ribosomal protein S16 [Drosophila melanogaster]
62	CG4169, isoform A [Drosophila melanogaster]
63	LD07532p, partial [Drosophila melanogaster]
64	lipid storage droplet-1, isoform A [Drosophila melanogaster]
65	heat shock protein cognate 72 [Drosophila melanogaster]
66	WNK homolog [Drosophila melanogaste]
67	ribosomal protein S14a, isoform B [Drosophila melanogaster]
68	GM12408 [Drosophila sechellia]
69	mitochondrial ATP synthase [Drosophila melanogaster]
70	Unc-89, isoform B [Drosophila melanogaster]
71	actin 87E, isoform A [Drosophila melanogaster]
72	canoe [Drosophila melanogaster]
73	T complex protein [Drosophila melanogaster]
74	RACK1 [Drosophila melanogaster]
75	Rab11, isoform B [Drosophila melanogaster]
76	microsomal glutathione S-transferase-like protein [Drosophila melanogaster]
77	ribosomal protein S17 [Drosophila melanogaster]
78	ribosomal protein L13, isoform A [Drosophila melanogaster]
79	CCT-gamma protein [Drosophila melanogaster]
80	karyopherin beta 3, isoform A [Drosophila melanogaster]
81	GG16451 [Drosophila erecta]
82	GE22904 [Drosophila yakuba]
83	juvenile hormone epoxide hydrolase 3 [Drosophila melanogaster]

84	RH21091p [Drosophila melanogaster]
85	Lola [Drosophila melanogaster]
86	Z band alternatively spliced PDZ-motif protein 52, isoform F [Drosophila melanogaster]
87	Moira [Drosophila melanogaster]
88	ADP ribosylation factor 79F, isoform B [Drosophila melanogaster]
89	GM20048 [Drosophila sechellia]
90	NADH:ubiquinone reductase 23kD subunit precursor [Drosophila melanogaster]
91	GG19820 [Drosophila erecta]
92	glutathione S-transferase D1 [Drosophila simulans]
93	neuroglian, isoform A [Drosophila melanogaster]
94	phosphofructokinase, isoform A [Drosophila melanogaster]
95	Vap-33-1, isoform B [Drosophila melanogaster]
96	T-cp1zeta [Drosophila melanogaster]
97	RH09294p [Drosophila melanogaster]
98	GF15209 [Drosophila ananassae]
99	Polychaetoid [Drosophila melanogaste]
100	GE25915 [Drosophila yakuba]
101	GE23773 [Drosophila yakuba]
102	GH05567p [Drosophila melanogaster]
103	GG18722 [Drosophila erecta]
104	lipid storage droplet-2, isoform B [Drosophila melanogaster]
105	ribosomal protein L19, isoform A [Drosophila melanogaster]
106	GA18510 [Drosophila pseudoobscura pseudoobscura]
107	lethal (2) essential for life, isoform A [Drosophila melanogaster]
108	ribosomal protein S25, isoform A [Drosophila melanogaster]
109	thioredoxin peroxidase 1, isoform A [Drosophila melanogaster]
110	GA17461 [Drosophila pseudoobscura pseudoobscura]
111	NTPase, isoform A [Drosophila melanogaster]
112	GM24402 [Drosophila sechellia]
113	Acyl-CoA synthetase long-chain, isoform C [Drosophila melanogaster]
114	Bbg, Isoform C [Drosophila melanogaster]
115	mushroom body defect, isoform H [Drosophila melanogaster]
116	Bub3 [Drosophila melanogaster]
117	Fruitless [Drosophila melanogaster]
118	GM12765 [Drosophila sechellia]
119	aldehyde dehydrogenase [Drosophila melanogaster]
120	CG33303, isoform A [Drosophila melanogaster]
121	receptor of activated protein kinase C 1, isoform A [Drosophila melanogaster]
122	toucan [Drosophila melanogaster]
123	Trip1 [Drosophila melanogaster]
124	GG14652 [Drosophila erecta]

125	epi {drosophila melanogaster]

Number	Bbg+IgG overlapping interactors
1	hyperplastic discs [Drosophila melanogaster]
2	heterogeneous nuclear ribonucleoprotein at 98DE, isoform D [Drosophila melanogaster]
3	ribosomal protein S6, isoform A [Drosophila melanogaster]
4	no-on-transient A product form I [Drosophila melanogaster]
5	heat shock cognate 4 [Drosophila melanogaster]
6	Chain C, Crystal Structure Of A Filament-like Actin Trimer Bound To The Bacterial Effector Vopl
7	LD44733p [Drosophila melanogaster]
8	heterogeneous nuclear ribonucleoprotein at 87F, isoform A [Drosophila melanogaster]
9	GG15623 [Drosophila erecta]
10	CG9684 [Drosophila melanogaster]
11	GD13105 [Drosophila simulans]
12	glorund, isoform A [Drosophila melanogaster]
13	ribosomal protein S9, isoform A [Drosophila melanogaster]
14	GA20600 [Drosophila pseudoobscura pseudoobscura]
15	ribosomal protein L38, isoform A [Drosophila melanogaster]
16	ribosomal protein S13, isoform A [Drosophila melanogaster]
17	little imaginal discs, isoform A [Drosophila melanogaster]
18	LD09503p [Drosophila melanogaster]
19	GD12620 [Drosophila simulans]
20	longitudinals lacking, isoform C [Drosophila melanogaster]
21	Muscle-specific protein 300, isoform G [Drosophila melanogaster]
22	belle, isoform A [Drosophila melanogaster]
23	Tpr homolog [Drosophila melanogaster]
24	GG14270 [Drosophila erecta]
25	GA10310 [Drosophila pseudoobscura pseudoobscura]
26	CG11882, isoform A [Drosophila melanogaster]
27	fondue, isoform B [Drosophila melanogaster]
28	ribosomal protein L5, isoform A [Drosophila melanogaster]
29	ribosomal protein S19a, isoform A [Drosophila melanogaster]

30	ribosomal protein S15, isoform A [Drosophila melanogaster]
31	no circadian temperature entrainment, isoform A [Drosophila melanogaster]
32	ribosomal protein L14 [Drosophila melanogaster]
33	GG16013 [Drosophila erecta]
34	LD11664p [Drosophila melanogaster]
35	GA14837 [Drosophila pseudoobscura pseudoobscura]
36	suppressor of forked, isoform E [Drosophila melanogaster]
37	Ulp1 [Drosophila melanogaster]
38	CG5787, isoform A [Drosophila melanogaster]
39	ribosomal protein S24, isoform A [Drosophila melanogaster]
40	polyA-binding protein, isoform A [Drosophila melanogaster]
41	fibrillarin [Drosophila melanogaster]
42	ribosomal protein L8, isoform A [Drosophila melanogaster]
43	ribosomal protein S15Aa, isoform D [Drosophila melanogaster]
44	GG22596 [Drosophila erecta]
45	GH18602 [Drosophila grimshawi]
46	GF20391 [Drosophila ananassae]
47	CG10777 [Drosophila melanogaster]
48	ribosomal protein S14, isoform B [Drosophila melanogaster]
49	ribosomal protein S7, isoform A [Drosophila melanogaster]
50	caprin [Drosophila melanogaster]
51	ribosomal protein L18A [Drosophila melanogaster]
52	ribosomal protein S20 [Drosophila melanogaster]
53	ubiquitin, partial [Drosophila melanogaster]
54	combgap, isoform F [Drosophila melanogaster]
55	GF17624 [Drosophila ananassae]
56	GM24117 [Drosophila sechellia]
57	GM13911 [Drosophila sechellia]
58	GE12955 [Drosophila yakuba]
59	GA21399 [Drosophila pseudoobscura pseudoobscura]
60	GA10657 [Drosophila pseudoobscura pseudoobscura]
61	GG20113 [Drosophila erecta]

Number	IgG interactors
1	ADP/ATP translocase [Drosophila pseudoobscura]
2	dihydrodipicolinate reductase [Escherichia coli O157:H7 str. EDL933]
3	dihydrodipicolinate reductase [Citrobacter rodentium ICC168]
4	dihydrodipicolinate reductase [Shigella]
5	dihydrodipicolinate reductase [Salmonella enterica subsp. enterica serovar Paratyphi A str. ATCC 9150]
6	HL06604p [Drosophila melanogaster]
7	desmoglein type 1 [Homo sapiens]
8	Na ATPase alpha subunit [Drosophila melanogaster]
9	Aspartokinase [Salmonella enterica subsp. enterica serovar Inverness str. R8-3668]
10	bifunctional aspartokinase/homoserine dehydrogenase 2 [Enterobacter cloacae EcWSU1]
11	keratin 1 [Homo sapiens]
12	Keratin 10 [Homo sapiens]
13	keratin_ type II cytoskeletal 2 epidermal [Homo sapiens]
14	bifunctional aspartate kinase II/homoserine dehydrogenase II [Salmonella enterica]
15	cytokeratin 9 [Homo sapiens]
16	aspartate kinase [Shigella dysenteriae]
17	PREDICTED: keratin_ type II cytoskeletal 5 [Saimiri boliviensis boliviensis]

References

Aegerter-Wilmsen, T., Aegerter, C.M., Hafen, E., Basler, K. (2007). **Model for the regulation of size in the wing imaginal disc of Drosophila.** Mech. Dev. 124(4): 318--326.

Alves, C. H. *et al.* (2012) **Loss of CRB2 in the mouse retina mimics human retinitis pigmentosa due to mutations in the *CRB1* gene.** Hum. Mol. Genet. 22, 35–50.

Ambegaonkar, A.A., Pan, G., Mani, M., Feng, Y., Irvine, K.D. (2012). **Propagation of Dachsous-Fat planar cell polarity.** Curr. Biol. 22(14): 1302--1308.

Arai, Y., Pulvers, J.N., Haffner, C., Schilling, B., Nusslein, I., Calegari, F., Huttner, W.B. (2011) **Neural stem and progenitor cells shorten S-phase on commitment to neuron production.** Nat. Commun. 2, 154.

Aranjuez, G., Kudlaty, E., Longworth, M.S., McDonald, J.A. (2012). **On the role of PDZ domain-encoding genes in Drosophila border cell migration.** G3 (Bethesda) 2(11): 1379--1391.

Bachmann, A., Draga, M., Grawe, F., Knust, E. (2008). **On the role of the MAGUK proteins encoded by Drosophila varicose during embryonic and postembryonic development.** BMC Dev. Biol. 8(): 55.

Bachmann, A., Schneider, M., Theilenberg, E., Grawe, F., Knust, E. (2001). **Drosophila Stardust is a partner of Crumbs in the control of epithelial cell polarity.** Nature 414(6864): 638--643.

Bachmann, A., Timmer, M., Sierralta, J., Pietrini, G., Gundelfinger, E. D., Knust, E. and Thomas, U. (2004). **Cell type-specific recruitment of Drosophila Lin-7 to distinct MAGUK-based protein complexes defines novel roles for Sdt and Dlg-S97.** J. Cell Sci. 117, 1899-1909.

Baum B and Georgiou M. (2011) **Dynamics of adherens junctions in epithelial establishment, maintenance, and remodeling.** JCB vol. 192 no. 6 907-917.

Berger, C., Renner, S., Lüer, K., Technau, G.M. (2007). **The commonly used marker ELAV is transiently expressed in neuroblasts and glial cells in the Drosophila embryonic CNS.** Dev. Dyn. 236(12): 3562--3568.

Bilder, D., Perrimon, N. (2000). **Localization of apical epithelial determinants by the basolateral PDZ protein Scribble.** Nature 403(6770): 676--680.

Bilder, D., Schober, M., Perrimon, N. (2003). **Integrated activity of PDZ protein complexes regulates epithelial polarity.** Nat. Cell Biol. 5(1): 53--58.

Bonnay, F., Cohen-Berros, E., Hoffmann, M., Kim, S.Y., Boulianne, G.L., Hoffmann, J.A., Matt, N., Reichhart, J.M. (2013). **big bang gene modulates gut immune tolerance in Drosophila.** Proc. Natl. Acad. Sci. U.S.A. **110(8)**: 2957--2962.

Bossinger, O., Klebes, A., Segbert, C., Theres, C., Knust, E. (2001) **Zonula adherens formation in Caenorhabditis elegans requires dlg-1, the homologue of the Drosophila gene discs large**. Dev Biol. 2001 Feb 1;230(1):29-42.

Brittle, A., Thomas, C., Strutt, D. (2012). **Planar polarity specification through asymmetric subcellular localization of Fat and Dachsous.** Curr. Biol. 22(10): 907--914.

Bulgakova NA, Knust E. (2009) **The Crumbs complex: from epithelial-cell polarity to retinal degeneration.** J Cell Sci. 1;122(Pt 15):2587-96.

Bulgakova, N.A., Kempkens, O., Knust, E. (2008). **Multiple domains of Stardust differentially mediate localisation of the Crumbs-Stardust complex during photoreceptor development in Drosophila.** J. Cell Sci. 121(12): 2018--2026.

Chang :, Kreko T, Davison H, Cusmano T, Rothenfluh A, Eaton BA. (2013) **Normal dynactin complex function during synapse growth in Drosophila requires membrane binding by Arfaptin.** Mol Biol Cell Jun;24(11):1749-64, S1-5

Chartier, F. J., Hardy, E. J. & Laprise, P. (2012) **Crumbs limits oxidase-dependent signaling to maintain epithelial integrity and prevent photoreceptor cell death.** J. Cell Biol. 198, 991–998.

Chen J, Zhang M (2013) **The Par3/Par6/aPKC complex and epithelial cell polarity.** Exp Cell Res. 319(10):1357-64.

Chen, S., Zhang, Y.E., Long, M. (2010). **New genes in Drosophila quickly become essential.** Science 330(6011): 1682--1685.

Chillakuri CR[1], Sheppard D, Lea SM, Handford PA. (2012) **Notch receptor-ligand binding and activation: insights from molecular studies**. Semin Cell Dev Biol. (4):421-8.

Choi, W., Jung, K.C., Nelson, K.S., Bhat, M.A., Beitel, G.J., Peifer, M., Fanning, A.S. (2011). **The single Drosophila ZO-1 protein Polychaetoid regulates embryonic morphogenesis in coordination with Canoe/afadin and Enabled.** Mol. Biol. Cell 22(12): 2010--2030.

Clark, H.F., Brentrup, D., Schneitz, K., Bieber, A., Goodman, C., Noll, M. (1995). **Dachsous encodes a member of the cadherin superfamily that controls imaginal disc morphogenesis in Drosophila.** Genes Dev. 9(12): 1530--1542.

Conlon I, Raff M. **Size control in animal development**. Cell. ;96(2):235-44.

Cruz AF and Edgar BA. (2008). **Flow cytometric analysis of Drosophila cells. Methods Mol Biol.** 2008;420:373-89

Cunningham R, Biswas R, Steplock D, Shenolikar S, Weinman E. (2010**) Role of NHERF and scaffolding proteins in proximal tubule transport.** Urol Res 38:257–262.

den Hollander, A. I., Roepman, R., Koenekoop, R. K. and Cremers, F. P. (2008). **Leber congenital amaurosis: genes, proteins and disease mechanisms.** Prog. Retin. Eye Res. 27, 391-419.

den Hollander, J.B. ten Brink, Y.J.M. de Kok, S. van Soest, L.I. van den Born, M.A. van Driel, D.J.R. van de Pol, A.M. Payne, S.S. Bhattacharya, U. Kellner, C.B. Hoyng, A. Westerveld, H.G. Brunner, E.M. Bleeker-Wagemakers, A.F. Deutman, J.R. Heckenlively, F.P.M. Cremers, A.A.B. Bergen. (1999) **Mutations in a human homologue of *Drosophila crumbs* cause retinitis pigmentosa (RP12).** Nat. Genet., 23 (1999), pp. 217–221.

Dunst, S., Kazimiers, T., von Zadow, F., Jambor, H., Sagner, A., Brankatschk, B., Mahmoud, A., Spannl, S., Tomancak, P., Eaton, S., Brankatschk, M. (2015). **Endogenously tagged rab proteins: a resource to study membrane trafficking in Drosophila.** Dev. Cell 33(3): 351--365.

Ganot P, Zoccola D, Tambutte E, Voolstra C, Aranda M, Allemand D,and Tambutte S. **Structural Molecular Components of Septate Junctions in Cnidarians Point to the Origin of Epithelial Junctions in Eukaryotes.** Mol. Biol. Evol.

Gateff, E. (1978) **Malignant neoplasms of genetic origin in *Drosophila melanogaster*.** Science 200, 1448–1459.

Grusche, F.A., Degoutin, J.L., Richardson, H.E., Harvey, K.F. (2011). **The Salvador/Warts/Hippo pathway controls regenerative tissue growth in Drosophila melanogaster.** Dev. Biol. 350(2): 255--266.

Grzeschik, N.A., Parsons, L.M., Allott, M.L., Harvey, K.F., Richardson, H.E. (2010). **Lgl, aPKC, and Crumbs regulate the Salvador/Warts/Hippo pathway through two distinct mechanisms.** Curr. Biol. 20(7): 573--581.

Hafezi, Y., Bosch, J.A., Hariharan, I.K. (2012). **Differences in levels of the transmembrane protein Crumbs can influence cell survival at clonal boundaries.** Dev. Biol. 368(2): 358--369.

Halder G and Johnson RL (2011). **Hippo signaling: growth control and beyond.** Development.;138(1):9-22.

Hand A and Gobel S (1971). **The structural organization of the septate and gap junctions of hydra.** THE JOURNAL OF CELL BIOLOGY • VOLUME 52.

Herranz, H., Stamataki, E., Feiguin, F., Milan, M. (2006). **Self-refinement of Notch activity through the transmembrane protein Crumbs: modulation of gamma-Secretase activity.** EMBO Rep. 7(3): 297--302.

Hong, Y., Stronach, B., Perrimon, N., Jan, L.Y., Jan, Y.N. (2001). **Drosophila Stardust interacts with Crumbs to control polarity of epithelia but not neuroblasts.** Nature 414(6864): 634--638.

Hong, Y., Stronach, B., Perrimon, N., Jan, L.Y., Jan, Y.N. (2001). **Drosophila Stardust interacts with Crumbs to control polarity of epithelia but not neuroblasts.** Nature 414(6864): 634--638.

Izaddoost, S., Nam, S.C., Bhat, M.A., Bellen, H.J., Choi, K.W. (2002). **Drosophila Crumbs is a positional cue in photoreceptor adherens junctions and rhabdomeres.** Nature 416(6877): 178--182.

Johnson, K., Grawe, F., Grzeschik, N., Knust, E. (2002). **Drosophila crumbs is required to inhibit light-induced photoreceptor degeneration.** Curr. Biol. 12(19): 1675--1680.

Jordan, P., Karess, R. (1997). **Myosin light chain-activating phosphorylation sites are required for oogenesis in Drosophila**. J. Cell Biol. 139(7): 1805--1819.

Jurgens, G., Wieschaus, E., Nusslein-Volhard, C., Kluding, H. (1984). **Mutations affecting the pattern of the larval cuticle in Drosophila melanogaster. II. Zygotic loci on the third chromosome.** Rouxs Arch. Dev. Biol. 193: 283--295.

Kim Sabrina Yoon-Gyung (2006) **Characterization of *big bang*, a novel *Drosophila* gene encoding PDZ domain-containing proteins involved in locomotor behavior.** PhD thesis, University of Toronto, Canada.

Kim NG, Koh E, Chen X, Gumbiner BM. (2011) **E-cadherin mediates contact inhibition of proliferation through Hippo signaling-pathway components.** Proc Natl Acad Sci U S A. ;108(29):11930-5.

Kim, S.Y., Renihan, M.K., Boulianne, G.L. (2006). **Characterization of big bang, a novel gene encoding for PDZ domain-containing proteins that are dynamically expressed throughout Drosophila development.** Gene Expr. Patterns6(5): 504--518.

Klebes, A., Knust, E. (2000). **A conserved motif in Crumbs is required for E-cadherin localisation and zonula adherens formation in Drosophila.** Curr. Biol. 10(2): 76--85.

Klose, S., Flores-Benitez, D., Riedel, F., Knust, E. (2013). **Fosmid-based structure-function analysis reveals functionally distinct domains in the cytoplasmic domain of Drosophila crumbs.** G3 (Bethesda) 3(2): 153--165.

Kornau H-C, Schenker LT, Kennedy MB, Seeburg PH. **Domain interaction between NMDA receptor subunits and the postsynaptic density protein PSD-95.** Science.1995;269:1737–1740.

Krahn PM, Bückers J, Kastrup L and Wodarz A. **Formation of a Bazooka–Stardust complex is essential for plasma membrane polarity in epithelia.** JCB v2010. vol. 190 no. 5 751-760.

Lecuyer, E., Yoshida, H., Parthasarathy, N., Alm, C., Babak, T., Cerovina, T., Hughes, T.R., Tomancak, P., Krause, H.M. (2007). **Global analysis of mRNA localization reveals a prominent role in organizing cellular architecture and function.** Cell 131(1): 174--187.

Lee, C.Y., Andersen, R.O., Cabernard, C., Manning, L., Tran, K.D., Lanskey, M.J., Bashirullah, A. and Doe, C.Q. (2006) ***Drosophila* Aurora-A kinase**

inhibits neuroblast self-renewal by regulating aPKC/Numb cortical polarity and spindle orientation. Genes Dev. 20, 3464–3474.

Lee, M. and Vasioukhin, V. (2008) **Cell polarity and cancer: cell and tissue polarity as a non- canonical tumor suppressor.** J. Cell Sci. 121, 1141–1150.

Lemmers, C., Medina, E., Delgrossi, M.H., Michel, D., Arsanto Bivic, J.P., Le Bivic, A. (2002). **hINADI/PATJ, a homolog of Discs lost, interacts with crumbs and localizes to tight junctions in human epithelial cells.** J. Biol. Chem.277(28): 25408--25415.

Levayer, R., Moreno, E. (2013). **Mechanisms of cell competition: Themes and variations.** J. Cell Biol. 200(6): 689--698.

Lin Ya-Huei (2015) **The AP2 complex regulates epithelial polarity via regulating Crumbs endocytosis.** PhD thesis, Technical University of Dresden, Germany.

Ling, C., Zheng, Y., Yin, F., Yu, J., Huang, J., Hong, Y., Wu, S., Pan, D. (2010). **The apical transmembrane protein Crumbs functions as a tumor suppressor that regulates Hippo signaling by binding to Expanded.** Proc. Natl. Acad. Sci. U.S.A. 107(23): 10532--10537.

Macara Ian G. (2004) **Parsing the Polarity code.** Nature Reviews Molecular Cell Biology 5, 220-231.

Major RJ and Irvine KD. (2005) **Influence of Notch on dorsoventral compartmentalization and actin organization in the Drosophila wing.** Development Sep;132(17):3823-33.

Manzanares et al., (2009) **Non-muscle myosin II takes centre stage in cell adhesion and migration.** Nat Rev Mol Cell Biol. (11): 778–790.

Manzanares,[*] Xuefei Ma,[‡] Robert S. Adelstein,[‡§] and Alan Rick Horwitz[*§]

Mao, Y., Tournier, A.L., Bates, P.A., Gale, J.E., Tapon, N., Thompson, B.J. (2011). **Planar polarization of the atypical myosin Dachs orients cell divisions in Drosophila.** Genes Dev. 25(2): 131--136.

Marmorstein AD, Finnemann SC, BonilhaVL, Rodriguez-Boulan E. (1998). **Morphogenesis of the retinal pigment epithelium:toward understanding retinal degenera-tive diseases.** Ann N Y Acad Sci. 857:1–12.

McGuire, S.E., Le, P.T., Osborn, A.J., Matsumoto, K., Davis, R.L. (2003). **Spatiotemporal rescue of memory dysfunction in Drosophila.** Science 302(5651): 1765--1768.

McKinley, R.F., Yu, C.G., Harris, T.J. (2012). **Assembly of Bazooka polarity landmarks through a multifaceted membrane-association mechanism.** J. Cell Sci. 125(5): 1177--1190.

Mehalow AK, Kameya S, Smith RS, Hawes NL, Denegre JM, Young JA, Bechtold L, Haider NB, Tepass U, Heckenlively JR, Chang B,Naggert JK, Nishina PM. (2003) **CRB1 is essential for external limiting membrane integrity and photoreceptor morphogenesis in the mammalian retina.** Hum Mol Genet.12(17):2179-89**.**

Milan, M., Campuzano, S., Garcia-Bellido, A. (1996). **Cell cycling and patterned cell proliferation in the Drosophila wing during metamorphosis.** Proc. Natl. Acad. Sci. U.S.A. 93(21): 11687--11692.

Ohata S, Aoki R, Kinoshita S, Yamaguchi M, Tsuruoka-Kinoshita S, et al. (2011). **Dual roles of Notch in regulation of apically restricted mitosis and apicobasal polarity of neuroepithelial cells.** Neuron 69:215–30.

Ohata S, Aoki R, Kinoshita S, Yamaguchi M, Tsuruoka-Kinoshita S, Tanaka H, Wada H, Watabe S, Tsuboi T, Masai I, Okamoto H. (2011) **Dual roles of Notch in regulation of apically restricted mitosis and apicobasal polarity of neuroepithelial cells.** Neuron. ;69(2):215-30.

Omori, Yoshihiro, Malicki, Jarema, (2006). **oko meduzy and Related crumbs Genes Are Determinants of Apical Cell Features in the Vertebrate Embryo.** Current biology : CB16(10): 945-957.

Pellikka, M., Tanentzapf, G., Pinto, M., Smith, C., McGlade, C.J., Ready, D.F., Tepass, U. (2002). **Crumbs, the Drosophila homologue of human CRB1/RP12, is essential for photoreceptor morphogenesis** . Nature 416(6877): 143--149.

Pielage, J., Stork, T., Bunse, I., Klaembt, C. (2003). **The Drosophila cell survival gene discs lost encodes a cytoplasmic Codanin-1-like protein, not a homolog of tight junction PDZ protein Patj.** Dev. Cell 5(6): 841--851.

Pinheiro, E., Montell, D.J. (2003). **Identification of two PDZ-domain proteins, PAR-6 and Bazooka, that function in border cell migration.** A. Dros. Res. Conf. 44 : 557B.

Rauskolb, C., Pan, G., Reddy, B.V., Oh, H., Irvine, K.D. (2011). **Zyxin links fat signaling to the hippo pathway.** PLoS Biol. 9(6): e1000624.

Rauskolb, C., Sun, S., Sun, G., Pan, Y., Irvine, K.D. (2014). **Cytoskeletal Tension Inhibits Hippo Signaling through an Ajuba-Warts Complex**. Cell 158(1): 143--156.

Richardson, E.C., Pichaud, F. (2010). **Crumbs is required to achieve proper organ size control during Drosophila head development** . Development 137(4): 641--650.

Ridley AJ. **Life at the leading edge.** Cell. 2011;145(7):1012–1022.

Robinson, B.S., Huang, J., Hong, Y., Moberg, K.H. (2010). Crumbs regulates Salvador/Warts/Hippo signaling in Drosophila via the FERM-domain protein expanded. Curr. Biol. 20(7): 582--590.

Roh, M. H., Makarova, O., Liu, C. J., Shin, K., Lee, S., Laurinec, S., Goyal, M., Wiggins, R. and Margolis, B. (2002). **The Maguk protein, Pals1, functions as an adapter linking mammalian homologues of Crumbs and Discs Lost.** J. Cell Biol. 157, 161-172.

Sansores-Garcia, L., Bossuyt, W., Wada, K., Yonemura, S., Tao, C., Sasaki, H., Halder, G. (2011). **Modulating F-actin organization induces organ growth by affecting the Hippo pathway.** EMBO J. 30(12): 2325--2335.

Saraste and Pulkki (2000) **Morphologic and biochemical hallmarks of apoptosis.** Cardiovasc Res.;45(3):528-37.

Sasaki N, Sasamura T, Ishikawa HO, Kanai M, Ueda R, Saigo K, Matsuno K. (2007) **Polarized exocytosis and transcytosis of Notch during its apical localization in *Drosophila* epithelial cells.** Genes Cells. 2007 Jan;12(1):89-103.

Schlegelmilch K, Mohseni M, Kirak O, Pruszak J, Rodriguez JR, Zhou D, Kreger BT, Vasioukhin V, Avruch J, Brummelkamp TR, et al. (2011). **Yap1 acts downstream of α-catenin to control epidermal proliferation.** Cell 144: 782–795.

Silvis MR, Kreger BT, Lien WH, Klezovitch O, Rudakova GM, Camargo FD, Lantz DM, Seykora JT, Vasioukhin V (2011)**. α-catenin is a tumor suppressor that controls cell accumulation by regulating the localization and activity of the transcriptional coactivator Yap1.** Sci Signal 4: ra33.

Staley B, Irvine K (2012) **Hippo signaling in Drosophila: recent advances and insights.** Dev Dyn. 241(1):3-15.

Sullivan, W., Ashburner, M., and Hawley, R.S. (2000). **Drosophila protocols**, Cold Spring Harbor, N.Y.: Cold Spring Harbor Laboratory Press.

Tepass U (2012). **The apical polarity protein network in Drosophila epithelial cells: regulation of polarity, junctions, morphogenesis, cell growth, and survival.** Annu Rev Cell Dev Biol. ;28:655-85.

Tepass, U., Knust, E. (1993). **Phenotypic and developmental analysis of mutations at the crumbs locus, a gene required for the development of epithelia in Drosophila melanogaster.** Rouxs Arch. Dev. Biol.

Tepass, U., Theres, C., Knust, E. (1990). ***crumbs*** **encodes an EGF-like protein expressed on apical membranes of Drosophila epithelial cells and required for organization of epithelia.** Cell 61(): 787--799.

Thompson B, Pichaud F & Röper K. (2013) **Sticking together the Crumbs — an unexpected function for an old friend.** Nature Reviews Molecular Cell Biology 14, 307-314.

van de Pavert, S. A., Kantardzhieva, A., Malysheva, A., Meuleman, J., Versteek, I., Levelt, C., Klooster, J., Geiger, S., Seeliger, M. W., Rashbass, P. et al. (2004). **Crumbs homologue 1 is required for maintenance of photoreceptor cell polarization and adhesion during light exposure.** J. Cell Sci. 117, 4169-4177.

Wodarz, A. and Nathke, I. (2007) **Cell polarity in development and cancer.** Nat. Cell Biol. 9, 1016–1024.

Wodarz, A., Hinz, U., Engelbert, M., Knust, E. (1995). **Expression of crumbs confers apical character on plasma membrane domains of ectodermal epithelia of Drosophila.** Cell 82(1): 67--76.

Wodarz, A., Ramrath, A., Grimm, A., Knust, E. (2000). **Drosophila atypical protein kinase C associates with Bazooka and controls polarity of epithelia and neuroblasts.** J. Cell Biol. 150(6): 1361--1374.

Zhou, W., Hong, Y. (2012). **Drosophila Patj plays a supporting role in apical-basal polarity but is essential for viability.** Development 139(16): 2891--2896.

Acknowledgements

First, I would like to thank my mentor, Prof. Dr. Elisabeth Knust, for giving me the opportunity to conduct my PhD in a great place, and for her scientific advice, motivation and enthusiasm all these four years. What I learnt from her is how to conduct good science.

I would also like to thank Prof. Dr. Christian Dahmann for his willingness to review this PhD thesis. I would like to thank my TAC members Prof. Dr. Elly Tanaka and Dr. Pavel Tomancak for scientific advice and motivation for my project.

I am grateful to Linda Nemetschke, post-doc in our lab, that she shared her screen and results with me. I want to thank all of my labmates and especially, Ya-Huei Lin for fruitful discussions and technical support. I am thankful to Srija Bhagavatula, for revising this thesis. Our present and past technicians and fly keepers: Catrin, Petra, Michi, Weihua, Conny, Sven and Stefan, for giving a helping hand and a great working atmosphere. I would like to thank the former and past members of the lab: Vicki, Ani, Marta and João, that except from co-workers they are great friends. Natalie Dye, post-doc in S. Eaton group for the live-imaging experiments and Anna Shevchenko for the MS screen. Last but not least, a special thanks to the MPI-CBG facilities (light microscopy, MS, FACS sequencing, antibody and protein expression) that made my PhD life much easier.

I would like to thank my second family here in Dresden, consisting of my friends Franky and Grigoris. I will never forget my closest friends that I spent so much funny time both in Dresden: Marci, Robi, Giannis, Vivian and Vania, and in Greece: Vasillis, Kapanida and Dritsa.

Finally, I am really greatfull to the people that they always supported, support and will support my choices, the people that are most proud for me: my parents Manolis and Maria and my sister Olga. My family is always my driving force.

Erklärung entsprechend §5.5 der Promotionsordnung/ Declaration according to §5.5 of the doctorate regulations

PhD Thesis **"*big bang*, a novel regulator of tissue growth in *Drosophila melanogaster*.** Submitted by **Georgios Tsoumpekos.**

Hiermit versichere ich, dass ich die vorliegende Arbeit ohne unzulässige Hilfe Dritter und ohne Benutzung anderer als der angegebenen Hilfsmittel angefertigt habe; die aus fremden Quellen direkt oder indirekt übernommenen Gedanken sind als solche kenntlich gemacht. Die Arbeit wurde bisher weder im Inland noch im Ausland in gleicher oder ähnlicher Form einer anderen Prüfungsbehörde vorgelegt.

Die Dissertation wurde im Zeitraum vom starting 09/01/2012 bis 21/12/2015 of finish verfasst und von Prof. Dr. Elisabeth Knust *,* Max Planck Institute of Molecular Cell Biology and Genetics in Dresden, Germany*.*

Meine Person betreffend erkläre ich hiermit, dass keine früheren erfolglosen Promotionsverfahren stattgefunden haben.
Ich erkenne die Promotionsordnung der Fakultät für Mathematik und Naturwissenschaften, Technische Universität Dresden an.

I herewith declare that I have produced this paper without the prohibited assistance of third parties and without making use of aids other than those specified; notions taken over directly or indirectly from other sources have been identified as such. This paper has not previously been presented in identical or similar form to any other German or foreign examination board.

The thesis work was conducted from *09/01/2012 to 21/12/2015* under the supervision of Prof.Dr. Elisabeth Knust at the Max Planck Institute of Molecular Cell Biology and Genetics in Dresden, Germany.

I declare that I have not undertaken any previous unsuccessful doctorate proceedings.
I declare that I recognize the doctorate regulations of the *Fakultät für Mathematik und Naturwissenschaften* of the *Technische Universität Dresden*.

Date Signature